1-1-2014

Explorations into host defense against Plasmodium falciparum: mechanistic and structure-function studies of antimalarial chemokines

Melissa Suzanne Love
University of Pennsylvania, mlove73085@gmail.com

Explorations into host defense against Plasmodium falciparum: mechanistic and structure-function studies of antimalarial chemokines

Abstract
Antimicrobial peptides (AMPs) are small (2-8kDa) peptides that have remained an important part of innate immunity over evolutionary time. AMPs vary greatly in sequence and structure, but display broad-spectrum activity against bacteria, yeast, and fungi via direct perturbation of the pathogen membrane. AMPs are typically amphipathic, and contain 2-4 positively charged amino acid residues. It has been previously shown that many chemokines also display AMP activity, both via their canonical function recruiting immune cells to the site of an infection and by direct interaction with the pathogen itself. Many antimicrobial chemokines have the same tertiary structure: an N-terminal loop responsible for receptor recognition; a three-stranded antiparallel β-sheet domain that provides a stable scaffold; and a C-terminal α-helix that folds over the β-sheet and helps to stabilize the overall structure. The α-helix of these chemokines tends to be amphipathic and retains AMP activity on its own. The work presented here focuses on two antimicrobial chemokines - platelet factor 4 (CXCL4/PF4) and macrophage inflammatory protein-3α (CCL20/MIP-3α) - and shows that they have activity against the malaria parasite. Chapter 2 details the exploration into the mechanism of action of PF4 against *P. falciparum*, and the translation of this mechanism to small molecules that mimic antimicrobial peptides. Additionally, this antimalarial activity is also present in a mouse model of malaria. Chapter 3 focuses on finding additional chemokines with antimalarial activity, and explores the structure-function relationship between the conserved domains and how they modulate i) the antimalarial activity, and ii) provide a protective scaffold to prevent harm to host cells. We provide evidence that PF4 and small molecule mimics of AMPs kill parasites by exclusively lysing the digestive vacuole. Furthermore, the C-terminal α-helix of PF4 and CCL20 are the active components of each chemokine, and are necessary for parasite killing. The N-terminal loop is necessary to stabilize the tertiary structure of each chemokine, providing a stable scaffold that aides in the selectivity to protect host cells. Taken together, these data suggest that antimicrobial chemokines and small molecule mimics may provide an interesting scaffold and mechanism for potential therapeutics for the fight against malaria.

Degree Type
Dissertation

Degree Name
Doctor of Philosophy (PhD)

Graduate Group
Pharmacology

First Advisor
Doron C. Greenbaum

Keywords
Antimicrobial Peptides, CCL20, Malaria, Mimics of AMPs, PF4, Structure-function

EXPLORATIONS INTO HOST DEFENSE AGAINST *PLASMODIUM FALCIPARUM*:

MECHANISTIC AND STRUCTURE-FUNCTION STUDIES OF ANTIMALARIAL CHEMOKINES

Melissa Suzanne Love

A DISSERTATION

in

Pharmacology

Presented to the Faculties of the University of Pennsylvania

in

Partial Fulfillment of the Requirements for the

Degree of Doctor of Philosophy

2014

Supervisor of Dissertation:

_____

Doron C. Greenbaum, PhD, Assistant Professor of Pharmacology

Graduate Group Chairperson:

_____

Julie Blendy, PhD, Professor of Pharmacology

Dissertation Committee:

Dennis E. Discher, PhD, Robert D. Bent Chaired Professor of Chemical and Biomolecular Engineering, Bioengineering, and Mechanical Engineering and Applied Mechanics

Mortimer Poncz, MD, Professor of Pediatrics

Vladimir Muzykantov, MD, PhD, Professor and Vice Chair of Pharmacology, Professor of Medicine

David S. Roos, PhD, E. Otis Kendall Professor of Biology

EXPLORATIONS INTO HOST DEFENSE AGAINST *PLASMODIUM FALCIPARUM:* MECHANISTIC AND STRUCTURE-FUNCTION STUDIES OF ANTIMALARIAL CHEMOKINES

I dedicate this work to the members of my family,
who have always lived up to our name.

ACKNOWLEDGMENT

As with all great things in life, this was not achieved alone. I would like to thank a number of people who have made this work possible, the first of which is my adviser, Dr. Doron Greenbaum. It is rare to find someone who is consistently excited about his work and show such scientific ingenuity, and he has always fostered a creative and challenging environment in the lab. I would also like to thank the past and present members of the Greenbaum lab, especially Drs. Mike Harbut, Melanie Millholland, Nataline Meinhardt, and Swapnil Kulkarni. They provided invaluable experimental and emotional support, and made lab a fun place to be.

I greatly appreciate the time and helpful insight from my thesis committee: Drs. Dennis Discher, Morty Poncz, Vlad Muzykantov, and David Roos. I would also like to extend my thanks to our many collaborators at various companies and institutions without whom this work would not have happened. I am also grateful for my funding through the Pharmacology Training Grant, as well as our other NIH funding sources.

I would like to thank my friends in the Pharmacology Graduate Group. The camaraderie at Penn was one of the biggest deciding factors in my choice of graduate school, and I don't think I could have made it without everyone always readily lending an ear, hand, or beer. I especially want to thank my classmates Dr. Edward Chen, and the future Drs. Hilary McCarren, Corey Cannon, and Shane Poplawski for always being great friends, and giving tough love when needed. I also would like to thank Drs. Gabriel Krigsfeld and Michael Brewer, for figuring things out a year ahead, and for all the food and fun they provided. I also need to acknowledge all of the friends I've met through people in PGG, who have long suffered many boring science conversations.

I would also like to thank my friends from home as well as the numerous housemates and friends I've made since moving to Philadelphia. I've had an extremely good streak of luck for sharing rooms, houses, and apartments with a great group of people who were always supportive and excited for me to get my PhD.

Lastly, I would like to thank my family. My parents have always encouraged me, and I don't believe I would be where I am today without their love and support. I am more thankful to them than I can express here. I also need to thank my siblings, who are the best big brother and sister anyone could ask for. To Dr. Erik Love, who blazed the PhD trail in the family and always gave me a wizened perspective when necessary. And to Katie Love, who started on this journey with me by moving to Philadelphia on a whim, and has not only been a great sister, but a best friend. I would also like to thank their partners, Dr. Helene Lee and Erin Love, whom I'm grateful to now call my family.

ABSTRACT

EXPLORATIONS INTO HOST DEFENSE AGAINST *PLASMODIUM FALCIPARUM*: MECHANISTIC AND STRUCTURE-FUNCTION STUDIES OF ANTIMALARIAL CHEMOKINES

Melissa Suzanne Love

Doron C. Greenbaum, PhD

Antimicrobial peptides (AMPs) are small (2-8kDa) peptides that have remained an important part of innate immunity over evolutionary time. AMPs vary greatly in sequence and structure, but display broad-spectrum activity against bacteria, yeast, and fungi via direct perturbation of the pathogen membrane. AMPs are typically amphipathic, and contain 2-4 positively charged amino acid residues. It has been previously shown that many chemokines also display AMP activity, both via their canonical function recruiting immune cells to the site of an infection and by direct interaction with the pathogen itself. Many antimicrobial chemokines have the same tertiary structure: an N-terminal loop responsible for receptor recognition; a three-stranded antiparallel β-sheet domain that provides a stable scaffold; and a C-terminal α-helix that folds over the β-sheet and helps to stabilize the overall structure. The α-helix of these chemokines tends to be amphipathic and retains AMP activity on its own. The work presented here focuses on two antimicrobial chemokines – platelet factor 4 (CXCL4/PF4) and macrophage inflammatory protein-3α (CCL20/MIP-3α) – and shows that they have activity against the malaria parasite. Chapter 2 details the exploration into the mechanism of action of PF4 against *P. falciparum*, and the translation of this mechanism to small molecules that mimic antimicrobial peptides. Additionally, this antimalarial activity is also present in a mouse model of malaria. Chapter 3 focuses on finding additional chemokines with

antimalarial activity, and explores the structure-function relationship between the conserved domains and how they modulate i) the antimalarial activity, and ii) provide a protective scaffold to prevent harm to host cells. We provide evidence that PF4 and small molecule mimics of AMPs kill parasites by exclusively lysing the digestive vacuole. Furthermore, the C-terminal α-helix of PF4 and CCL20 are the active components of each chemokine, and are necessary for parasite killing. The N-terminal loop is necessary to stabilize the tertiary structure of each chemokine, providing a stable scaffold that aides in the selectivity to protect host cells. Taken together, these data suggest that antimicrobial chemokines and small molecule mimics may provide an interesting scaffold and mechanism for potential therapeutics for the fight against malaria.

TABLE OF CONTENTS

LIST OF TABLES

LIST OF FIGURES

CHAPTER 1: Introduction

1.1 Malaria

Malaria continues to be a large global health burden, particularly on the African continent, where 90% of malaria deaths occur, most of which are in children under the age of 5. The WHO estimates there were 207 million new cases leading to over 600,000 deaths in 2012 [1]. Coupled with the impact of tuberculosis and HIV/AIDS, malaria has had severely negative consequences for the socio-economics of Africa [2]. Malaria is characterized by cyclic recurrent fevers, metabolic acidosis, respiratory distress, and anemia. Severe cases can lead to severe anemia, hemoglobinuria, acute kidney failure, hypoglycemia, and cerebral symptomology [3].

The disease is caused by protozoan parasites of the *Plasmodium* genus, with four species that infect humans through the bite of an *Anopheles* mosquito. The most deadly of these four species is *P. falciparum*, which is responsible for the majority of malaria fatalities. *P. falciparum,* the most recently evolved human-infecting species of malaria parasites, is the most virulent; this is likely due to its ability to vastly remodel the host red blood cell upon invasion. The most significant adaptation *P. falciparum* imparts to its host cell are exported surface proteins, which cause the infected cells to adhere to the endothelial walls, leading to obstructions of the microvasculature in organs such as the lungs, kidneys, and brain [4].

Current malaria control efforts consist of two primary methods: vector control (insecticide-treated nets and residual indoor spraying), and chemotherapy. Significant effort has been put into developing a malaria vaccine, but after multiple decades of development, the most promising vaccine (RTS,S plus adjuvant AS01) has only shown

modest short-term effectiveness [5, 6]. Drug treatment of malaria also faces a myriad of problems, as resistance to most antimalarials is spreading throughout the endemic regions, rendering many of them ineffective. Chloroquine, which kills parasites by inhibiting the detoxification of heme, was the mainstay treatment for almost 50 years due to its effectiveness and low cost. However, resistance started within 20 years of its implementation, and the spread of resistant strains has left the effectiveness of chloroquine all but nullified. The combination antimalarial sulfadoxine/pyrimethamine, which targets two enzymes in the folate metabolism pathway, and other similar drugs have produced resistant parasites at an even faster rate [7].

Modern malaria chemotherapy relies on artemisinin-based combination therapies (ACTs). The benefit of a combination of two drugs with different mechanisms of action is a lower propensity to induce resistance – a necessity in the fight to eradicate malaria. The mechanism of artemisinin is still being investigated, but the site is believed to be in the parasite digestive vacuole [8]. ACTs are currently effective in areas where there is rampant resistance to other antimalarials, though areas of artemisinin monotherapy have emerging resistance [9]. The current state of affairs in managing the malaria burden indicate that new therapeutics with novel targets are needed in the pipeline, ideally with a low propensity to cause resistance [10].

1.2 The *Plasmodium falciparum* life cycle

Plasmodium falciparum is a protozoan parasite with a complicated lifecycle involving two different host organisms. Female mosquitoes of the *Anopheles gambiae* species ingest *P. falciparum* gametocytes from an infected human when taking a blood meal. In the mosquito gut, the gametocytes transition into male and female gametes, which then fuse to form a zygote. The zygote develops into an ookinete that penetrates the gut wall to

form a sporozoite-filled oocyst. This oocyst ruptures, and the released sporozoites move to the insect's saliva, where they wait to be injected into a human upon the mosquito's next blood meal.

When sporozoites are injected into a human host's blood, they first migrate to the liver, whereupon they go through multiple stages of development over several weeks. The final hepatocytic stage, merozoites, are released en masse into the blood stream.

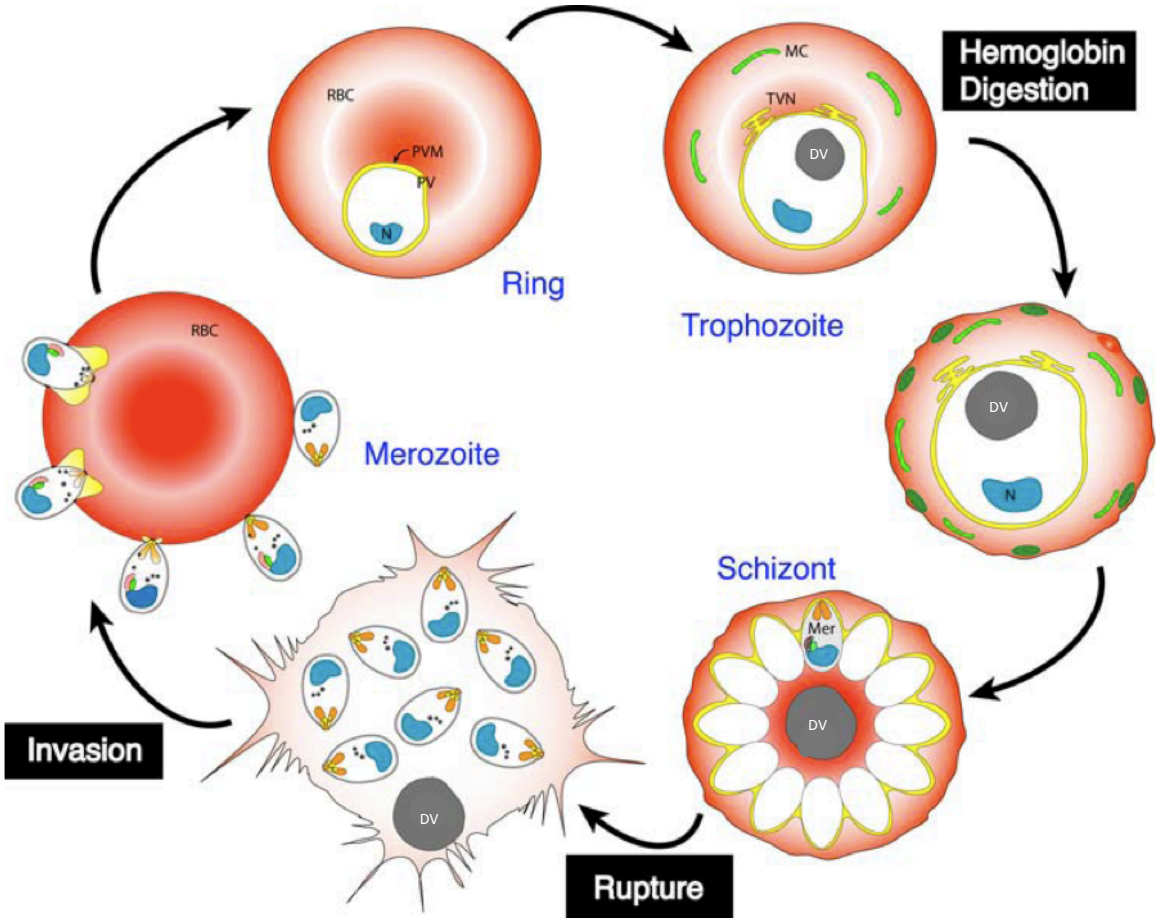

Figure 1.1: The malaria parasite erythrocytic pathway. Merozoite parasites invade the erythrocyte (RBC) and develop into ring stage parasites within the parasitophorous vacuole (PV). The peak of the parasite's metabolic activity occurs during the growing trophozoite stage, during which host cell cytoplasm is endocytosed and large-scale hemoglobin proteolysis in carried out within the digestive vacuole (DV). In addition, the parasite sets up a complex secretory pathway during this stage for delivering proteins to the PV and host cell. During the schizont stage multiple rounds of nuclear division occur, which results in the formation of daughter merozoites. At roughly 48 hrs post infection (for *P. falciparum*), the parasite ruptures from the host cell. PVM, parasitophorous vacuole membrane; N, nucleus; Mer, merozoite.

The merozoites infect red blood cells (RBCs), beginning the intraerythrocytic cycle responsible for the pathology of malaria. The newly invaded merozoites develop into the ring stage, which then become metabolically active trophozoites approximately 24 hours post RBC invasion. Trophozoites develop into schizonts, which replicate their DNA and form 16-32 daughter merozoites via cellular segmentation. At 48 hours post invasion, the merozoites rupture, or egress, out of the erythrocyte and go on to infect new cells, thus beginning the cycle again (Figure 1.1) [11].

During parasite invasion, *Plasmodium falciparum* causes invagination of the RBC membrane, forming a double membrane derived vacuolar space termed the parasitophorous vacuole (PV). The parasite spends its entire time in this vacuole while it is within the RBC, until egress, digesting ~75% of the host cell's hemoglobin [12-14]. Host cell cytoplasm begins to be taken up by the parasite in mid-ring stage via specialized structures called cytostomes. The acidified (pH 4.5-5.5) vesicles that bud off of the cytostome digest hemoglobin. As more form, they eventually coalesce into a large digestive vacuole (DV) in the early trophozoite stage. This site of hemoglobin digestion, and subsequent formation of hemozoin – an insoluble polymer of hematin – is a target for many antimalarials [15].

1.3 Antimicrobial peptides

Antimicrobial peptides (AMPs), also known as host defense peptides (HDPs), play a central role in the innate immune system [16-18]. They are comprised of two types: ribosomally and nonribosomally synthesized peptides. Over 1000 AMPs have been identified to date, and they vary greatly in length (12-80 residues), amino acid sequence, and three-dimensional structure [19]. Most AMPs are either α-helical (e.g. magainin and cecropin), disulfide-rich β-sheets (e.g. bactenecin and defensin), or an extended

structure (e.g. indolicidin) [20]. AMPs are particularly important in organisms that lack an adaptive immune response based on T-cells and antibodies, and furthermore AMPs display broad-spectrum activity against bacteria, fungi, protozoa, and even viruses, which has prompted development of AMP-based antibiotics [17].

Though they are vastly different in sequence and structure, the common features shared among AMPs include highly amphipathic topologies in which the hydrophilic and hydrophobic side chains segregate onto distinct or opposing faces or regions of the overall structure. Figure 1.2 demonstrates this facial amphipathicity in Magainin 2 [21]. Numerous studies with linear and cyclic peptides suggest that the physicochemical properties of AMPs, rather than a specific sequence or structure, are responsible for their activities. The general theory of the AMP mechanism of action is via insertion into and eventual disruption of the pathogen cytoplasmic membrane, which causes pathogen death. The amphipathic topology is believed to be essential for this membrane interaction [17].

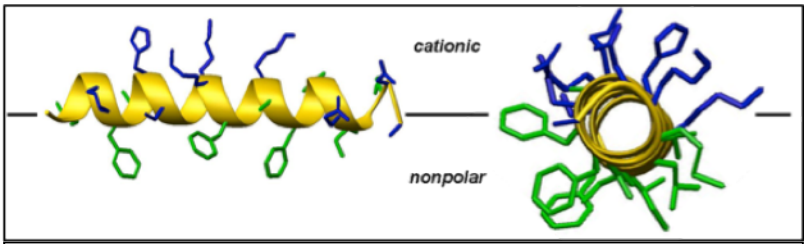

Figure 1.2: Magainin 2 shown with cationic groups in blue and nonpolar groups in green. The peptide backbone is shown as a yellow ribbon (left) side view and end view (right) highlights the spatial amphipathic distribution of cationic and nonpolar amino acid side chains that confers the mechanism of action against membranes. Adapted from Som, A., et al., *Synthetic mimics of antimicrobial peptides.* Biopolymers, 2008. **90**(2): p. 83-93. Reprinted with permission.

The basis of the cytotoxic activity and pathogen specificity of these cationic and amphipathic AMPs has been greatly studied in bacteria. The specificity for bacteria over mammalian (host) cells is likely due to the fundamental differences in membrane structure and characteristics: bacteria have a large proportion of negatively charged phospholipid head groups on the surface of their membranes, while the outer leaflet of

animal cells is composed mainly of neutral lipids [17]. The presence of cholesterol in animal cell membranes also appears to reduce AMP activity.

There have been several mechanisms proposed for this process of cell killing [22-26], which occurs within minutes after bacteria are exposed to lethal doses of peptide. It appears that AMPs bind to the membrane surface in a non-cooperative fashion, and then aggregate when a threshold concentration is achieved, leading to rapid membrane permeabilization. Membrane permeabilization is associated with a variety of other events including membrane depolarization, leakage of cellular metabolites, loss of compositional integrity due to enhanced membrane flip-flopping, and translocation of peptides to the cytoplasm where additional targets, such as RNA, DNA, and various enzymes, can be encountered [27]. It is unclear which of these events are primarily responsible for bacterial killing, and may depend on the peptide and the bacterium [28]. It is also worth noting that AMPs have remained an effective weapon against bacterial infection over evolutionary time, indicating that their mechanism of action thwarts bacterial responses that normally lead to resistance against toxic substances. This premise is supported by data showing that no appreciable resistance to AMPs occurs after multiple passages of bacteria in the presence of sublethal concentrations of the peptides [29-31].

1.4 Synthetic mimics of antimicrobial peptides

Because of difficulties with tissue distribution and toxicity of AMPs, as well as the high cost of synthesis and purification, a library of small molecule synthetic mimics of antimicrobial peptides (smAMPs) has been developed [31, 32]. These small molecules mimic the amphipathic structure of AMPs, and display good broad-spectrum activity against bacteria while having low toxicity in animals. The Greenbaum laboratory has

tested well over 1000 of these compounds, demonstrating that many of them kill *P. falciparum* in culture with IC50s in the low nanomolar range, and display a high degree of safety [33]. An added advantage of these compounds is that they are small molecules, and are thus able to be more easily chemically modified to optimize specificity, stability, and tissue distribution.

1.5 Antimicrobial chemokines

Chemokines are a superfamily of chemotactic proteins that have many roles in cellular functions, such as inflammation, development, angiogenesis, and immunity [34-36]. Almost 50 human chemokines have been identified to date, along with 20 different G-protein-coupled 7-pass transmembrane receptors (GPCRs) that control the various downstream effects [37]. Although there is some redundancy among which receptors certain chemokines can activate (or antagonize), each chemokine differs in stimuli that induce their release, cells that produce them, binding affinities, and biological potencies and efficacies [38, 39].

With regard to function, chemokines can be divided into inflammatory (inducible) chemokines or homeostatic (constitutively expressed) chemokines. The inflammatory chemokines play a key role in innate immune response by attracting a diverse array of effector leukocytes to inflammatory sites: neutrophils, monocytes/macrophages, dendritic cells, and natural killer cells. Homeostatic chemokines have important roles in migration of antigen-presenting cells, lymphocytes into the lymph node, and effector T cells reaching tissues that contain their cognate antigen, all of which are crucial in the adaptive immune response [39].

Chemokines are small (8-12 kDa), and have a remarkably similar structure consisting of an N-terminal loop necessary for receptor activation, a central domain

comprised of 3 antiparallel β-strands that provide a stable scaffold, and a C-terminal α-helix that folds across the β-sheet to stabilize the overall structure (Figure 1.3) [40]. Chemokines have four conserved cysteines (two in the N-terminal loop, and 2 in the β-sheet) that form two essential disulfide bonds (Cys1-Cys3 and Cys2-Cys4). Chemokines are traditionally divided into four groups based on the positioning of the first two cysteines: C, CC, CXC, and CX_3C, where X is any non-cysteine amino acid [36, 37, 41].

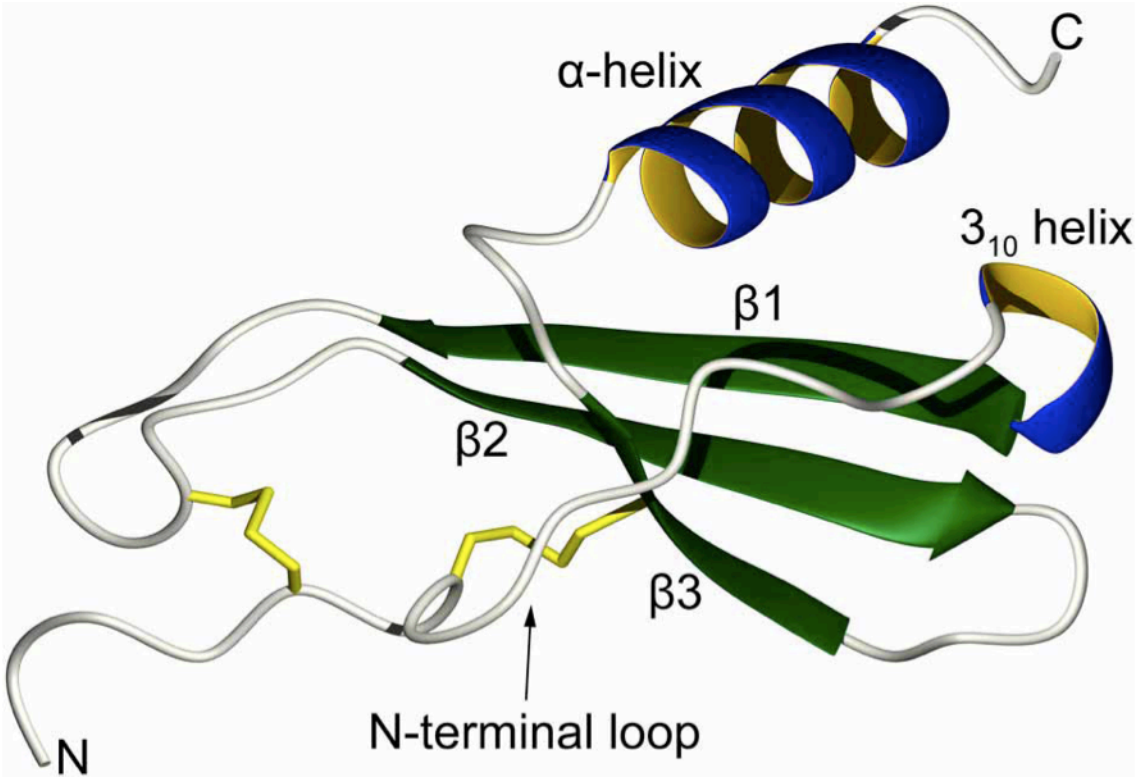

Figure 1.3: Topology of a typical chemokine. The N-terminal loop, which is responsible for receptor recognition, is restrained by two disulfide bonds (in yellow). This is followed by a short turn of a 3_{10} helix that leads to a three-stranded antiparallel β-sheet. The C-terminal α-helix folds over the β-sheet and helps to stabilize the overall tertiary structure. Reprinted from Nguyen, L.T. and H.J. Vogel, *Structural perspectives on antimicrobial chemokines.* Front Immunol, 2012. **3**: p. 384.

In addition to the roles that chemokines play in immunity through cell trafficking, many chemokines also have direct microbicidal activity [40, 42-46]. These antimicrobial chemokines are expressed directly in the bloodstream, and therefore necessarily have

low host toxicity. This is in contrast to classical AMPs, which are typically expressed in phagocytes or on mucosa. Because chemokines have a highly conserved tertiary structure, examining the key structure-function relationships in antimicrobial chemokines may deconvolute their biological role in host defense, and may provide insights into new therapeutics against drug-resistant pathogens with minimal host toxicity.

1.6 Host defense activity against malaria

The pathogenesis of malaria is modulated both positively and negatively by many human cell types in blood including monocytes, neutrophils and platelets [47-52]. While platelets have long been known to interact cooperatively with erythrocytes in thrombogenesis, both generally and in the specific case of sickle cell disease [53], only recently have platelets been shown to bind infected erythrocytes and kill intracellular malaria parasites [54]. Previous studies have suggested that thrombocytopenia is a poor prognostic marker in malaria [55] and is significantly associated with cerebral malaria [56, 57].

Mature platelet factor 4 (PF4), or CXCL4, is a 70 amino acid protein. It exists as a homotetramer in solution, and like other antimicrobial chemokines, consists of an N-terminal cytokine domain, a central domain responsible for tetramerization, and a C-terminal domain that binds heparin and also can act as an AMP [46]. PF4 was the first characterized chemokine [58], though unlike other chemokines, PF4 does not have strong chemotactic properties and does not interact with common chemokine receptors except human CXCR3B, an alternatively-spliced CXCR3 [59]. PF4 is a cationic molecule, especially in its tetrameric state, with high affinity for heparin and other large, negatively-charged molecules [60]. Upon platelet activation, PF4 is released from platelet alpha-granules in high local concentrations, up to 100 μM proximal to a clot [61].

PF4 has been implicated in both inflammation [62, 63] and thrombosis [64]. PF4 released from activated platelets forms complexes with endogenous glycosaminoglycans on the surface of platelets [65] and monocytes [65] and likely on other hematopoietic and vascular cells. Mice that are knockout for the *cxcl4* gene [64] (deficient in PF4 (PF4 KO)) or overexpress human PF4 ($hPF4^{+}$) have proven to be important tools in understanding *in vivo* PF4 biology during thrombosis and megakaryopoiesis [66, 67].

Conversely, Srivastava *et al.* have recently shown that PF4 may have detrimental effects in the pathogenesis of cerebral malaria [62]. A knockout PF4 mouse model infected with *P. berghei* ANKA had improved survival compared to their wild-type littermates. Further, a CXCR3 knockout mouse had 100% survival 10 days after infection, suggesting that the effects of PF4 on the cerebral symptomology was modulated through its chemokine domain. It is unclear whether these observations are clinically relevant to cerebral malaria in humans, given that this murine model is complicated by severe inflammation in the brain and CNS, unlike human cerebral malaria in which little, if any, inflammation is seen [68-70]. As human cerebral malaria is a consequence of intravascular sequestration of infected erythrocytes in the brain vessels and capillaries, rather than increased inflammation, it is unlikely that human PF4 mediates increased inflammation during this disease process. Murine models of cerebral malaria are further complicated by the marked accumulation of leukocytes and platelets in the brain venules and capillaries, a phenomenon not seen in human pathology [70].

Human macrophage-inflammatory protein-3α (MIP-3α), or CCL20 is a 70 amino acid, 8-kDa protein. It has been linked to numerous diseases, such as cancer, rheumatoid arthritis, and diseased periodontal issues [71-73]. CCL20 exclusively binds the CCR6 receptor, and interestingly, is the only chemokine that will bind it [74].

Surprisingly, the human β-defensins, β-defensin-1 and β-defensin-2, can also bind and activate CCR6 [75]. CCL20 and the human β-defensins have no obvious amino acid sequence homology, but there are many structural similarities between them that may explain the overlap between their chemotactic and microbicidal activities [76]. CCL20 and its amphipathic C-terminus have both been shown to have antimicrobial activity against *E. coli* and *S. aureus* [36, 76, 77].

In this work, I show that the CXC chemokine CXCL4/PF4 is active against *P. falciparum* at an IC50 of 5-10 μM (Chapters 2 and 3). Chapter 2 focuses on mechanistic studies of the direct microbicidal activity of PF4 against the malaria parasite. Chapter 3 focuses on a closer investigation of the structure-function relationship of the various domains of antimicrobial chemokines. In addition to platelet factor 4 (PF4), I also show that the CC chemokine CCL20/MIP-3α is potent against *P. falciparum* (IC50 of ~5 μM), and that the hemolytic potential, or host toxicity, is modulated by the tertiary structure.

CHAPTER 2: Platelet Factor 4 Activity Against *Plasmodium falciparum* and its Translation to Nonpeptidic Mimics as a New Class of Antimalarials*

2.1 Introduction

Malaria is a devastating disease and continues to be a global health burden, causing significant morbidity and mortality [78]. The pathogenesis of malaria is modulated both positively and negatively by many human cell types in blood including monocytes, neutrophils and platelets [47-52]. Recently platelets have been shown to bind infected erythrocytes and kill intracellular malaria parasites [54]. Previous studies have suggested that thrombocytopenia is a poor prognostic marker in malaria [55] and is associated with cerebral malaria [56, 57]. We therefore pursued the hypothesis that host cells found in the bloodstream that are known to secrete proteins with host defense peptide (HDP) activity [43, 54] could contribute to the host's control of malaria parasite proliferation in the blood stage.

HDPs play a central role in the innate immune system [16-18, 79]. HDPs display broad-spectrum action against bacteria, fungi, protozoa, and viruses, which has promoted their use as new leads for developing antibiotics [79]. A unifying characteristic of HDPs is an amphipathic topology in which the cationic and hydrophobic side chains segregate onto opposing faces of the overall folded molecule. It is thought that the

*The text of this chapter has been published (Love *et al. Platelet Factor 4 Activity against P. falciparum and Its Translation to Nonpeptidic Mimics as Antimalarials*. Cell Host Microbe, 2012. **12**(6): p. 815-23.) It is printed here with permission.

physicochemical properties of HDPs, rather than any specific sequence or structure, are responsible for their activities. HDPs are thought to bind the membrane surface in a non-cooperative fashion and then aggregate once a threshold concentration is reached causing membrane permeabilization [22-24, 26, 80]. It is believed that amphipathic topology is essential for insertion into and disruption of membranes leading to pathogen death. From this background, we hypothesized that naturally occurring bloodstream HDPs especially from platelets might have the ability to kill *P. falciparum* early in erythrocytic infection.

2.2 Results

Identification of human platelet factor 4 (hPF4) as an antiparasitic HDP that kills P. falciparum via lysis of the parasite DV

A screen of HDPs found in the bloodstream, secreted by a variety of cells including platelets, neutrophils, or lymphocytes, was performed to assess their anti-parasitic activity (Figure 2.1). This screen revealed that several proteins killed *P. falciparum in vitro* without affecting the host erythrocyte. Most notably, hPF4 showed high potency against *P. falciparum* with an IC50 of 4.2 μM and no significant hemolysis. Considering local concentrations of hPF4 have been reported to reach at least 280 μM surrounding activated platelets [81], the antiparasitic IC50 of hPF4 has *in vivo* relevance. Platelets harvested from wild-type (WT), mouse PF4 (mPF4) knock-out (mPF4 KO), or overexpressing hPF4 ($hPF4^+$) mice were tested against *P. falciparum* in culture with recombinant mPF4 and hPF4 as controls (Figure 2.2). Because there is no evidence to suggest that mouse platelets bind to or are activated by human infected erythrocytes, platelets were pre-activated with AYP prior to their addition to parasite cultures. Pre-activated WT and $hPF4^+$ mouse platelets were able to kill *P. falciparum* in culture, while

Figure 2.1

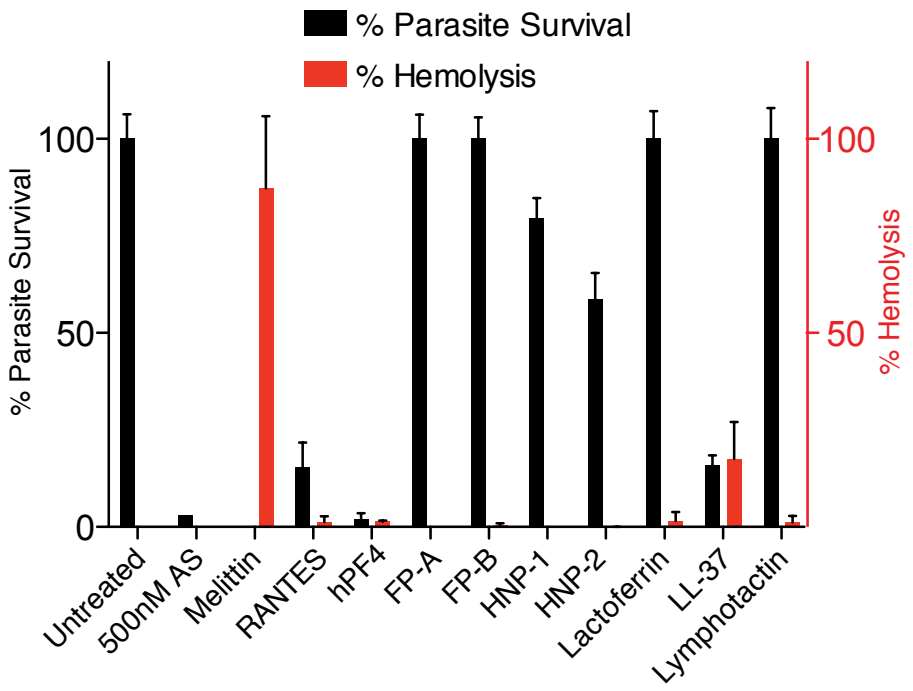

Figure 2.1: Screen of human HDPs found in blood for *P. falciparum* killing and hemolysis. All HDPs were tested at 15 μM. Regulated upon Activation, Normal T-cell Expressed, and Secreted (RANTES); hPF4; Fibrinopeptide-A (FP-A); Fibrinopeptide-B (FP-B); Human Neutrophil Peptides 1 and 2 (HNP-1; HNP-2); Cathelicidin (LL-37). Parasite survival was normalized to an untreated control. Artesunate (500 nM) and the HDP melittin (15 μM) were used as positive controls for parasite death without and with hemolysis, respectively. Data shown are means ± SEM.

Figure 2.2

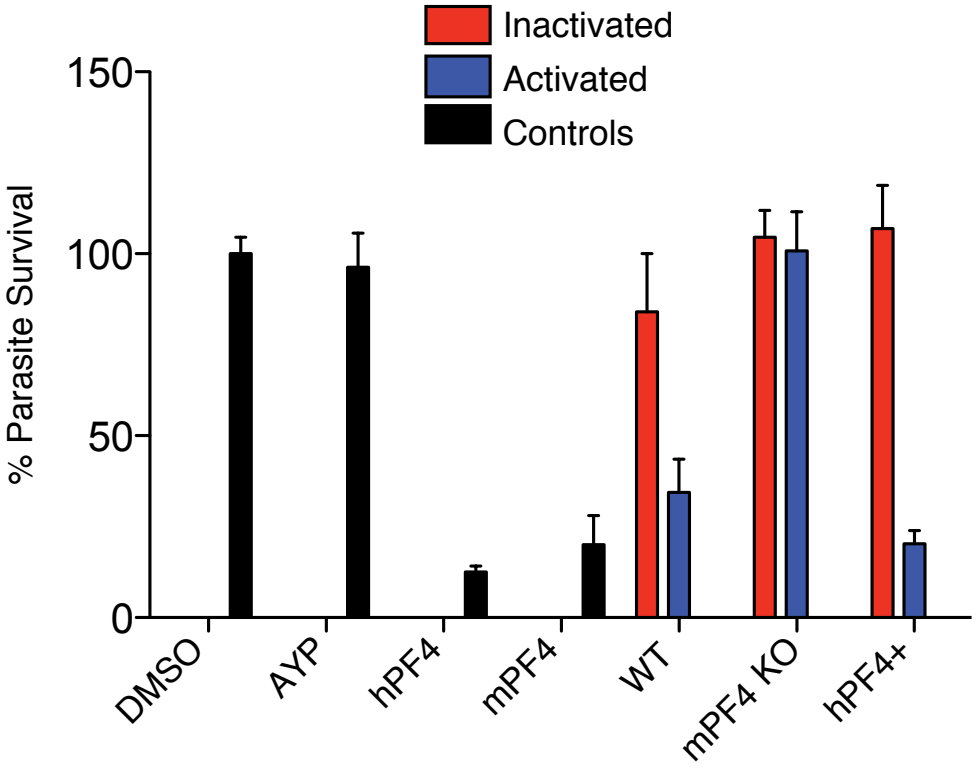

Figure 2.2: PF4-containing platelets kill *P. falciparum in vitro*. Parasite-infected erythrocytes were incubated for 24 hours with 2.5 x 10^8 platelets from either littermate WT, PF4 KO, or hPF4+ mice in the presence or absence of 5 μM AYP to induce platelet activation. Parasite survival assayed by flow cytometry using SYTOX green as a measurement of DNA content and normalized to an untreated control. Recombinant hPF4 and mPF4 (10 μM) were used as positive controls. Data shown are means ± SEM.

littermate PF4 KO platelets showed no killing capacity. Thus it appears that PF4 is a major antimalarial component of activated platelets.

As membrane perturbation is an established mechanism of action for HDPs [25, 79, 82-84], we examined the integrity of potential target parasite membranes upon hPF4 treatment. Since hPF4 had little hemolytic capability we reasoned the erythrocyte integrity was not significantly compromised. Parasite plasma membrane (PPM) potential assays showed no discernible loss of potential following 4 hours of hPF4 exposure (Figure 2.3). Next the integrity of established intracellular parasite organelle targets, including the mitochondria and lysosome-like digestive vacuole (DV) was assessed post hPF4 treatment. Analysis of membrane potential revealed no perturbation of the mitochondria, however a significant loss of proton potential was observed in the DV within minutes of treatment (Figure 2.3). To further investigate this novel perturbation to the DV, transgenic parasites expressing green fluorescent protein (GFP)-tagged plasmepsin-II in the DV [85] were treated with hPF4 and followed by fluorescence microscopy over a 10-minute time course. Parasites were assayed for both hPF4 localization using immunofluorescence analysis (IFA) and direct GFP signal (integrity of the DV; Figure 2.4). Within 1 minute of hPF4 incubation, hPF4 staining could be detected in the cytoplasm of only infected erythrocytes. hPF4 continued to accumulate over the next several minutes, wherein it entered the parasite cytoplasm and colocalized with the parasite DV. Next, severe perturbation of the DV allowed GFP to diffuse throughout the parasite cytoplasm (Figures 2.4,8,9). Western blot analysis of hPF4 confirmed the IFA results showing entry into erythrocytes by 1 minute followed by accumulation into the parasite within 5 minutes (Figure 2.5). To assess the loss of DV integrity on the population level, we utilized quantitative flow cytometry to first capture images of individual parasite-infected cells, then quantitatively differentiate based on DV

Figure 2.3

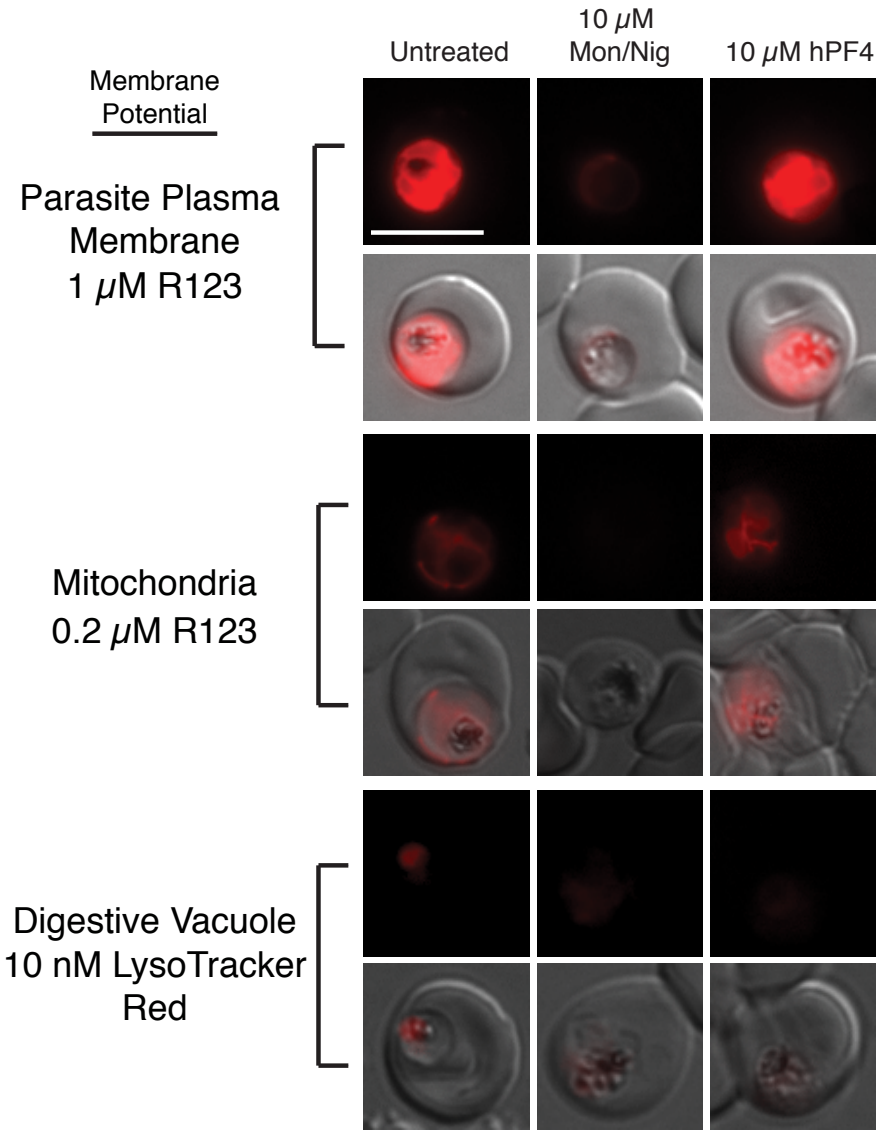

Figure 2.3: hPF4 causes loss of membrane potential of the DV. Parasite-infected erythrocytes pre-incubated with rhodamine 123 (1 μM for parasite plasma membrane potential; 0.2 μM for mitochondrial potential) or 10 nM LysoTracker Red and then treated over a 4-hr time course with 10 μM hPF4 or a 10 μM mixture of ionophores Monensin and Nigericin (Mon/Nig). Length bar is 10 μm in each figure.

Figure 2.4

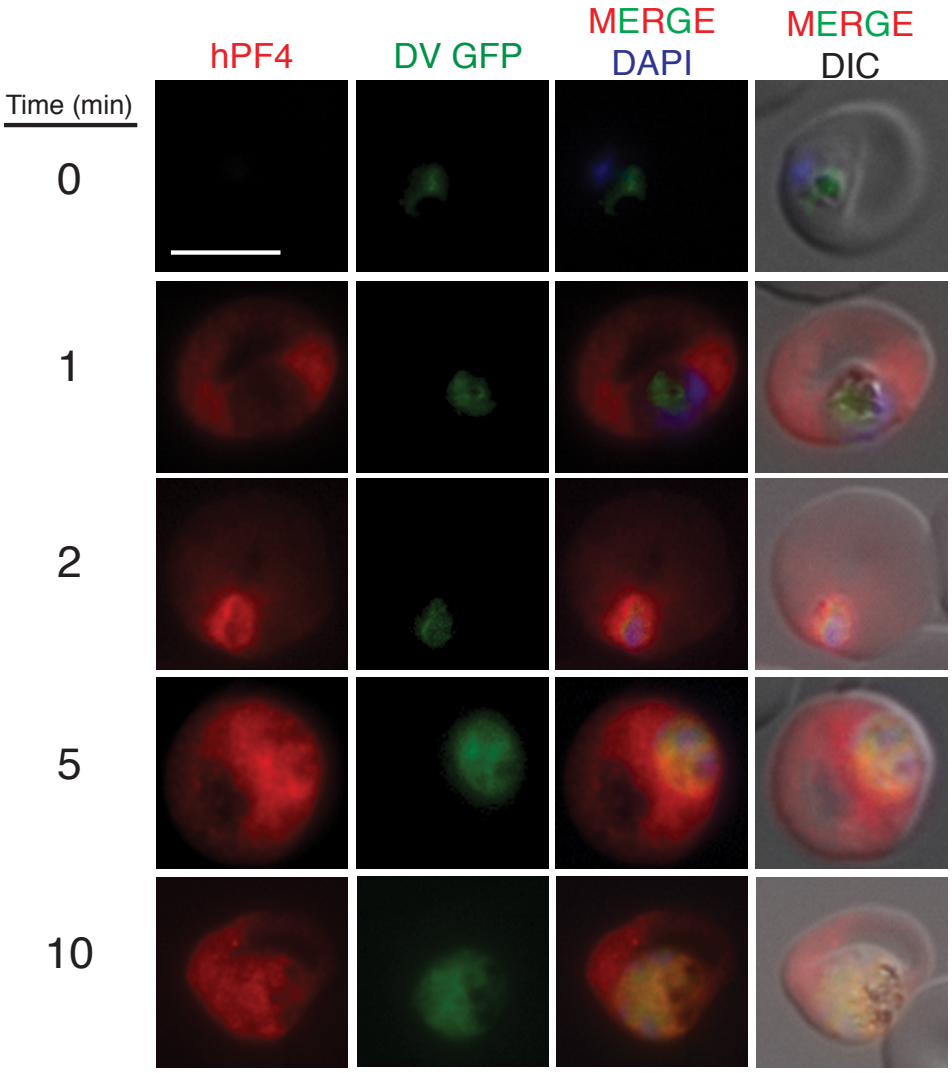

Figure 2.4: hPF4 causes lysis of the DV. hPF4 accumulates in the infected erythrocyte cytoplasm prior to lysis of the DV by immunofluorescence. Erythrocytes infected with parasites expressing plasmepsin-II-GFP (PM-II-GFP) were treated with 1 μM hPF4 over a 10 min time course. Within 1 minute of PF4 incubation, PF4 staining is seen in the cytoplasm of infected erythrocytes until entering and inducing lysis of the parasite DV, as shown by GFP signal diffusion through the entire parasite cytoplasm. (Green: PM-II-GFP [DV]; red: hPF4 IFA; blue: parasite nuclei.)

Figure 2.5

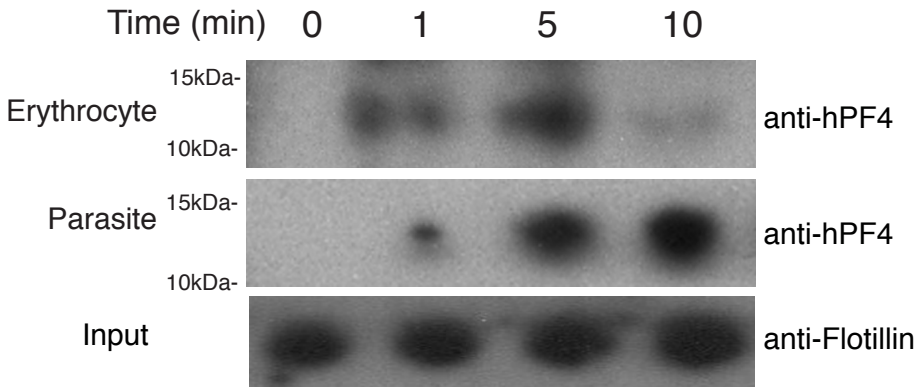

Figure 2.5: Western blot analysis of hPF4 accumulation in infected erythrocytes. Western blot analysis of erythrocyte fractions or parasite lysates shows early accumulation of hPF4 in infected erythrocytes, followed by persistence in the parasite.

Figure 2.6

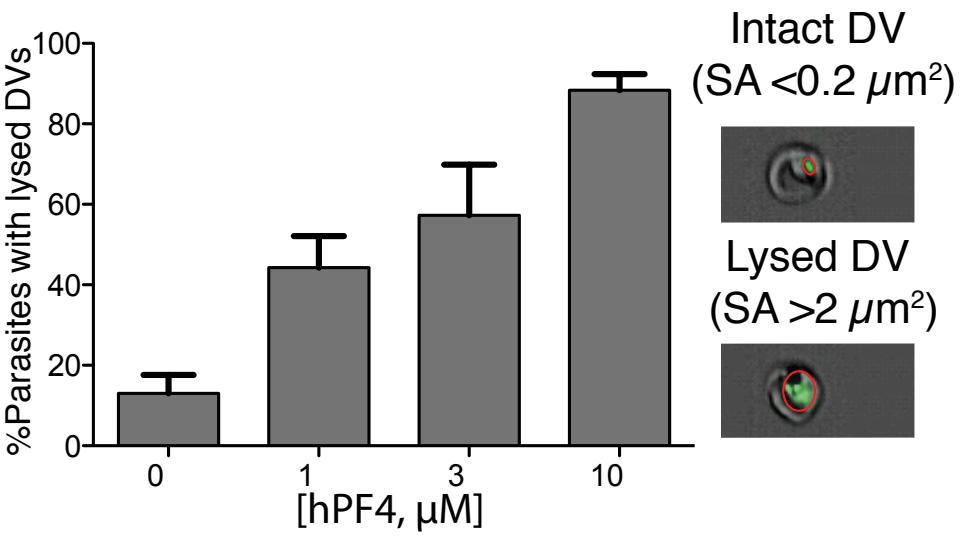

Figure 2.6: Quantitative analysis of DV lysis by hPF4. ImageStream flow cytometry shows a dose-dependent increase in PM-II-GFP parasites with a fluorescence surface area of >2 μm^2, an indication of DV lysis, upon treatment with hPF4. Intact DVs have fluorescent surface areas <0.2 μm^2. Data shown are means ± SEM. (*p<0.05, **p<0.01)

Figure 2.7

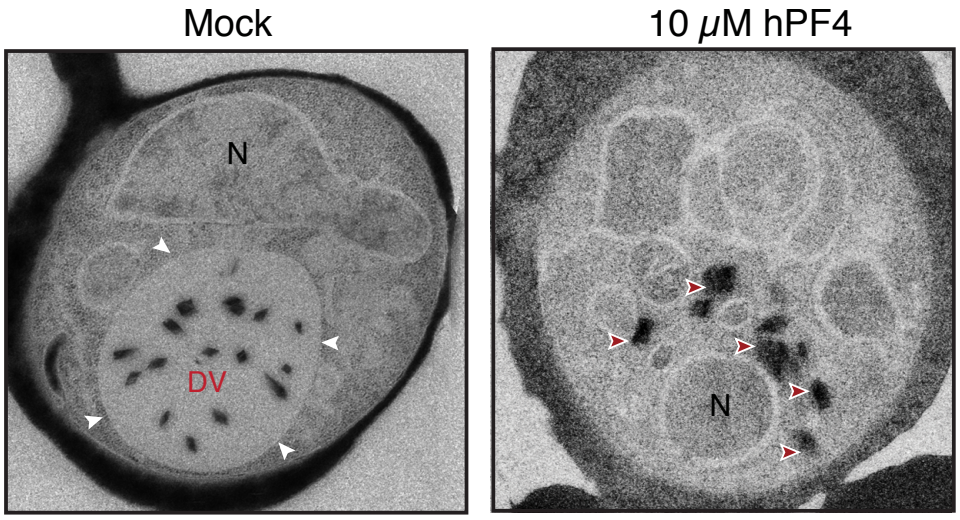

Figure 2.7: Transmission Electron Microscopy images of DV lysis by hPF4. TEM images reveal dissolution of the DV membrane upon treatment with 10 μM PF4, as well as dispersal of hemozoin fragments throughout the cytoplasm (red arrowheads). Mock-treated controls showed complete integrity of the DV membrane (white arrowheads), encapsulating all hemozoin crystals. (N: parasite nucleus).

Figure 2.8

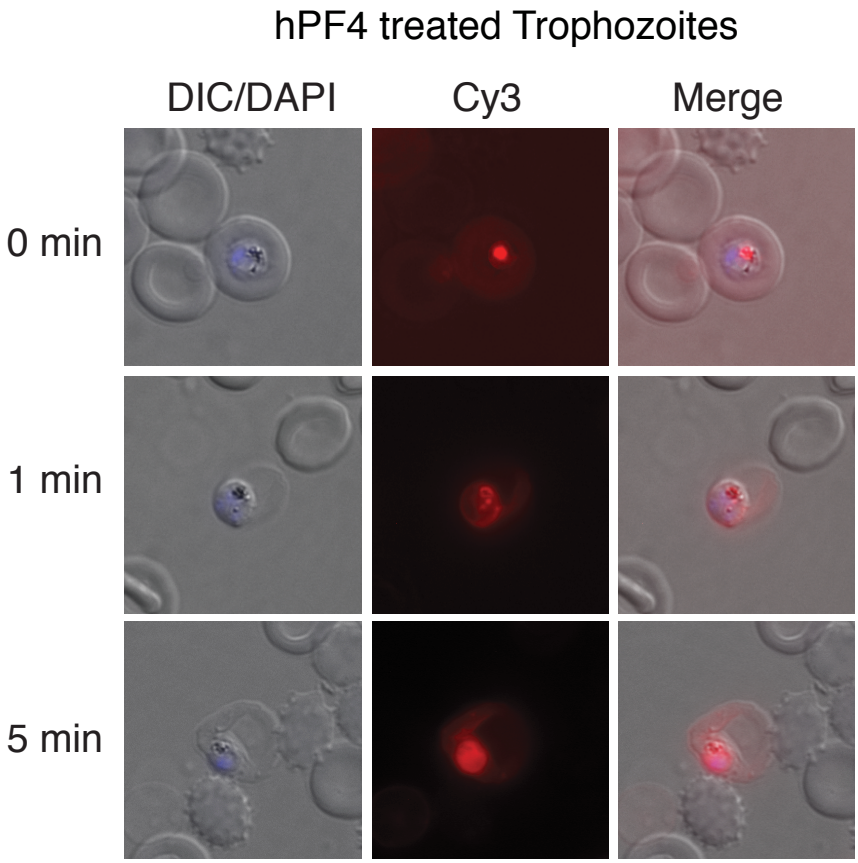

Figure 2.8: Texas Red Dextran imaging of trophozoite DV lysis by hPF4. Trophozoite-infected Texas Red Dextran-loaded erythrocytes show dispersal of fluorescence into the parasite cytoplasm (indicating DV lysis) following 5 min of treatment with hPF4.

Figure 2.9

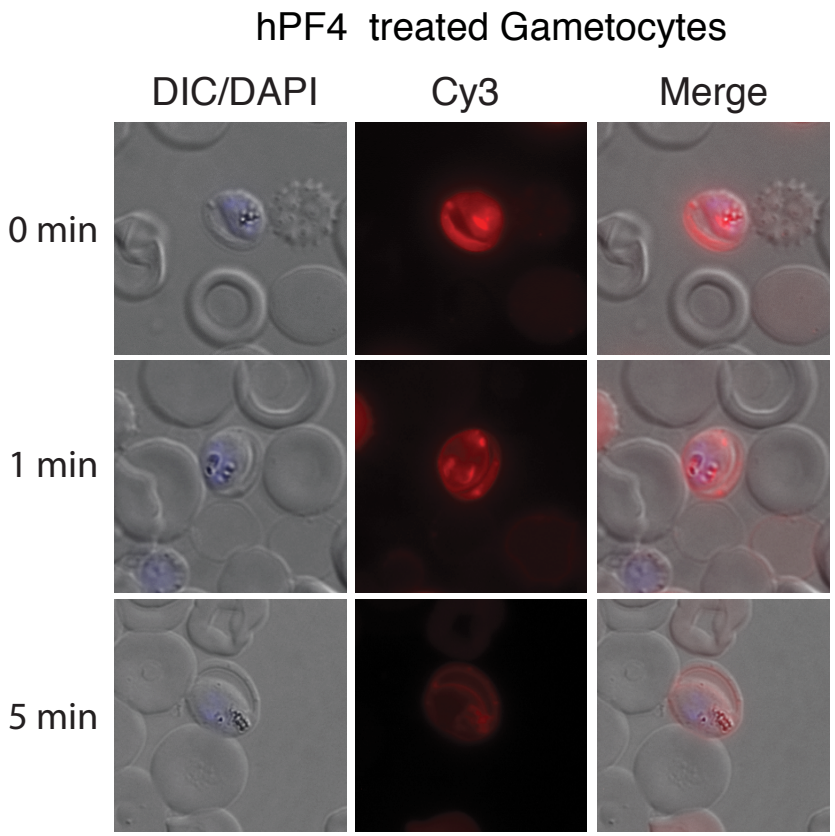

Figure 2.9: Texas Red Dextran imaging of gametocyte DV lysis by hPF4. Gametocyte-infected Texas Red Dextran-loaded cells show dispersal of fluorescence into the parasite cytoplasm (indicating DV lysis) upon 5 min of treatment with hPF4.

fluorescent surface area (SA) intact DVs (<0.2 μm^2) from lysed DVs (>2 μm^2; Figure 2.6, Figure 2.10). hPF4 treatment caused dose-dependent DV lysis, with nearly complete DV lysis on a population level upon exposure to 10 μM hPF4. The loss of DV integrity was confirmed at high resolution using transmission electron microscopy imaging to compare untreated and hPF4-treated parasites, revealing the complete loss of DV integrity in the hPF4-treated parasites versus mock-treated parasites with a clearly delineated DV membrane (white arrowheads; Figure 2.7). In addition to the loss of DV organellar structure, hemozoin crystals were seen dispersed throughout the parasite (red arrowheads). Thus, DV lysis appears to be the primary and novel mechanism of hPF4 action against parasites. Parasite stages that rely heavily on DV function were especially susceptible to hPF4 treatment (Figure 2.11).

The HDP-like C-terminus of hPF4 has antiparasitic activity

hPF4 is comprised of three domains: an N-terminal chemokine domain, a central domain responsible for homotetramerization, and a C-terminal amphipathic helical region with HDP activity [46]. To test the hypothesis that the HDP-like C-terminus has activity against the malaria parasite, the 12-residue domain (C12, Figure 2.12A) was synthesized and tested against *P. falciparum in vitro* (Figure 2.12B). C12 acted similarly to the parental protein causing loss of parasite DV integrity, was not hemolytic, and did not perturb the PPM or mitochondrial membrane potential after a 4-hour treatment (Figure 2.13). Treatment of PM-II-GFP parasites with 100 μM C12 led to leakage of GFP into the parasite cytoplasm following 30 minutes of exposure, indicating loss of DV integrity (Figures 2.14,15). In order to ascertain localization of C12 upon treatment, Figure 2.16 shows that a fluorescently-tagged C12 peptide, C12-TAMRA, entered only infected erythrocytes within 15 minutes of treatment, with accumulation in the parasite

Figure 2.10

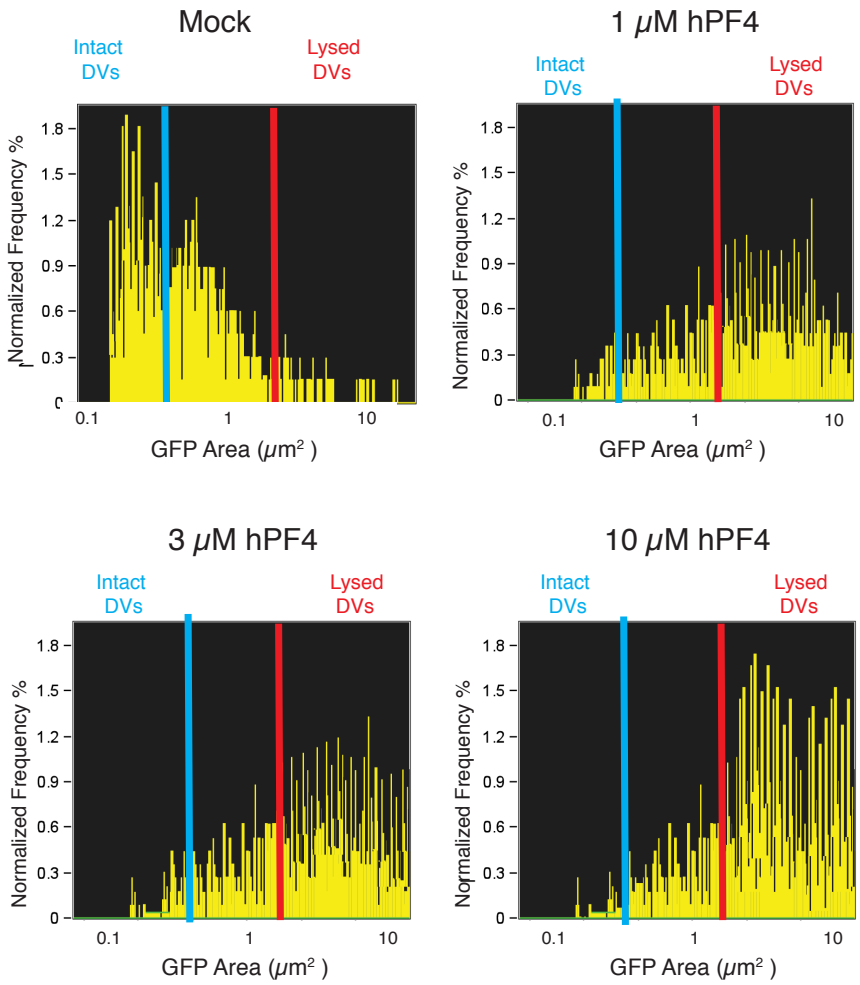

Figure 2.10: Representative flow plots from mock-treated parasites expressing PM-II-GFP or parasites treated with 1 μM hPF4, 3 μM hPF4, or 10 μM hPF4. Synchronous PM-II-GFP parasites were used to examine DV integrity upon treatment. DV lysis is defined as area of GFP signal greater than 2 μm^2 (red line is minimum area), as GFP signal would disperse into the entire parasite cytoplasm. Intact DVs show compact area (less than 0.2 μm^2; blue line is maximum area).

Figure 2.11

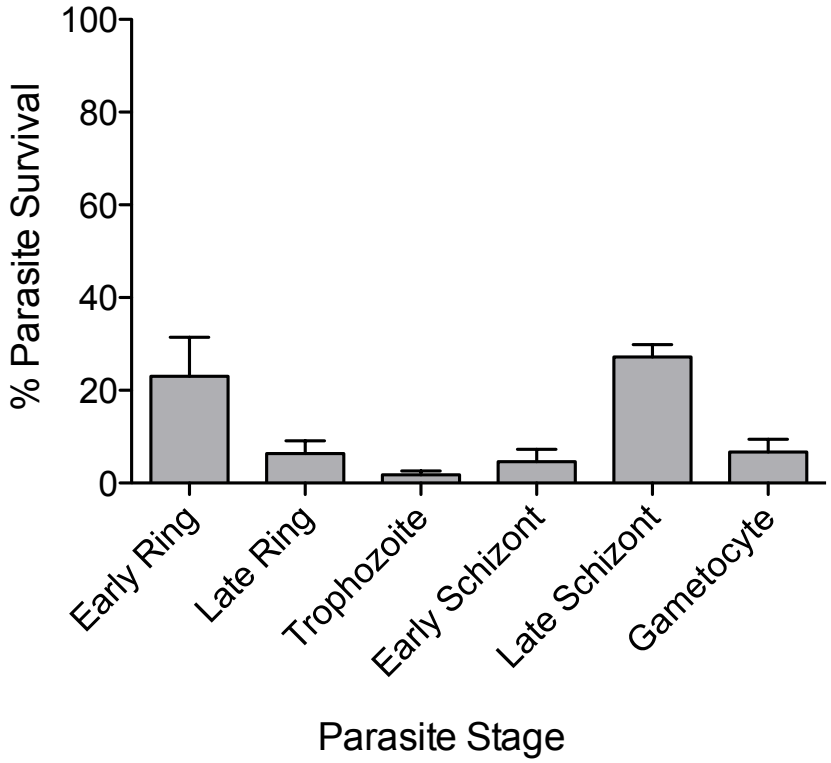

Figure 2.11: Parasite stages that rely on DV function are more susceptible to hPF4 killing. Stage-specific killing of PF4 shows increased efficacy during the stages that rely heavily on DV function (late ring, trophozoite, schizont, gametocyte). Shown are means ± SEM; n=3.

Figure 2.12

A

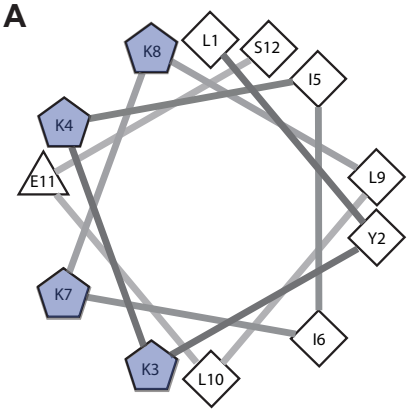

B

Peptide	Sequence	# of K→A	IC_{50} (μM)
PF4	–	–	4.2 ± 0.6
C12	LY^{3}K^{4}KII^{7}K^{8}KLLES	0	73.3 ± 8.1
C12 A3	LY**A**KIIKKLLES	1	84.0 ± 10.8
C12 A3,4	LY**AA**IIKKLLES	2	92.1 ± 16.3
C12 A3,4,7	LY**AA**II**A**KLLES	3	>200
C12 A3,4,7,8	LY**AA**II**AA**LLES	4	Not tested

C

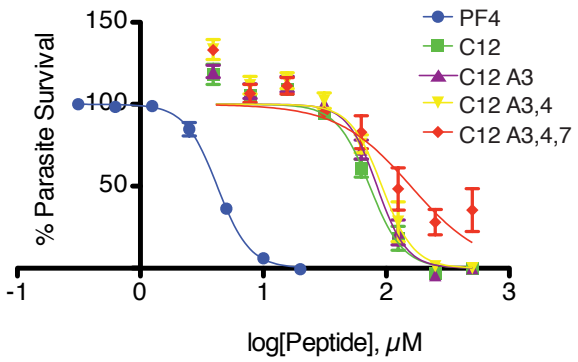

Figure 2.12: The C-terminal amphipathic helical domain of PF4 retains the HDP activity against *P. falciparum.* (**A**) Projected helical wheel of C12 with each amino acid numbered. (**B**) Peptide derivatives of the PF4 C-terminal domain with lysine residues mutated to alanines to determine the necessity of positive charges for C12 antimalarial activity. Mutated residues are denoted by "A" followed by the residue number. IC50s are means ± SEM (n=3). (**C**) Dose-response curves for PF4, C12, and the series of C12 lysine mutants. Data shown are means ± SEM.

Figure 2.13

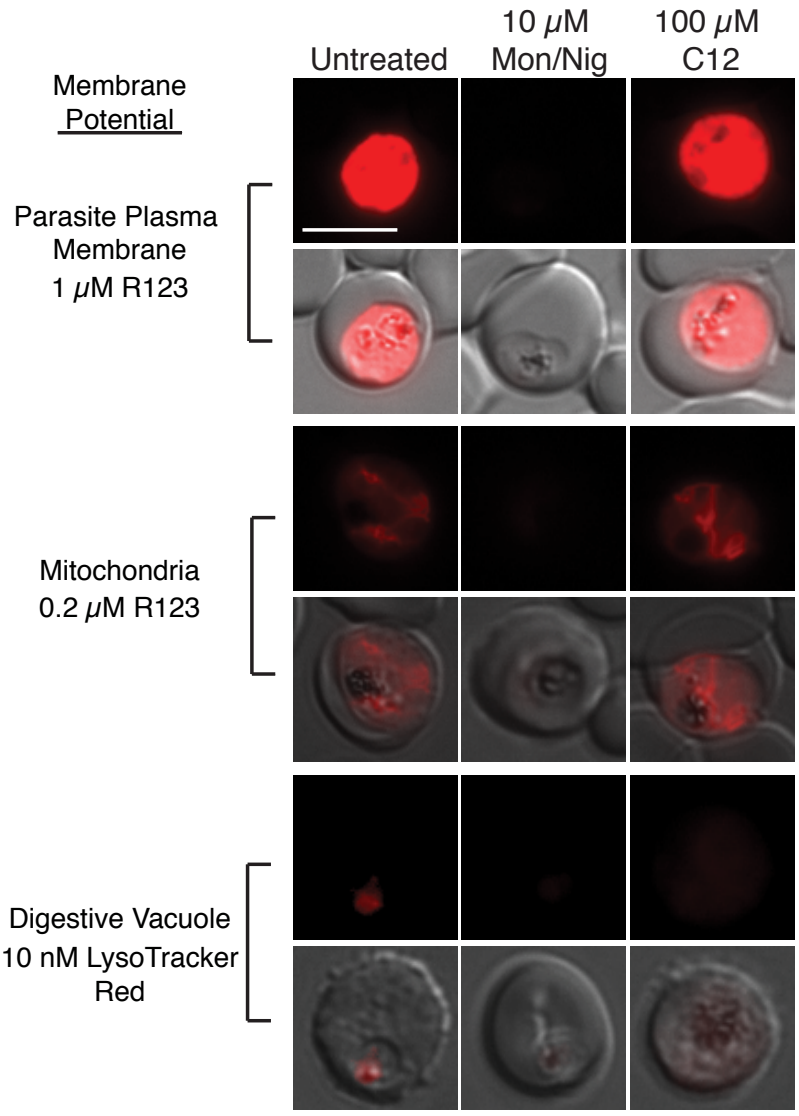

Figure 2.13: C12 causes loss of membrane potential of the DV. Parasite plasma membrane, mitochondrial, and DV potential were examined upon C12 treatment. Parasite-infected erythrocytes pre-incubated with rhodamine 123 (1 μM for parasite plasma membrane potential; 0.2 μM for mitochondrial potential) or 10 nM LysoTracker Red and then treated over a 4-hr time course with 100 μM C12 or a 10 μM mixture of ionophores Monensin and Nigericin (Mon/Nig). Length bar is 10 μm in each figure.

Figure 2.14

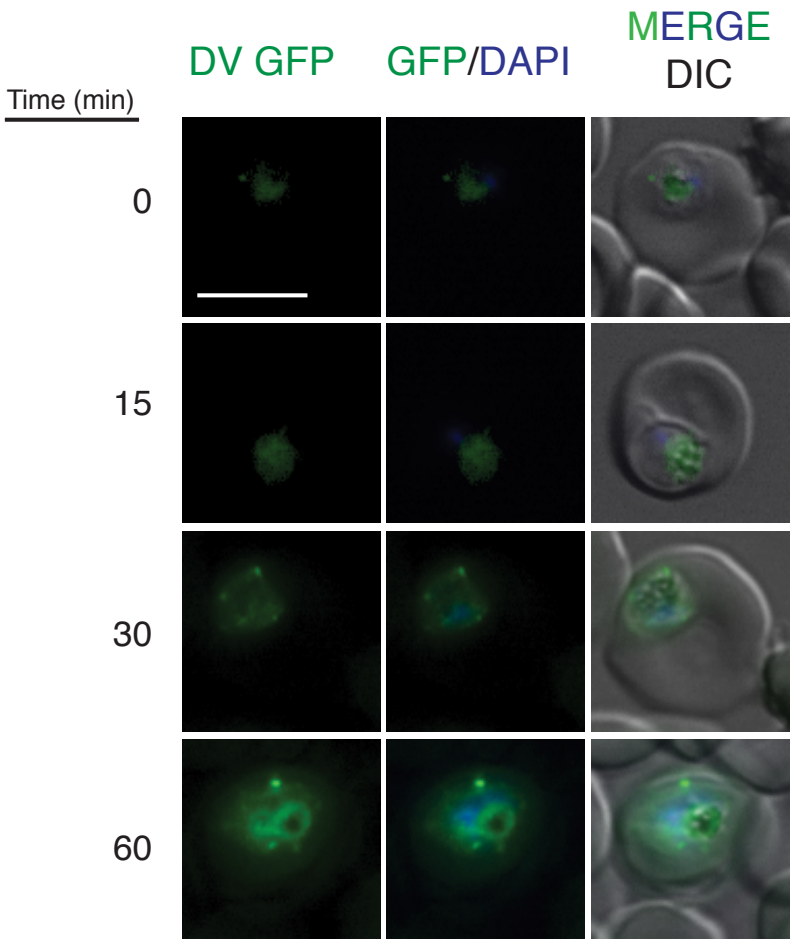

Figure 2.14: C12 causes DV lysis. C12-treated PM-II-GFP parasites showed loss of DV integrity. Green: PM-II-GFP (DV); blue: parasite nuclei.

Figure 2.15

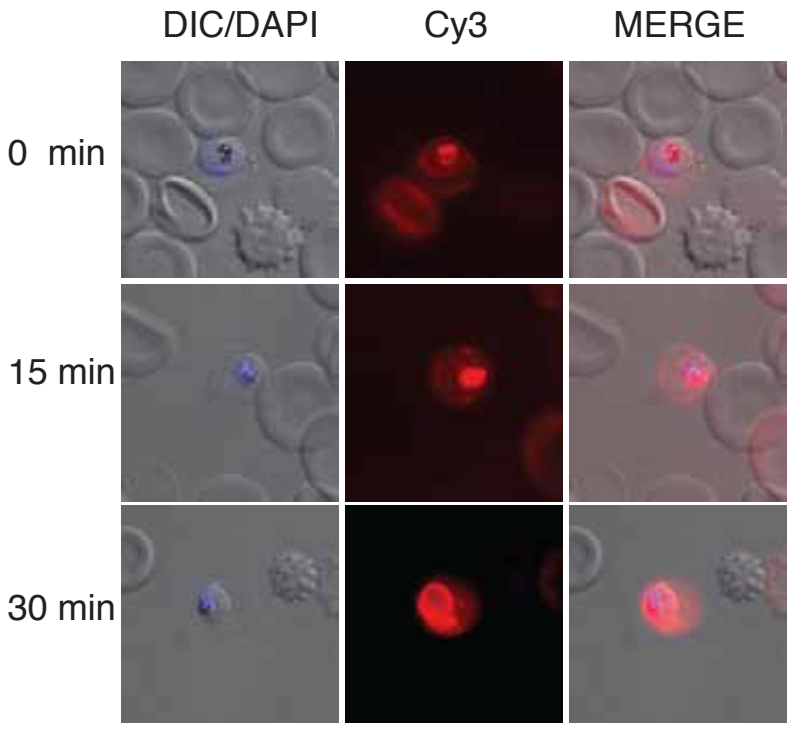

Figure 2.15: Texas Red Dextran imaging of trophozoite DV lysis by C12. Trophozoite-infected Texas Red Dextran-loaded erythrocytes show dispersal of fluorescence into the parasite cytoplasm (indicating DV lysis) following 30 min of treatment with 100 μM C12.

Figure 2.16

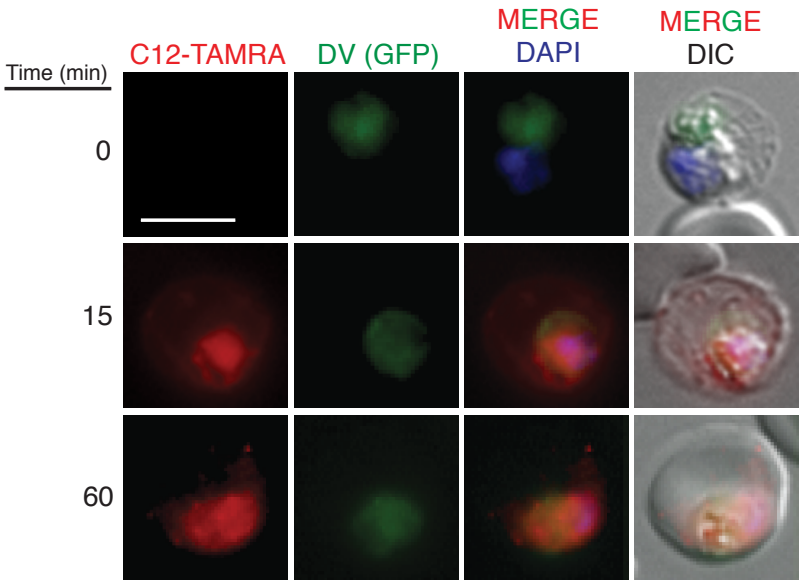

Figure 2.16: Imaging of fluorescent-tagged C12. C12-TAMRA treatment of PM-II-GFP parasites shows accumulation within infected erythrocytes and parasite bodies within 15 minutes of exposure, followed by DV lysis within 60 minutes of treatment. Red: C12-TAMRA; green: PM-II-GFP (DV); blue: parasite nuclei.

body and the erythrocyte cytoplasm while the DV remained intact. Within 60 minutes of treatment, GFP signal permeated throughout the parasite body, indicating lysis of the DV. As the cationic amphipathicity of HDPs is thought to be key to their mechanism of action, we reasoned that lowering the number of charges on C12 would adversely affect its activity. Starting at the N-terminus, mutation of the first or the first two of the four lysines caused only a minor decrease in activity (IC50 values of 84.0 μM and 92.1 μM, respectively), while mutation of the first three lysines ablated the antiparasitic activity of C12 (IC50 of > 200 μM; Figure 2.12B,C). The quadruple mutant was not tested due to its insolubility. These data suggest that, like most HDPs, activity of the amphipathic C12 peptide is dependent on a minimal cationic charge density.

Synthetic small molecule HDP mimics are potent against P. falciparum and have a mechanism similar to hPF4

Given their broad activity, HDPs appear to be ideal therapeutic agents, though significant pharmaceutical issues have severely hampered clinical progress, including poor tissue distribution, systemic toxicity, and difficulty and expense of manufacturing [86]. In addition, PF4 has been reported to worsen experimental cerebral pathology in mice, presumably mediated through the chemokine domain [62]. Thus, we reasoned that synthetic small molecules capable of adopting amphipathic secondary structures analogous to a HDP could potentially reproduce the potent, selective antiparasitic activity of PF4, while improving tissue distribution and decreasing complications arising from chemokine signaling. In addition, these small molecule HDP mimics (smHDPs) are significantly less expensive to produce (an example scaffold is shown in Figure 2.17). In order to exploit the DV lysis mechanism of PF4 in a drug discovery effort, a library of ~1000 nonpeptidic smHDPs [27, 87] was tested against *P. falciparum*. 132 compounds

Figure 2.17

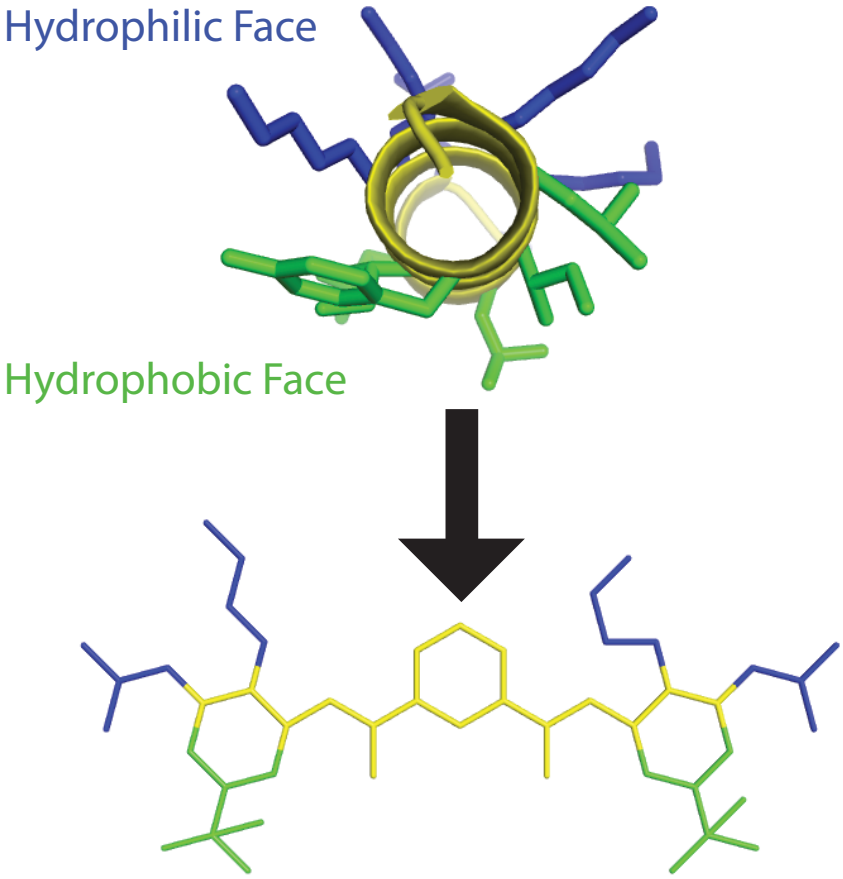

Figure 2.17: Conceptual design of smHDPs from HDPs. Top: Amphipathic structure of magainin 2; cationic groups in blue, nonpolar groups in green, peptide backbone in yellow. Bottom: *de novo* designed smHDPs capture the facially amphipathic architecture and critical physicochemical properties needed to establish robust antimicrobial activity.

were determined to be initial “hits” (14.3% hit rate), using a cutoff of 80% parasite death at 500 nM (Z’ = 0.720; Figure 2.18). 74 compounds were selected for follow-up IC50 determination (PMX004-1120, Table 2.3). Based on these hits, additional compounds were synthesized (PMX1154-1422, Table 2.3) and 7 structurally diverse compounds were chosen as “leads” based on high potency against *P. falciparum*, low hemolytic potential (Table 2.4), and low mammalian cell cytotoxicity. These lead compounds also showed similar potency across a panel of chloroquine-sensitive (3D7, HB3) and chloroquine-resistant (Dd2, 7G8, K1) parasite lines (Table 2.1). Several of the lead compounds displayed little activity against Gram-positive and Gram-negative bacteria, and mammalian cells, indicating that a high level of specificity can be built into these nonpeptidic scaffolds. Secondarily, specificity can also be found between simple single cell eukaryotic pathogens and mammalian cells (Table 2.2). Although all lead compounds showed a similar mechanism of action as PF4, based on acute animal tolerability studies, PMX1207 and PMX207 were selected for more rigorous mechanistic analysis (structures shown in Figure 2.19).

Treatment of *P. falciparum* parasites with either PMX1207 or PMX207 disrupted DV membrane potential within 15 minutes of treatment but did not disturb the PPM or mitochondrial potential, even after 4-hour treatment (Figure 2.20). In addition, treatment of the transgenic PM-II-GFP parasites with PMX1207 and PMX207 resulted in rapid diffusion of GFP through the parasite cytoplasm indicating a catastrophic loss of DV membrane integrity in a manner similar to that observed for hPF4 (Figure 2.21; other 5 leads shown in Figure 2.22). Quantitative flow cytometry analysis indicated a dose-dependent effect on DV lysis, with nearly complete DV lysis within the treated population upon treatment with 1 μM of PMX207 or PMX1207 (Figure 2.23). We further investigated the intracellular localization and distribution of the smHDPs using PMX496, a potent

Figure 2.18

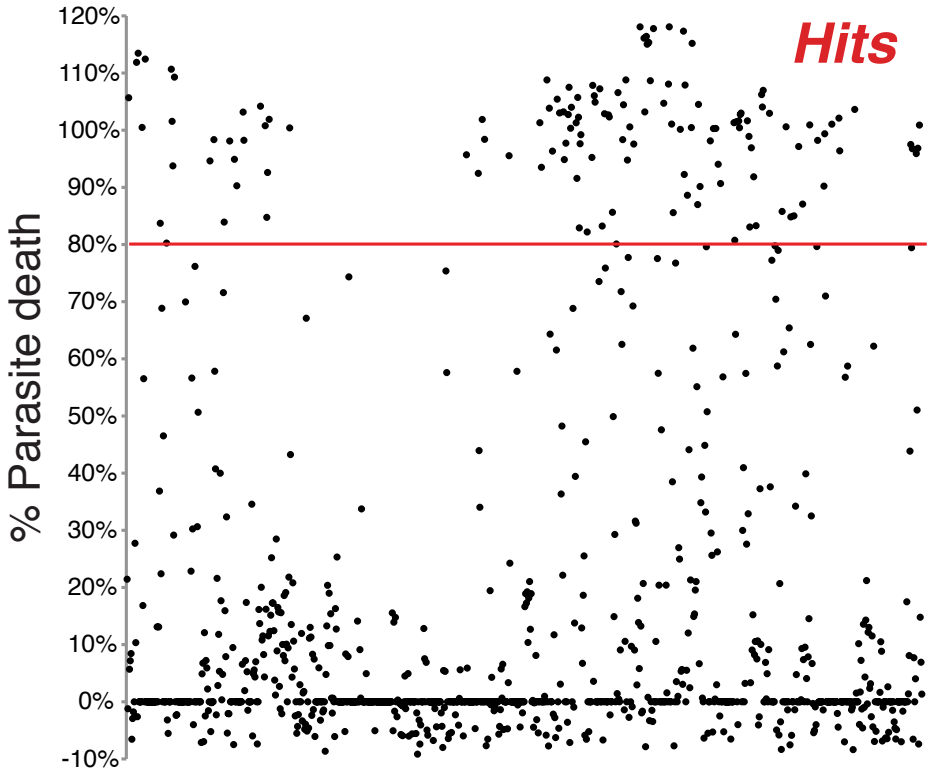

Figure 2.18: Screen of smHDPs reveals potent inhibitors of *P. falciparum* growth. Screen of 920 smHDPs at 500 nM against *P. falciparum*. Parasite death was normalized to a chloroquine control (14.3% hit rate, Z' = 0.720).

Table 2.1: Screen of lead smHDPs against a panel of *P. falciparum* strains. Lead smHDPs were screened against a panel of chloroquine-sensitive and chloroquine-resistant *P. falciparum* lines. Chloroquine was used as a positive control for parasite death. IC50s are as mean ± SEM, n>3 for each compound. Cytotoxicity (EC50) determined against mouse 3T3 fibroblasts and human transformed liver HepG2 cells using an MTS viability assay.

	CQ-sensitive *P. falciparum*		CQ-resistant *P. falciparum*			Mammalian Cells	
Compound	**3D7 IC_{50} (nM)**	**HB3 IC_{50} (nM)**	**Dd2 IC_{50} (nM)**	**7G8 IC_{50} (nM)**	**K1 IC_{50} (nM)**	**3T3 EC_{50} (μM)**	**HepG2 EC_{50} (μM)**
Chloroquine	8.7 ± 3.3	8.7 ± 1.0	24.6 ± 2.7	37.0 ± 5.8	47.1 ± 6.0	-	-
PMX611	60 ± 20	26 ± 8	49 ± 14	66 ± 14	57 ± 10	769	830
PMX1207	110 ± 12	104 ± 20	75 ± 11	91 ± 7	83 ± 4	65.1	165
PMX207	153 ± 13	133 ± 13	134 ± 10	104 ± 9	95 ± 13	463	536
PMX496	160 ± 60	150 ± 70	170 ± 70	160 ± 60	170 ± 70	139	80
PMX504	160 ± 60	160 ± 60	118 ± 16	113 ± 15	170 ± 70	322	356
PMX647	160 ± 60	170 ± 70	300 ± 100	300 ± 100	610 ± 66	284	433
PMX835	220 ± 50	200 ± 70	300 ± 100	200 ± 70	200 ± 70	>1000	>1000

Table 2.2: Screen of smHDPs against *P. falciparum* and bacteria. Comparison of anti-*P. falciparum* (*Pf;* 3D7 strain) and antibacterial activities. Bacteria strains: *E. coli* 25922 (EC), *S. aureus* 27660 (SA), *E. faecalis* 29212 (EF), *P. aeruginosa* 10145 (PA), *K. pneumoniae* 13883 (KP).

Compound	***Pf* IC_{50} (μg/mL)**	***Ec* MIC (μg/mL)**	***Sa* MIC (μg/mL)**	***Ef* MIC (μg/mL)**	***Pa* MIC (μg/mL)**	***Kp* MIC (μg/mL)**
PMX611	0.032	>50	12.5	25	>50	>50
PMX1207	0.089	0.78	0.78	0.78	6.25	12.5
PMX207	0.17	>50	>50	50	>50	>50
PMX496	0.093	50	50	50	>50	>50
PMX504	0.12	>50	12.5	25	>50	>50
PMX647	0.14	>50	50	25	>50	>50
PMX835	0.20	25	12.5	25	>50	50

Table 2.3: IC50 values of smHDP hits. IC50 values determined in 3D7 (CQ-sensitive) and Dd2 (CQ-resistant) *P. falciparum* for 74 hits from smHDP screen and derivative compounds not included in original screen. Parasites were treated in triplicate, n = 2.

Compound	3D7 IC50 (nM)	Dd2 IC50 (nM)	Compound	3D7 IC50 (nM)	Dd2 IC50 (nM)
Chloroquine	8.7	24.6	614	864	966
Artesunate	19.4	12.1	616	149	97
004	563	740	617	110	172
015	438	601	633	272	457
018	668	611	647	160	300
033	306	419	651	148	267
048	295	484	661	175	200
053	740	1154	730	1150	975
056	653	993	731	1164	964
058	1233	1219	734	610	980
062	413	426	781	147	207
073	204	274	800	610	431
092	1024	713	819	724	951
112	688	740	832	358	368
143	870	688	835	220	300
146	322	244	847	870	1076
152	221	170	848	625	709
158	683	827	868	881	886
160	151	168	893	200	301
192	1198	1010	1007	1283	2747
201	125	85	1011	880	795
207	153	134	1012	656	555
217	569	591	1032	1197	798
224	893	524	1045	706	398
235	146	108	1064	1098	1132
256	1064	344	1065	680	664
270	732	803	1068	644	682
459	1365	1632	1070	650	724
462	1283	2120	1076	N/A	N/A
474	991	1226	1086	812	1054
484	655	1095	1088	734	602
485	841	1006	1095	1141	786
493	904	1183	1096	58	90
496	160	170	1099	1163	667
501	593	393	1101	672	656
504	160	118	1107	1102	997
610	N/A	N/A	1115	696	829
611	60	49	1120	308	331

Compound	3D7 IC50 (nM)	Dd2 IC50 (nM)	Compound	3D7 IC50 (nM)	Dd2 IC50 (nM)
1154	530	N/T	1284	160	135
1158	563	N/T	1287	2819	N/T
1159	493	N/T	1301	226	N/T
1164	N/A	N/T	1302	160	132
1165	161	N/T	1305	N/A	N/T
1170	81	N/T	1306	1299	N/T
1179	1125	N/T	1307	1256	N/T
1185	15.5	N/T	1308	629	N/T
1199	2932	N/T	1310	2203	N/T
1200	2681	N/T	1324	602	N/T
1201	3376	N/T	1325	112	N/T
1206	3284	N/T	1338	N/A	N/T
1207	110	75	1364	N/A	N/T
1209	1503	N/T	1374	641	N/T
1210	658	N/T	1375	88.3	N/T
1211	976	N/T	1382	126	N/T
1213	N/A	N/T	1387	N/A	N/T
1219	3050	N/T	1398	131	N/T
1220	N/A	N/T	1399	N/A	N/T
1221	N/A	N/T	1400	473	N/T
1222	3603	N/T	1403	116	N/T
1223	3079	N/T	1407	795	N/T
1224	297	N/T	1408	77.1	N/T
1226	2523	N/T	1410	N/A	N/T
1229	202	N/T	1411	N/A	N/T
1237	255	N/T	1412	N/A	N/T
1249	1716	N/T	1413	N/A	N/T
1258	247	N/T	1414	N/A	N/T
1260	N/A	N/T	1415	N/A	N/T
1267	N/A	N/T	1416	N/A	N/T
1268	3480	N/T	1417	N/A	N/T
1269	3029	N/T	1418	187	N/T
1271	2318	N/T	1422	738	N/T
1283	2445	N/T			

N/A = Not Active
N/T = Not Tested

Table 2.4: Percent hemolysis of 15 smHDPs, PF4, and melittin. Hemolytic activity was determined for 15 smHDPs (2.5 μM), melittin (15 μM), hPF4 (15 μM), chloroquine (250 nM), and artesunate (250 nM). Parasite cultures were treated in triplicate, n = 3.

Compound	%Hemolysis (± SD)
Untreated	0.19% ± 0.28%
Chloroquine	0.01% ± 0.03%
Artesunate	0.18% ± 0.13%
Melittin	87.3% ± 18.5%
PF4	2.08% ± 0.78%
207	0.00% ± 0.00%
1096	0.09% ± 0.16%
647	0.16% ± 0.15%
160	0.22% ± 0.12%
235	0.00% ± 0.00%
201	0.00% ± 0.00%
152	0.00% ± 0.00%
496	0.42% ± 0.62%
504	0.19% ± 0.25%
611	0.00% ± 0.00%
661	0.35% ± 0.60%
835	0.15% ± 0.24%
616	0.12% ± 0.09%
617	0.30% ± 0.32%
1207	0.14% ± 0.06%

Figure 2.19

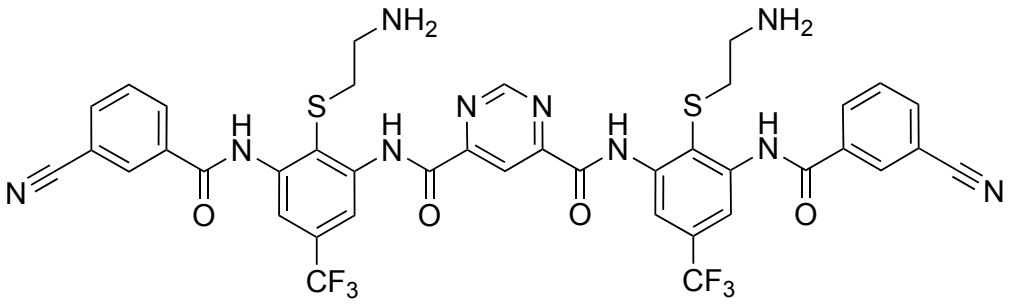

PMX207

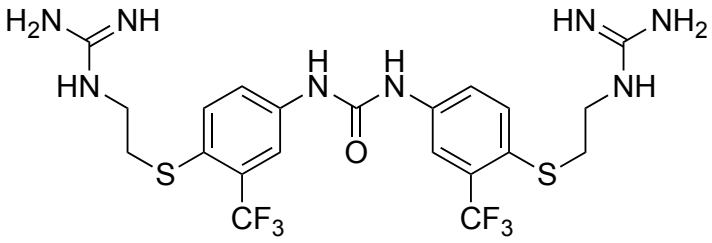

PMX1207

Figure 2.19: Chemical structures of PMX207 and PMX1207.

Figure 2.20

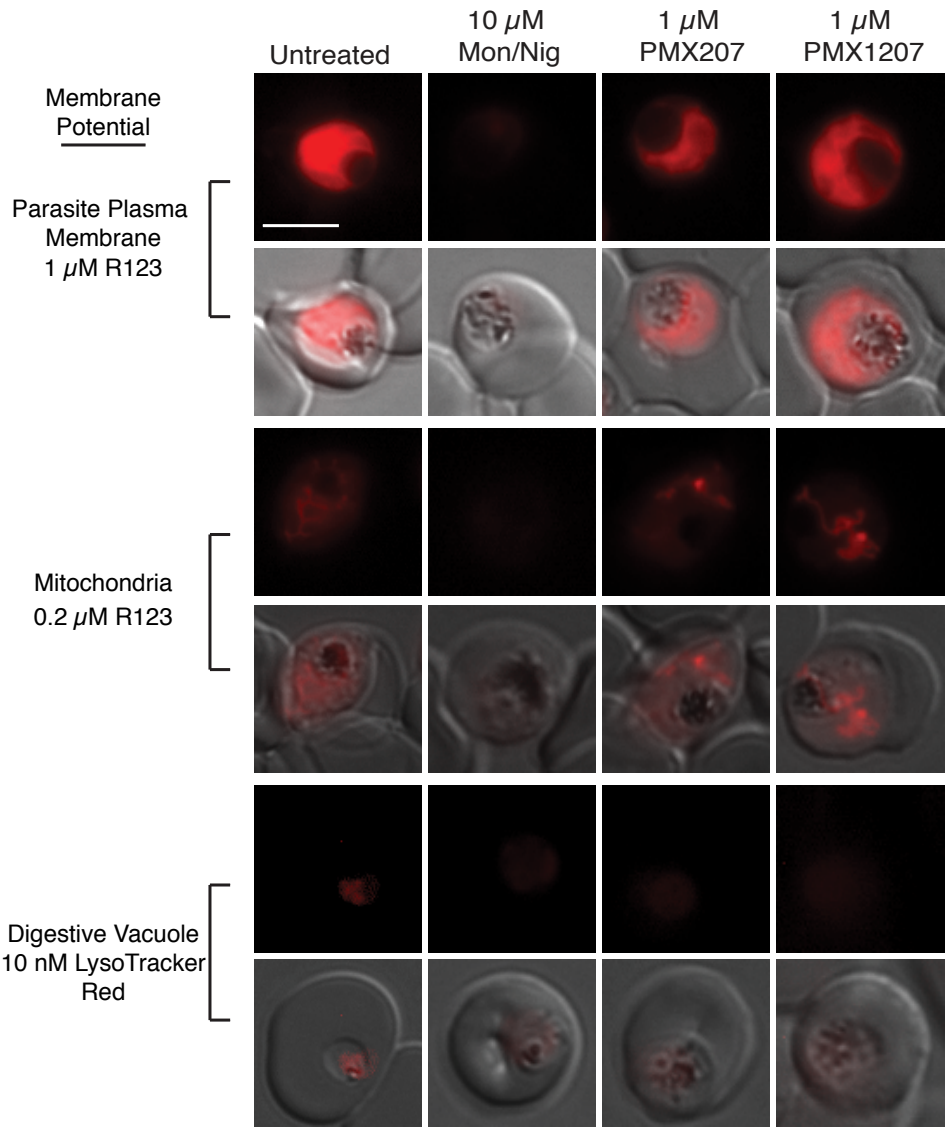

Figure 2.20: smHDP treatment causes loss of membrane potential of the DV. Parasite plasma membrane and mitochondrial potential was examined during treatment with PMX207 or PMX1207, with no discernible loss of fluorescence, unlike the positive controls. Compromise of DV integrity was monitored with LysoTracker Red, wherein loss of DV fluorescence was seen within 15 min of smHDP treatment, though no loss of parasite plasma membrane potential occurs.

Figure 2.21

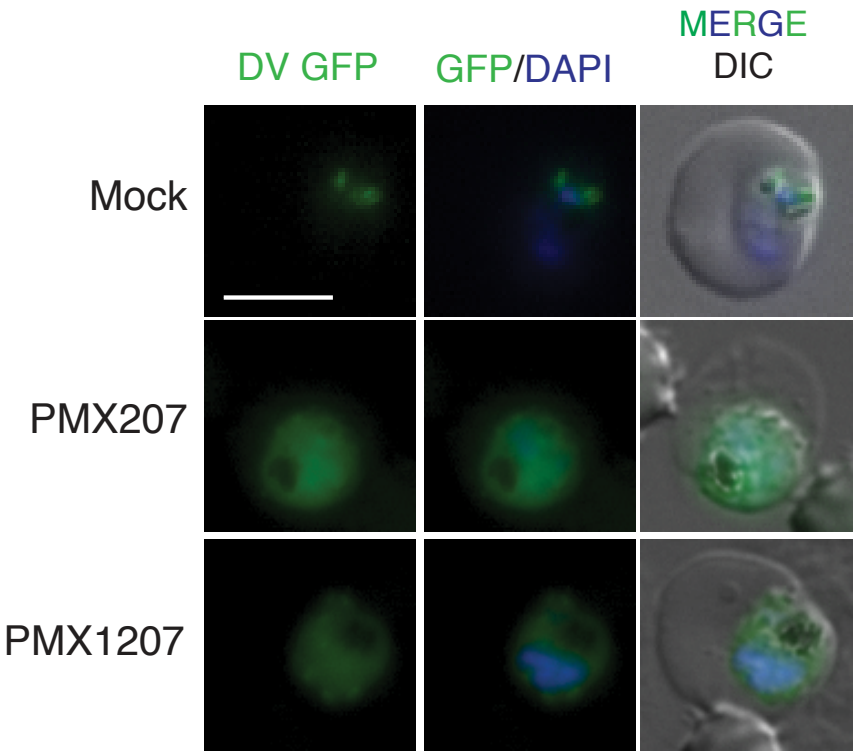

Figure 2.21: smHDP treatment causes DV lysis. Loss of DV integrity upon smHDP treatment of PM-II-GFP *P. falciparum* parasites. Green: PM-II-GFP (DV); blue: parasite nuclei.

Figure 2.22

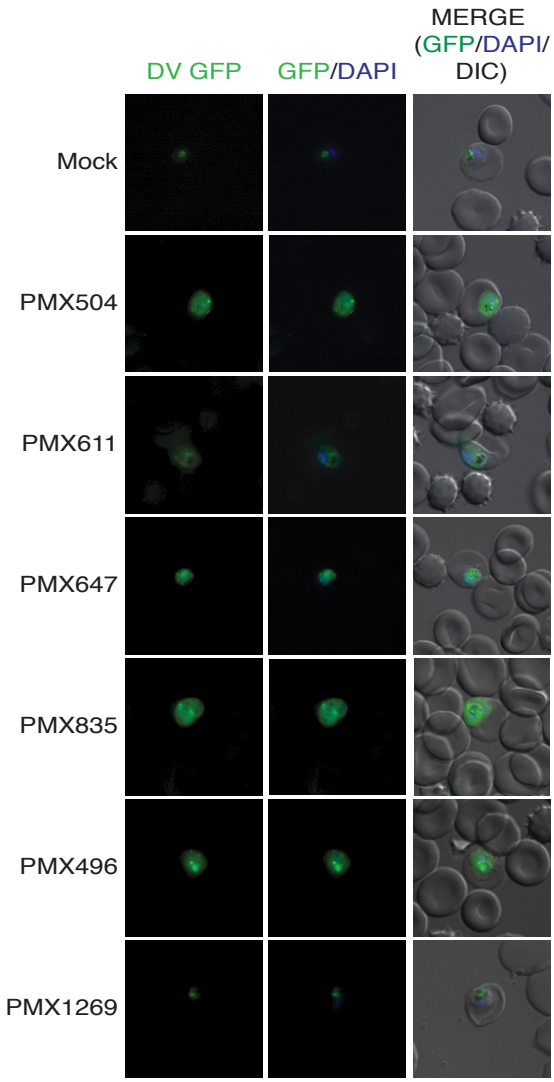

Figure 2.22: DV lysis imaging of 5 other smHDP leads. Visualization of DV lysis by smHDPs by fluorescence microscopy. PM-II-GFP *P. falciparum* parasites were treated with compounds PMX504, PMX611, PMX647, PMX835, PMX496, or PMX1269 (250 nM) over a 5-min time course and imaged via fluorescent microscopy. In untreated parasites, the GFP signal is an isolated structure, indicating an intact DV. The GFP signal after smHDP treatment spans the entire parasite body, indicating loss of digestive vacuole integrity. The uncharged analogue of PMX496, PMX1269, did not cause DV lysis. Green: PM-II-GFP (DV); blue: parasite nuclei.

smHDP with intrinsic fluorescence. PMX496 appeared to accumulate in the parasite body within 30 seconds, then concentrated in the DV at 1 minute, prior to dissipation throughout the parasite body, indicating a loss of DV membrane integrity (Figure 2.24). Since cationic amphipathicity is predicted to be necessary for smHDP antiparasitic action, an uncharged isosteric analog of PMX496 was synthesized (PMX1269, IC50 > 2.5 μM; structures in Figure 2.25). As expected, treatment with the uncharged analog did not result in DV lysis, as with the triple alanine C12 mutant. High-resolution transmission electron microscopy and 3D tomograms revealed a complete loss of integrity of the DV after treatment with either PMX1207 or PMX207 (Figure 2.26). In addition to free hemozoin crystals (red arrowheads), images showed an accumulation of undigested hemoglobin-containing vesicles (yellow arrowheads; Figures 2.26,27). Mock-treated parasites showed clear delineating DV membranes (white arrowheads). DV lysis and killing was also evident in Texas Red Dextran-loaded erythrocytes infected with either trophozoite-stage parasites (Figure 2.28) or gametocytes (Figure 2.29). Loss of gametocyte DV integrity would likely result in parasite death and indicates that smHDPs may have transmission-blocking potential. To further assess the antimalarial capacity of PMX207 and PMX1207, they were screened against an additional 5 *P. falciparum* isolates encompassing a diverse set of malaria endemic regions and antimalarial drug resistance characteristics (Table 2.5). All lines were comparably susceptible to these smHDPs, reiterating their potential as antimalarials.

HDP and smHDP activity reduce parasitemia in a murine malaria model

We next tested PF4 and its HDP domain C12 in a non-experimental cerebral malaria (non-ECM, *P. yoelii* 17XNL) murine malaria model using the 4-day Peters suppression test [88]. mPF4 treatment significantly reduced parasitemia by 4-fold, while the HDP

Figure 2.23

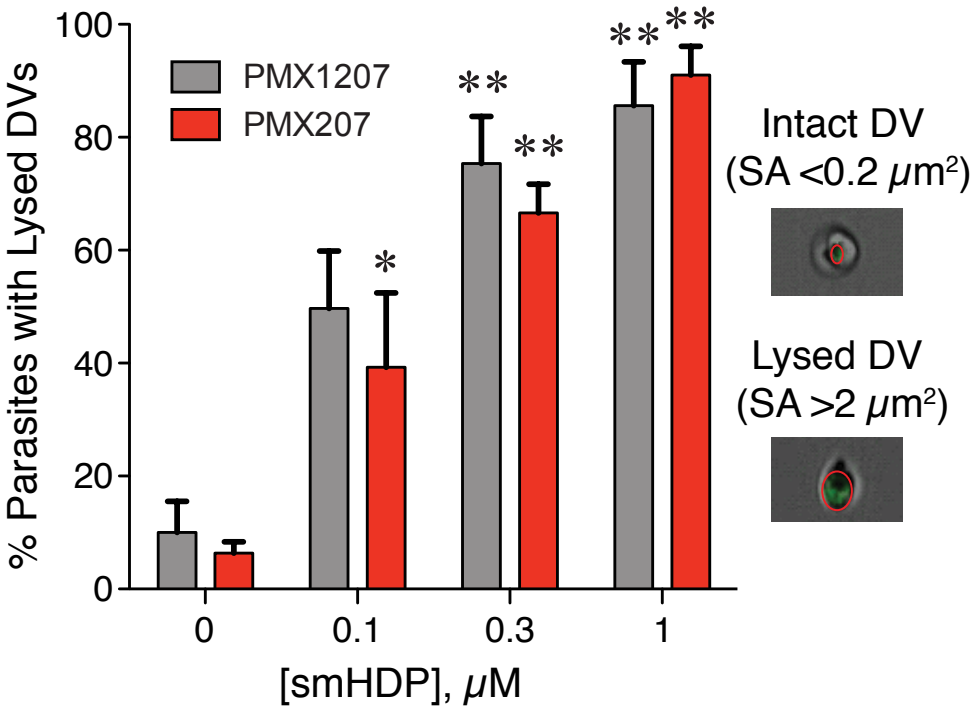

Figure 2.23: Quantitative analysis of DV lysis by smHDPs. ImageStream flow cytometry shows a dose-dependent increase in PM-II-GFP parasites showing a fluorescence surface area of >2 μm^2, an indication of DV lysis, upon treatment with PMX207 or PMX1207. Intact DVs have fluorescent surface areas <0.2 μm^2. Data shown are means ± SEM. (*p<0.05, **p<0.01).

Figure 2.24

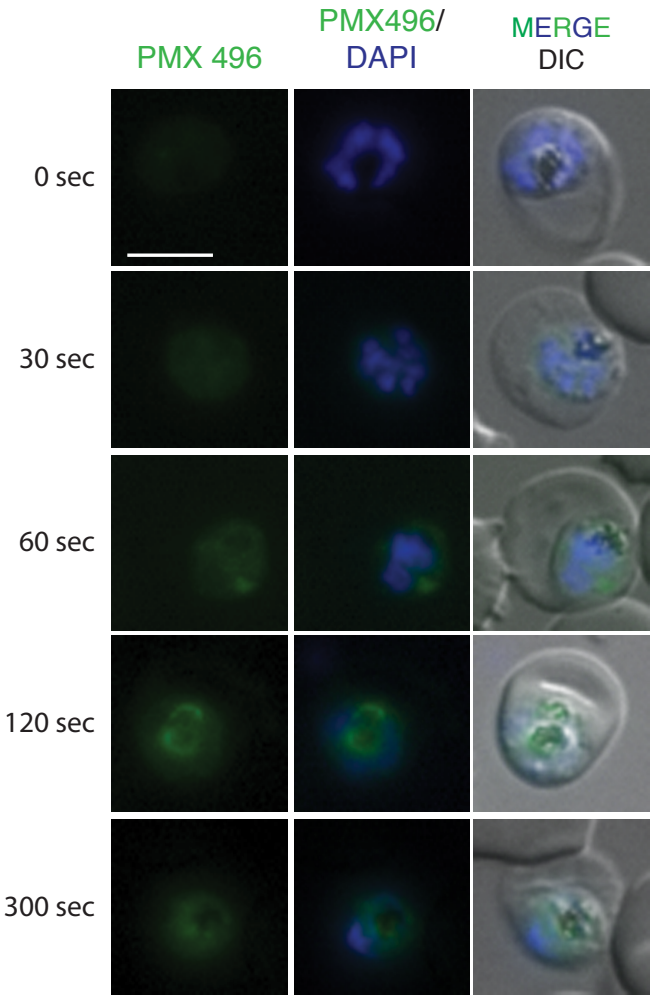

Figure 2.24: DV lysis imaging of the intrinsically fluorescent smHDP PMX496. Fluorescent microscopy of the intrinsically fluorescent PMX496 shows accumulation within the parasite cytoplasm and DV prior to DV lysis.

Figure 2.25

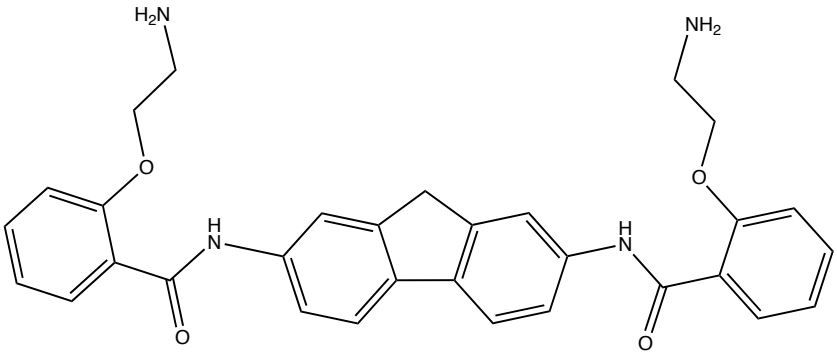

PMX496

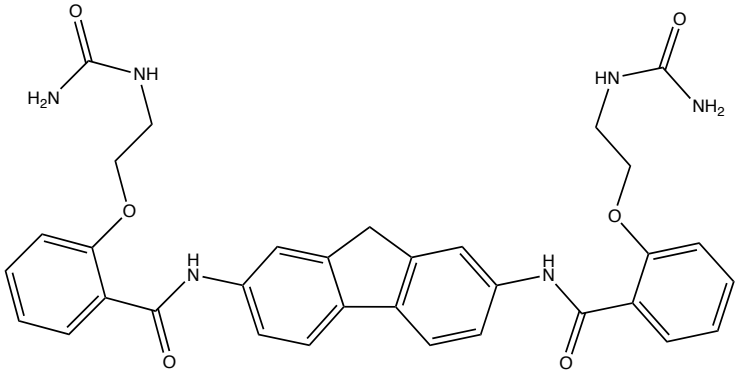

PMX1269

Figure 2.25: Chemical structures of PMX496 and its inactive analogue PMX1269.

Figure 2.26

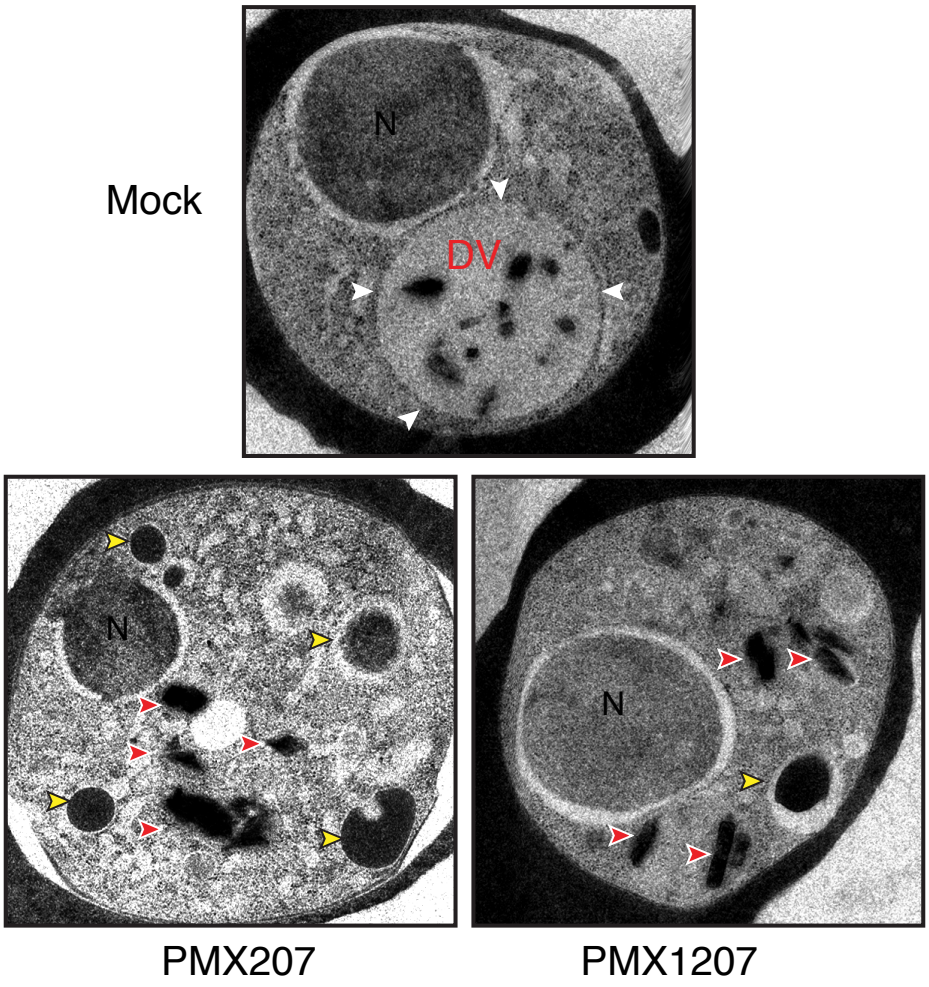

Figure 2.26: Transmission Electron Microscopy images of DV lysis by smHDPs. TEM images reveal complete dissolution of the DV membrane upon PMX207 or PMX1207 treatment, with dispersal of hemozoin crystals (red arrowheads) throughout the cytoplasm and an accumulation of undigested hemoglobin-containing vesicles (yellow arrowheads). Mock-treated parasites retained a clear delineating DV membrane (white arrowheads), encapsulating all hemozoin crystals. (N: parasite nucleus).

Figure 2.27

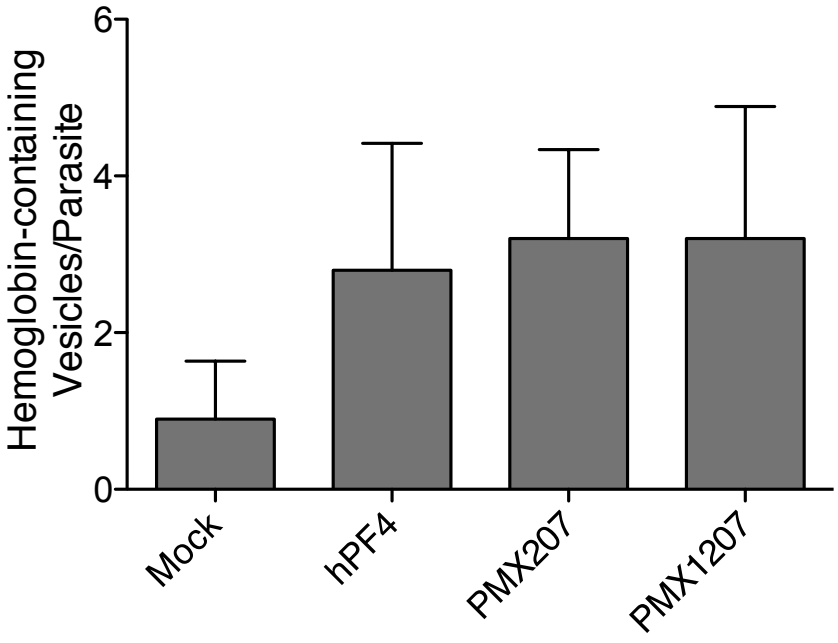

Figure 2.27: Quantification of hemoglobin-containing vesicles. Number of hemoglobin-containing vesicles in electron micrographs of parasites treated with 10 μM hPF4, 500 nM PMX207, or 500nM PMX1207 was counted and compared to mock (DMSO)-treated controls. Data shown is mean ± standard deviation of 50 parasites (*$p<0.05$).

Figure 2.28

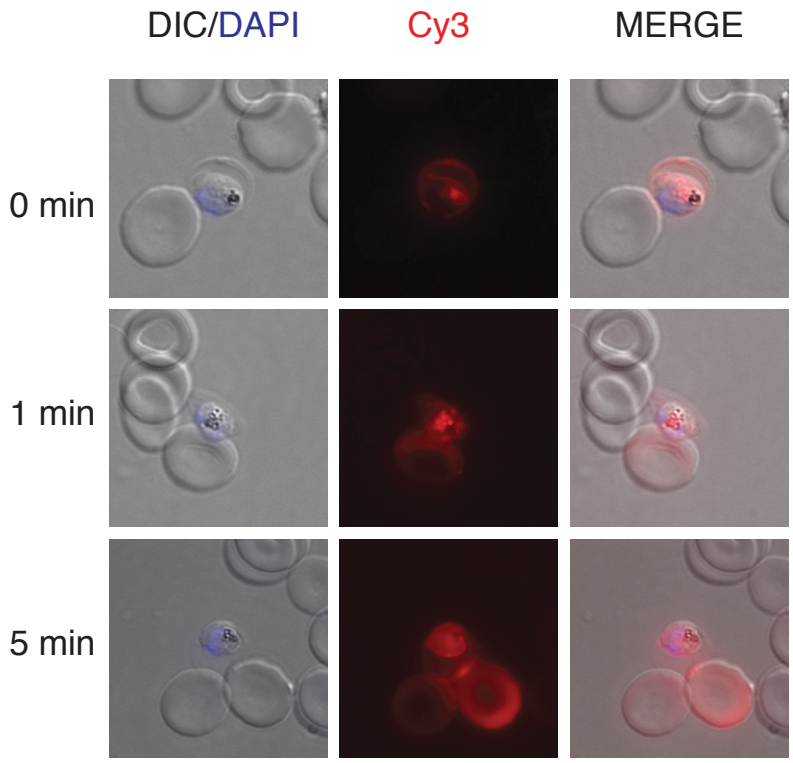

Figure 2.28: Texas Red Dextran imaging of trophozoite DV lysis by PMX1207. Visualization of DV lysis by PMX1207 with Texas Red Dextran-loaded erythrocytes. Trophozoite-infected Texas Red Dextran-loaded cells show dispersal of fluorescence into the parasite cytoplasm following treatment with PMX1207, indicating loss of DV integrity.

Figure 2.29

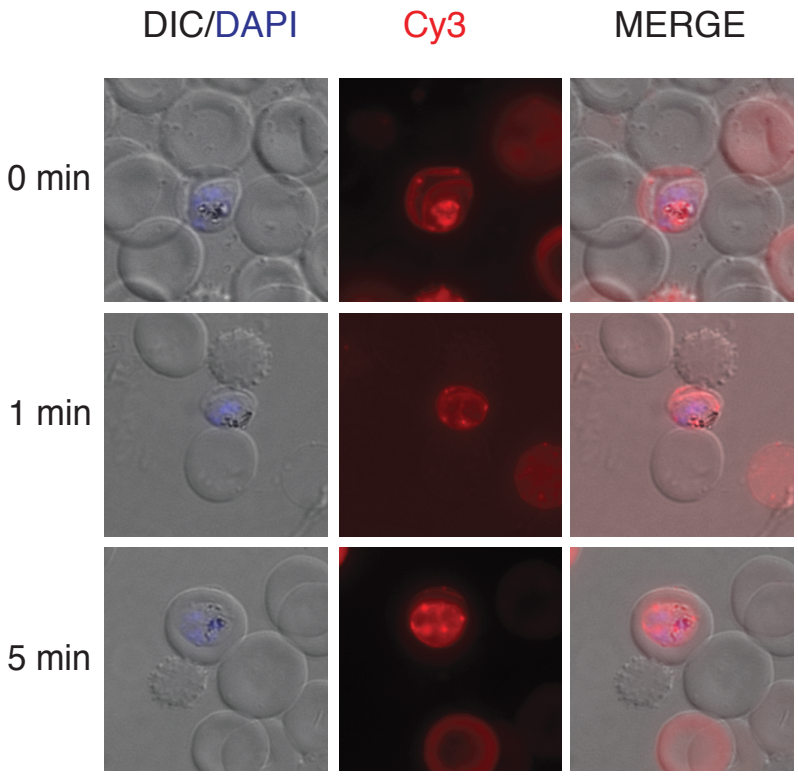

Figure 2.29: Texas Red Dextran imaging of gametocyte DV lysis by PMX1207. Visualization of DV lysis by PMX1207 with Texas Red Dextran-loaded erythrocytes. Gametocyte-infected Texas Red Dextran-loaded cells show dispersal of fluorescence into the parasite cytoplasm following treatment with PMX1207, indicating loss of DV integrity.

Table 2.5: IC50 values for PMX207 and PMX1207 in an expanded panel of *P. falciparum* strains. IC50 values are reported as means. Parasite cultures were treated in triplicate, n = 2.

P. falciparum strain	Chloroquine IC50 (nM)	PMX207 IC50 (nM)	PMX1207 IC50 (nM)
3D7	8.7	153	110
HB3	8.7	133	104
Dd2	24.6	134	75
7G8	37.0	104	91
K1	47.1	95	83
T2/C6	4.2	60	69
V1/S	74.4	165	65
Indo	41.8	190	134
NF54;E	8	117	110
MT/S1	6.7	157	73

domain C12 reduced parasitemia by 3-fold (Figure 2.30A,B), indicating that the HDP domain retained antimalarial activity during disease stages *in vivo*, aside from cerebral malaria. In an ECM model (*P. berghei* ANKA), C12 reduced parasitemia compared to controls on day 5, however, by day 7 (3 days after cease of treatment), parasitemia in the C12 treated mice were significantly higher than controls (Figure 2.30C). This data suggests that even the C12 domain of PF4 has some immunomodulatory activity that has a negative impact on survival in the *P. berghei* ANKA model of cerebral malaria; therefore, we felt that that the smHDPs have the best potential as antimalarials.

In order to further explore the antimalarial properties of lead smHDPs, PMX207 and PMX1207 were assessed for their ability to limit parasite growth *in vivo* in both a non-ECM and ECM murine malaria model. PMX207 and PMX1207 antiparasitic activity was assessed using the 4-day Peters suppression test against *P. yoelii* 17XNL and *P.*

Figure 2.30

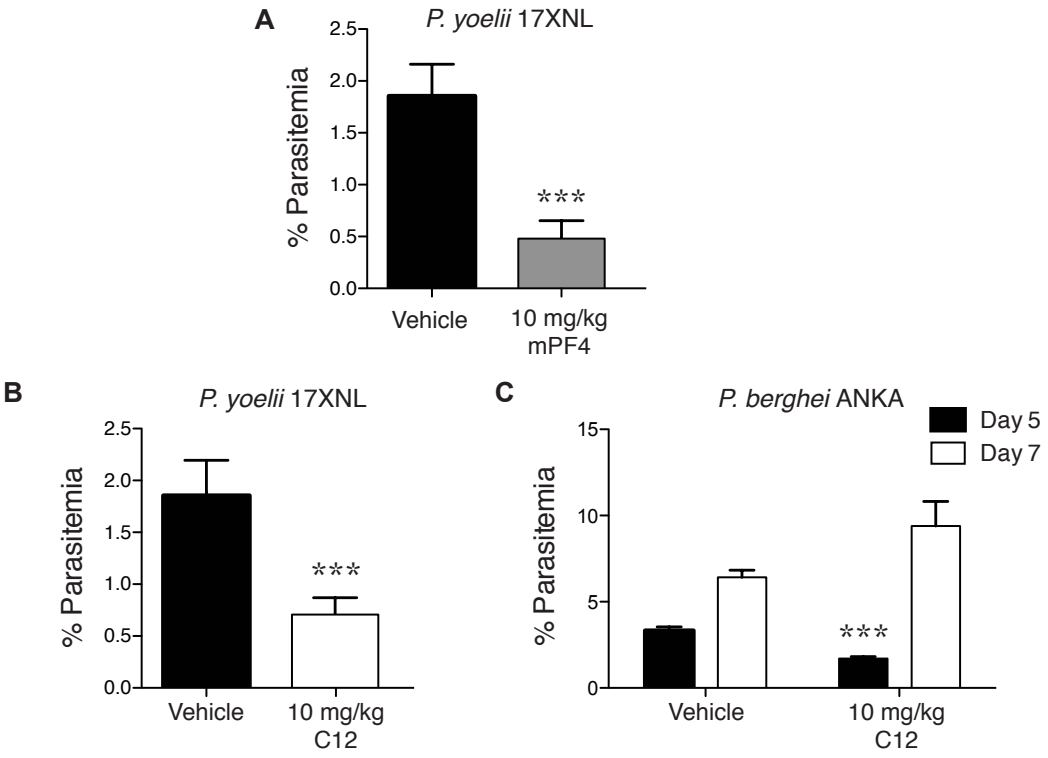

Figure 2.30: hPF4 and C12 reduce parasitemia in a mouse malaria model. (**A**) Mice infected with *P. yoelii* 17XNL show decreased parasitemia on day 4 when treated with 10 mg/kg mPF4 (n=3) compared to controls (n=5, $p < 0.001$). Shown are mean parasitemias ± SEM. (**B**) Mice infected with *P. yoelii* 17XNL show decreased parasitemia on day 4 when treated with C12 (n=4) compared to controls (n=5, $p < 0.001$). Shown are mean parasitemias ± SEM. (**C**) Mice infected with *P. berghei* ANKA showed a significant decrease in parasitemia upon treatment with 10 mg/kg C12 (n=5) compared to controls (n=5) on day 5 ($p < 0.001$). However, by day 7, C12-treated mice had significantly higher parasitemias than controls ($p < 0.05$). Shown are mean parasitemias ± SEM.

Figure 2.31

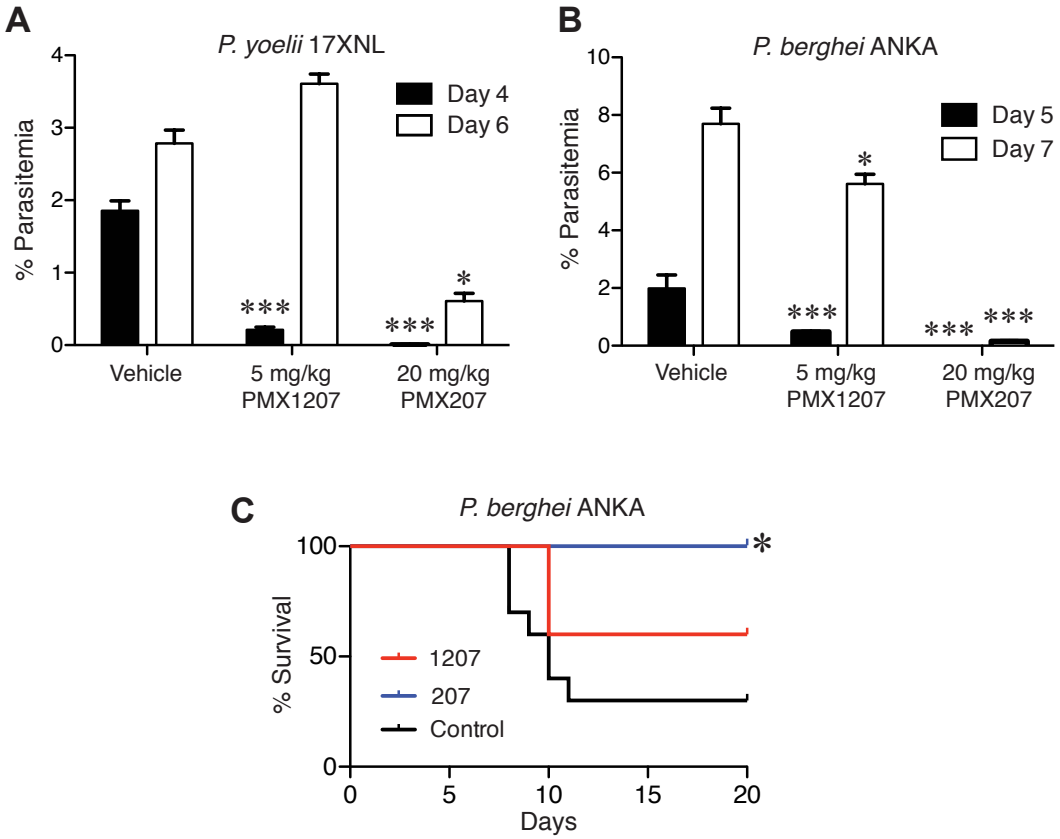

Figure 2.31: smHDP leads decrease parasitemia in a mouse malaria model. (**A**) Parasitemias of Swiss Webster mice infected with *P. yoelii* 17XNL parasitized erythrocytes via i.v. injection and treated with vehicle (n=5); 5 mg/kg PMX1207 (n=7); or 20 mg/kg of PMX207 (n=5). Parasitemia was assessed on days 4 and 6. Shown are the means ± SEM. (*p<0.05; ***p<0.001) (**B**) Parasitemias of C57Bl/6 mice infected with *P. berghei* ANKA parasitized erythrocytes via i.v. injection and treated with vehicle (n=10); 5 mg/kg PMX1207 (n=5); or 20 mg/kg of PMX207 (n=5). Parasitemia was assessed on days 5 and 7. Shown are the means ± SEM. (*p<0.05; ***p<0.001). (**C**) Survival curves for *P. berghei* ANKA infected mice. p = 0.14 in the log-rank Mantel-Cox test.

berghei ANKA (Figure 2.31A,B). PMX207 completely eliminated parasitemia in both models on days 4 and 5 while PMX1207 showed a significant decrease in parasite growth, suppressing parasitemia at least 5-fold over vehicle-treated controls. Both compounds also increased mouse survival in the ECM model (Figure 2.31C), with all PMX207 mice surviving through day 20. These data provide *in vivo* validation that smHDP compounds show promise as a new class of antimalarials.

2.3 Discussion

In this work we show that the human HDP protein, PF4, and its HDP domain alone (C12) kill *Plasmodium* parasites by lysing the parasite DV. Moreover, we screened a library of smHDPs and found molecules that preserved this mechanism of parasite killing while increasing potency (Figure 2.32). Thus, targeting the lysosome-like vesicles of protozoan parasites may be an evolutionarily selected mechanism for mammalian hosts to kill *Plasmodium*, and is a mechanism that may be exploited for drug discovery. How proteins such as PF4, just the C12 HDP domain of PF4, or smHDPs enter host cells is still an open question and beyond the scope of this work. However, we provide evidence these molecules enter only infected erythrocytes and that this entry process can be blocked by pre-incubating with protamine sulfate, a cationic peptide that can also bind to heparin (Figure 2.33). This indicates the importance of initial electrostatic interactions with the infected host cell membrane or membrane proteins. Since only infected cells are targeted, and parasite viability is important for uptake, this suggests that a parasite-derived or activated endocytosis-like mechanism could allow for large molecules such as PF4 or C12 to enter, while channels/pores or passive diffusion could be responsible for smHDP uptake.

In closing, human PF4 has the ability to kill blood stage parasites *in vitro*, and its

Figure 2.32

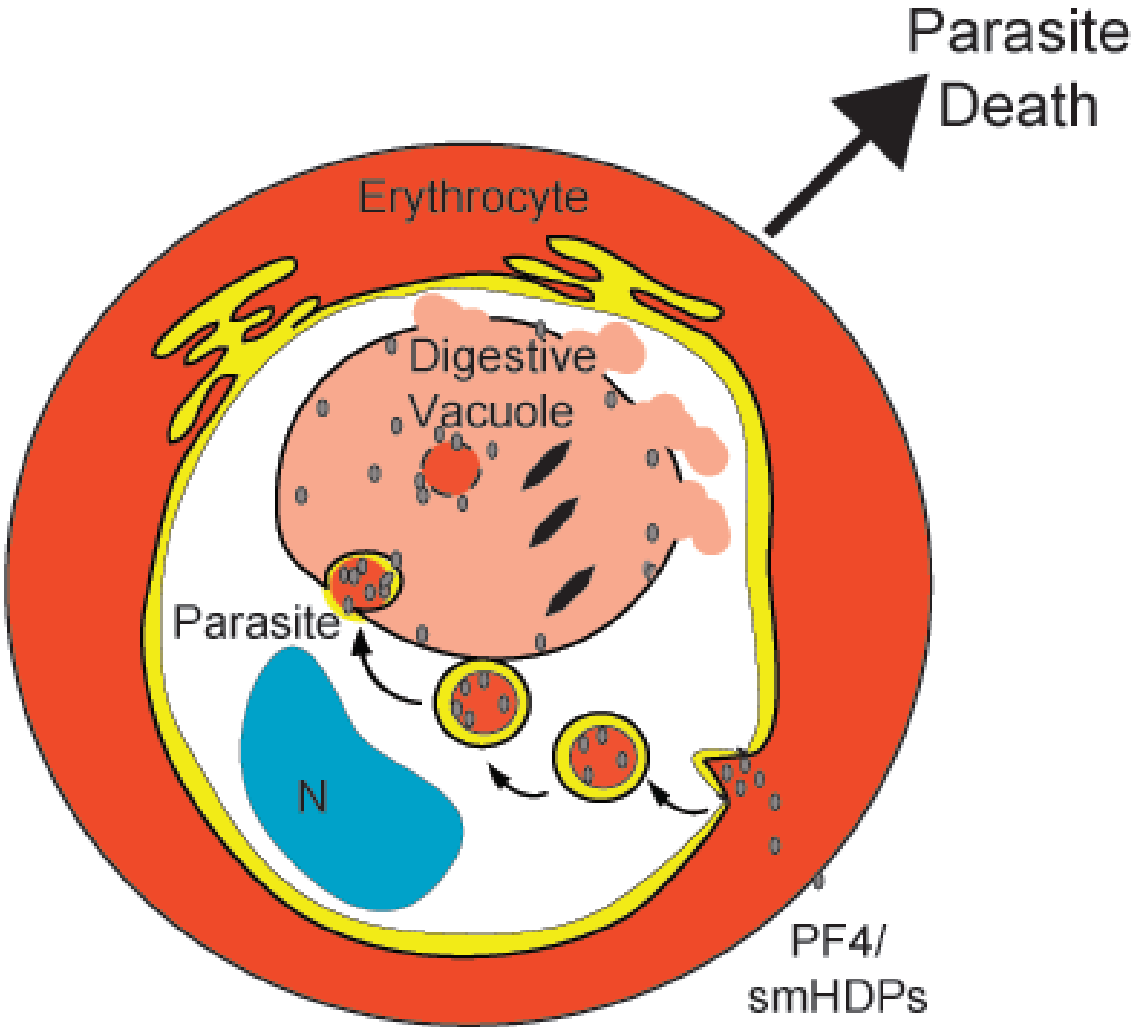

Figure 2.32: Proposed PF4 and smHDP mechanism of action. PF4/smHDPs enter the host erythrocyte via an unknown mechanism. The PF4 or smHDPs are then taken up through the cytostome with the host cell cytoplasm, packaged into vesicles, and then sent to the digestive vacuole for hemoglobin digestion. Upon reaching a critical concentration, the PF4/smHDPs insert into the digestive vacuole membrane, causing disruptions and lysis. This ultimately results in parasite death. N = nucleus.

Figure 2.33

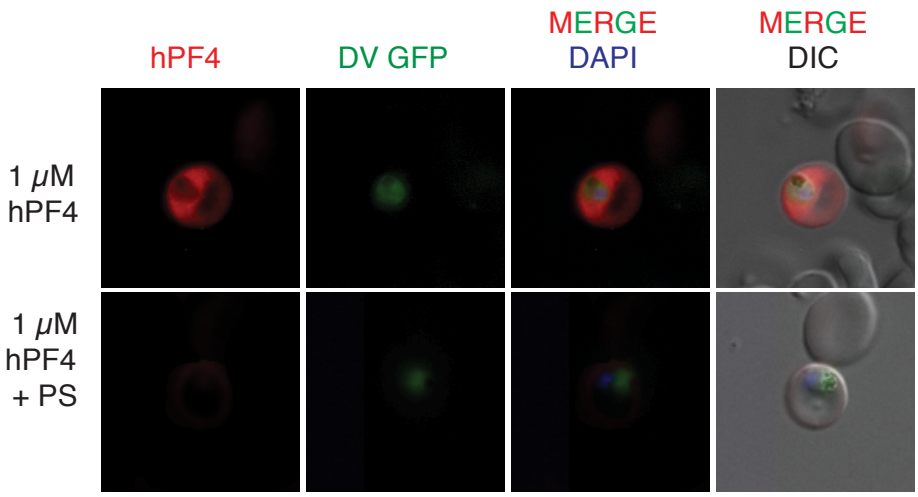

Figure 2.33: hPF4 causes dose-dependent DV lysis limited by protamine sulfate. PM-II-GFP parasite-infected erythrocytes were pretreated with 5 mM protamine sulfate or mock (DMSO) for 30 minutes, then treated with 10 μM hPF4 for 10 minutes prior to fixation and permeabilization. hPF4 immunofluorescence (red) shows no appreciable signal in the protamine sulfate pretreated erythrocytes, while mock-pretreated erythrocytes show hPF4 accumulation within the erythrocyte. Red: hPF4 IFA; green: PM-II-GFP (DV); blue: parasite nuclei.

low hemolytic potential and selective targeting of the parasite DV endow it with properties that are well tolerated in the bloodstream. However, it is unlikely that PF4 would make a useful therapeutic for malaria treatment due to the cost of goods and potential of increased inflammatory damage during cerebral malaria. Thus, we believe the development of smHDPs may overcome these issues while preserving this unique mechanism of action; thus smHDPs represent a new class of small molecules with effective therapeutic potential for combating this human disease where efforts are currently challenged with rampant drug resistance.

2.4 Experimental Procedures

Parasite culture and IC50 determination

P. falciparum parasites were cultured according to standard conditions [89] with minor modifications. Parasites were maintained in fresh human erythrocytes suspended at 4% hematocrit in RPMI 1640 supplemented with 0.5% Albumax II, 0.2% $NaHCO_3$, 50 µg/L hypoxanthine and 50 µg/l gentamicin and incubated at 37°C under a gas mixture of 5% O_2, 5% CO_2 and 90% N_2. For IC50 determinations, compounds were assayed for 72h, after which the cultures were fixed with a solution of 4% paraformaldehyde and 0.008% glutaraldehyde in PBS prior to permeabilization with 0.25% Triton X-100, and 5 µM SYTOX Green Nucleic Acid Stain and flow cytometry analysis (Accuri C6 Flow Cytometer with C-Sampler). IC50 curves were generated using GraphPad Prism.

HDP screen and assay for hemolysis.

P. falciparum parasites (3D7 strain) were cultured as described previously. Synchronized parasites were treated with 15 µM of 9 platelet-, neutrophil-, or lymphocyte-derived proteins containing HDP-domains or properties: Regulated upon Activation, Normal T-cell Expressed, and Secreted (RANTES, ProSpec); Platelet Factor-

4 (PF4, Haematologic Technologies Inc.); Fibrinopeptide-A (FP-A, AnaSpec); Fibrinopeptide-B (FP-B, AnaSpec); Human Neutrophil Peptide-1 (HNP-1, AnaSpec); Human Neutrophil Peptide-2 (HNP-2, AnaSpec); Cathelicidin (LL-37, AnaSpec); Lymphotactin (ProSpec); Lactoferrin (ProSpec). 15 μM melittin, the major active component of bee venom, was used as a positive control for HDP-killing of parasites with complete hemolysis. Parasite death was normalized to a 500 nM artesunate control. Parasites were treated for 72 hours, and then fixed and assayed for parasitemia via flow cytometry. Hemolysis was measured by removing 50 μL from each well (100 μL total in a 96-well plate) before fixing and transferring to a clear-bottom plate. Absorbance at 541 nm was measured and compared to a standard curve generated from Triton X-100-lysed erythrocytes (4% hematocrit serially diluted by 2).

Platelet activation

These studies were completed by Melanie G. Millholland at the University of Pennsylvania. Platelets were collected from C57BL/6 mice (WT), homozygous PF4 knockout mice (PF4 KO), and transgenic mice overexpressing human PF4 (hPF4+) [64] and added to cultures either with or without pre-activation *ex vivo* with 5 μM AYP. Parasitemia was assessed via flow cytometry after 24 hours treatment.

Parasite membrane potential assays

These studies were completed in collaboration with Melanie G. Millholland at the University of Pennsylvania. Parasite-infected erythrocytes were incubated at 37°C for 30 minutes with 1 μM rhodamine 123 (for parasite plasma membrane potential), 0.2 μM rhodamine 123 (for parasite mitochondrial potential) [90], or 10 nM LysoTracker Red (for digestive vacuole potential). After pre-incubation, parasites were treated for 4 hours with the test compound, a 10 μM mixture of the ionophores monensin (Sigma) and nigericin

(Calbiochem) as a positive control of membrane potential perturbation, or left untreated and then analyzed via fluorescence microscopy on a Leica DMI6000 B.

Fluorescence microscopy and quantification of digestive vacuole lysis

These studies were completed by Melanie G. Millholland at the University of Pennsylvania. Erythrocytes infected with synchronous cultures of PM-II-GFP expressing parasites were treated at 30 hours post invasion (hpi) and fixed at the indicated time points, stained with Hoechst and imaged by fluorescence microscopy. Cells were also analyzed on an Amnis ImageStream X high-resolution flow cytometer with gating for Hoechst-positive cells to isolate infected cells [91, 92].

PF4 immunofluorescence

These studies were completed by Melanie G. Millholland at the University of Pennsylvania. Erythrocytes infected with PM-II-GFP parasites were treated with 1 μM recombinant hPF4, fixed at specified time points, permeabilized with 0.1% Triton X-100 for 10 min and assayed for PF4 immunofluorescence with hPF4 primary antibody and an Alexa-568 conjugated anti-rabbit secondary antibody. Parasites were imaged via fluorescence microscopy.

Western blot analysis of PF4 accumulation

These studies were completed by Melanie G. Millholland at the University of Pennsylvania. Synchronous cultures of *P. falciparum*-infected erythrocytes were treated with 10 μM PF4 then 0.1% saponin to separate erythrocyte fractions from parasite material. Samples were run by standard SDS-PAGE, transferred to Immobilon Transfer PVDF membrane and incubated with 1:1000 primary antibody to human PF4 and

1:10000 anti-mouse secondary antibody. Input of total cell lysates was used as a loading control, using a primary antibody to flotillin and an anti-rabbit secondary antibody.

Peptide synthesis

Peptides were synthesized via the solid phase method at 0.092 mmol scales using Fmoc-CLEAR^{TM} Amide resin (Peptides International, substitution level 0.46 mmol/g). Activation of Fmoc-amino acids (5-fold excess) was achieved with (2-(6-Chloro-1H-benzotriazole-1-yl)-1,1,3,3-tetramethylaminium hexafluorophosphate) in the presence of 2-(N,N'-diisopropylamino) ethanol. The reaction solvent contains 100% *N*,*N*-Dimethylformamide (HPLC grade, Aldrich). Coupling, cleavage, and precipitation reagents were purchased from Sigma-Aldrich. Amino acids were purchased from Chem-Impex International Inc. Side chain deprotection and simultaneous cleavage from the resin were carried out using a mixture of trifluoroacetic acid/H_2O/Triisoproplysilane (46.5:2.5:1, v/v) at room temperature, for 3 hours. Crude peptide was obtained by ether precipitation and purified by reverse-phase chromatography. The mass of all peptides was verified by ESI-MS (Agilent MSD G1956B). Analytical and preparative HPLC was performed using a C18 reverse-phase column on an Agilent 1200 series system (Agilent Technologies), with Hewlett Packard Chemstation software.

smHDP screen

Synchronized parasites were treated with 500 nM of each smHDP for 72 hours. Cells were then fixed and assayed for parasitemia via flow cytometry. Compounds were deemed hits if they caused ≥80% parasite death, as compared to a 500 nM chloroquine-treated positive control. The Z-factor was calculated using the equation $Z' = 1 - \frac{3(\sigma_p + \sigma_n)}{|\mu_p - \mu_n|}$

where μ represents the means and σ represents the standard deviations of the positive (p) or negative (n) controls [93].

smHDP testing in multiple parasite, bacterial, and mammalian cell lines

Synchronized parasite cultures: 3D7, NF54;E, Dd2, 7G8, K1, HB3, T2/C6, INDO, V1/S, MT/s1 (MR4, ATCC) were treated with top smHDP hits for IC50 comparison. Titrations for the assay were performed as described previously. Cytotoxicity (EC50) was determined against mouse 3T3 fibroblasts and human transformed liver HepG2 cells using an MTS viability assay. Bacterial cultures were grown from isolated colonies in Cation-Adjusted Mueller-Hinton Medium II. Compounds to be tested were prepared in DMSO at 10 mg/mL, diluted 1:20 in water and the added to a 96-well round-bottom plate in concentrations ranging from 50 μg/mL to 0.024 μg/mL following 2-fold serial dilutions in water. Bacteria were added at 10^6 cfu/mL. The cultures were incubated for 18 hours at 37ºC. To determine inhibition, turbidity was read as ≥2mm button defined by CLSI or as a clear, agreeable change in the uniformity of the cultures, or defined as an 80% or greater reduction in pellet size compared to control wells.

Transmission Electron Microscopy

These studies were completed in collaboration with Melanie G. Millholland at the University of Pennsylvania. Synchronous cultures of *P. falciparum* parasites were magnet-purified at ~25 hpi and allowed to sit for 6 hours prior to a 10-min exposure to 10 μM hPF4, 500 nM PMX207 or PMX1207**.** DMSO was used as a negative control. Samples were frozen in an Abra high-pressure freezer. This material was freeze substituted in 2% OsO_4 in anhydrous acetone and embedded into Epon. Images were collected at 120KeV on a FEI Tecnai12 equipped with a Gatan 894 2k camera. Images were captured by Dewight R. Williams, Ph.D. at the Electron Microscopy Core at the

University of Pennsylvania. Tilt series were taken +/- 70° in 3° increments at 6500x magnification. Tilt images were decimated by a factor of 2 and initially aligned by cross-correlation in FEI's inspect3D. Tomograms were constructed from fiducially aligned stacks, orthogonal merged axes, and subsequent serial tomograms joined in the IMOD package "etomo". Montage images taken with 10x10 sampling at 3200x magnification were aligned with blendmont.

P. berghei ANKA mouse studies

These experiments were conducted with the assistance of Satish Mishra, Ph.D. in the laboratory of Photini Sinnis, M.D. at the Malaria Research Institute, Bloomberg School of Public Health, Johns Hopkins University. C57BL/6 mice were infected with $2.5x10^4$ *P. berghei* ANKA parasitized erythrocytes via intravenous injection. Mice were dosed once per day intravenously on days 1-4 with either 5 mg/kg PMX1207 (in 20% DMA in saline [n=5]); 20 mg/kg PMX207 (in 20% Kleptose HPB [n=5]); or untreated (Control, n=5). Parasitemias were determined on days 5 and 7 via Giemsa-stained blood smears.

Statistical analyses

We analyzed the statistical significance of DV lysis with one-tailed paired Student's *t* tests. Mouse parasitemias were analyzed with a one-way ANOVA with Dunnett's post-hoc test. A Mantel-Cox log rank test was performed on the survival data, with a Bonferroni correction for multiple analyses. Significance was assigned to an alpha of 0.01 for DV lysis.

PF4 and C12 P. yoelii 17XNL mouse studies

These experiments were conducted with the assistance of Satish Mishra, Ph.D. in the laboratory of Photini Sinnis, M.D. at the Malaria Research Institute, Bloomberg School of

Public Health, Johns Hopkins University. Swiss Webster mice were infected with $2x10^5$ *P. yoelii* 17XNL parasitized erythrocytes in 200 µL of RPMI medium via intravenous injection. Following a standard 4-day Peters suppression test protocol (Knight and Peters, 1980), the treatment regimen began on day 1 (the same day the mice were infected) and mice were dosed once per day intravenously on days 1-3 with vehicle (20% DMA in saline [n=3] or 20% Kleptose HPB [n=2]); 10 mg/kg mPF4 (in saline [n=3], R&D systems); or 10 mg/kg C12 (in saline [n=4]). Parasitemias were determined on day 4 via Giemsa-stained blood smears.

Texas Red Dextran-loaded erythrocyte analysis of DV lysis

These studies were completed by Melanie G. Millholland at the University of Pennsylvania. Erythrocytes were lysed and resealed as described previously [94], in the presence of 10 µM Texas Red Dextran prior to challenge with synchronous magnet-purified cultures of *P. falciparum*-schizont stage parasites. Infected erythrocytes containing Texas Red Dextran were treated at 30 hpi with hPF4, C12, or smHDPs as previously described and imaged on a Leica DMI6000B epifluorescent microscope to assess lysis of the parasite DV, denoted by Texas Red Dextran dispersion throughout the parasite body. Infected Texas Red Dextran-loaded cells were also subjected to gametocytogenesis as previously described [95] and treated with hPF4 or PMX1207 at stage 2 prior to fluorescent microscopy analysis of DV lysis.

Protamine sulfate studies

These studies were completed by Melanie G. Millholland at the University of Pennsylvania. hPF4 immunofluorescence was assayed as described previously with pretreatment of cultures with 5 mM protamine sulfate or mock (DMSO) for 30 min prior to hPF4 treatment.

CHAPTER 3: Structure-Function Analysis of the Antimalarial Activity of Platelet Factor 4 and CCL20 Chemokines

3.1 Introduction

Malaria continues to be a global health burden with an estimated 207 million new cases leading to over 600,000 deaths in 2012; most of which were in children under the age of 5 (77%) [1]. New treatments are needed in the pipeline as resistance to the first-line therapy – artemisinin-based combination therapy (ACTs) – has emerged in Cambodia, threatening the control of Malaria worldwide [9]. Ideally, novel treatments will minimize resistance, though most approaches to develop therapeutics generate resistant parasites in the laboratory and field.

Malaria parasites are obligate intracellular pathogens with life cycles involving both sexual and asexual stages of growth, where the asexual phase is thought to be the cause of all clinical symptoms of malaria. The asexual phase for *Plasmodium sp*. involves the intracellular infection of erythrocytes. This chronic erythrocytic stage begins when extracellular parasites (merozoites), initially released from the liver, invade erythrocytes. Over the next 48 hours, internalized parasites differentiate (ring stage), metabolize vast amounts of hemoglobin (trophozoite stage) in the specialized digestive vacuole (DV), and replicate (schizont stage) to produce expanded populations of invasive merozoites that are released upon rupture of the host cell [11]. Parasites must interact and dramatically remodel their host cell to facilitate invasion, intracellular development, and avoid innate/adaptive host defenses to continue this lytic cycle. Therapeutic agents must necessarily kill the intracellular or extracellular forms of these parasites to cure the disease.

Antimicrobial peptides (AMPs) are small (2-8 kDa) molecules that are an important part of innate immunity [79]. AMPs have been shown to have activity against a broad-range of pathogens, including bacteria, fungi, viruses, and parasites [79, 96]. Though they vary greatly in amino acid sequence and structure, they are united by an amphipathic topology that is thought to be essential to their antimicrobial activity. AMPs kill by interacting with pathogen membranes and causing disruptions via permeabilization [97]. Over 1000 AMPs have been identified to date [19], and new classes of proteins with antimicrobial activity continue to be discovered.

Chemokines are small (8-12 kDa) chemotactic proteins that have roles in many cellular functions, including inflammation, development, angiogenesis, and immunity through their regulation of leukocyte cell trafficking [34-36]. There are roughly 50 human chemokines and 20 different transmembrane chemokine receptors have been identified [37]. Although they control many different functions, chemokines are remarkably structurally similar, consisting of an N-terminal loop necessary for receptor activation, a central domain comprised of 3 antiparallel β-strands that provide a stable scaffold, and a C-terminal α-helix that folds across the β-sheet to stabilize the overall structure (Figure 3.1). Virtually all chemokines have four conserved cysteines (two in the N-terminal loop, and 2 in the β-sheet) that form two essential disulfide bonds (Cys1-Cys3 and Cys2-Cys4). Chemokines are traditionally divided into four groups based on the positioning of the first two cysteines: C, CC, CXC, and CX_3C, where X is any non-cysteine amino acid [36, 37, 41].

Over the past decade, many chemokines have been shown to have direct antimicrobial activity, in addition to their role in immunity through leukocyte recruiting [40, 42-46]. Antimicrobial chemokines, which are expressed directly in the bloodstream, necessarily have low host toxicity. This is in contrast to classical AMPs, which are

typically expressed in phagocytes or on mucosa. Because chemokines have a highly conserved tertiary structure, examining the key structure-function relationships in antimicrobial chemokines may deconvolute their biological role in host defense, and may provide insights into new therapeutics against drug-resistant pathogens with minimal host toxicity.

We have previously shown that CXCL4/PF4 kills *P. falciparum* via selective lysis of the digestive vacuole [98]. Because antimicrobial chemokines share such similar topology, we hypothesized that other chemokines may also have antimalarial activity *in vitro*. As the amphipathic α-helical C-terminal domain of chemokines is the driving component of antimicrobial activity, a small screen of several CC and CXC chemokine C-terminal domains was performed against *P. falciparum* parasites.

3.2 Results and Discussion

Considering the similarity in structure of chemokines (Figure 3.1), and because the amphipathic α-helix is frequently the antimicrobial fragment, we hypothesized that several α-helices of chemokines could have antimalarial activity. We screened 4 α-helices from the CC and CXC groups against *P. falciparum* for antimalarial activity and hemolysis (Figure 3.2, Table 3.1). We previously determined that the helix of PF4, a CXC chemokine (CXCL4), was active against *P. falciparum* [98], and therefore included this peptide as a positive control. An additional CXC chemokine, CXCL8/IL8, with documented α-helical antimicrobial activity [99], was selected. Three CC-type chemokines with antimicrobial activity were also selected for the mini-screen: CCL5/RANTES [43], CCL13/MCP-4 [100], and CCL20/MIP-3α [76]. CCL13 helix was inactive, even at 250 μM, while the helices of CCL5 and IL8 showed moderate activity at the top concentration. All three were not hemolytic at 250 μM. Interestingly, the helix of

Figure 3.1

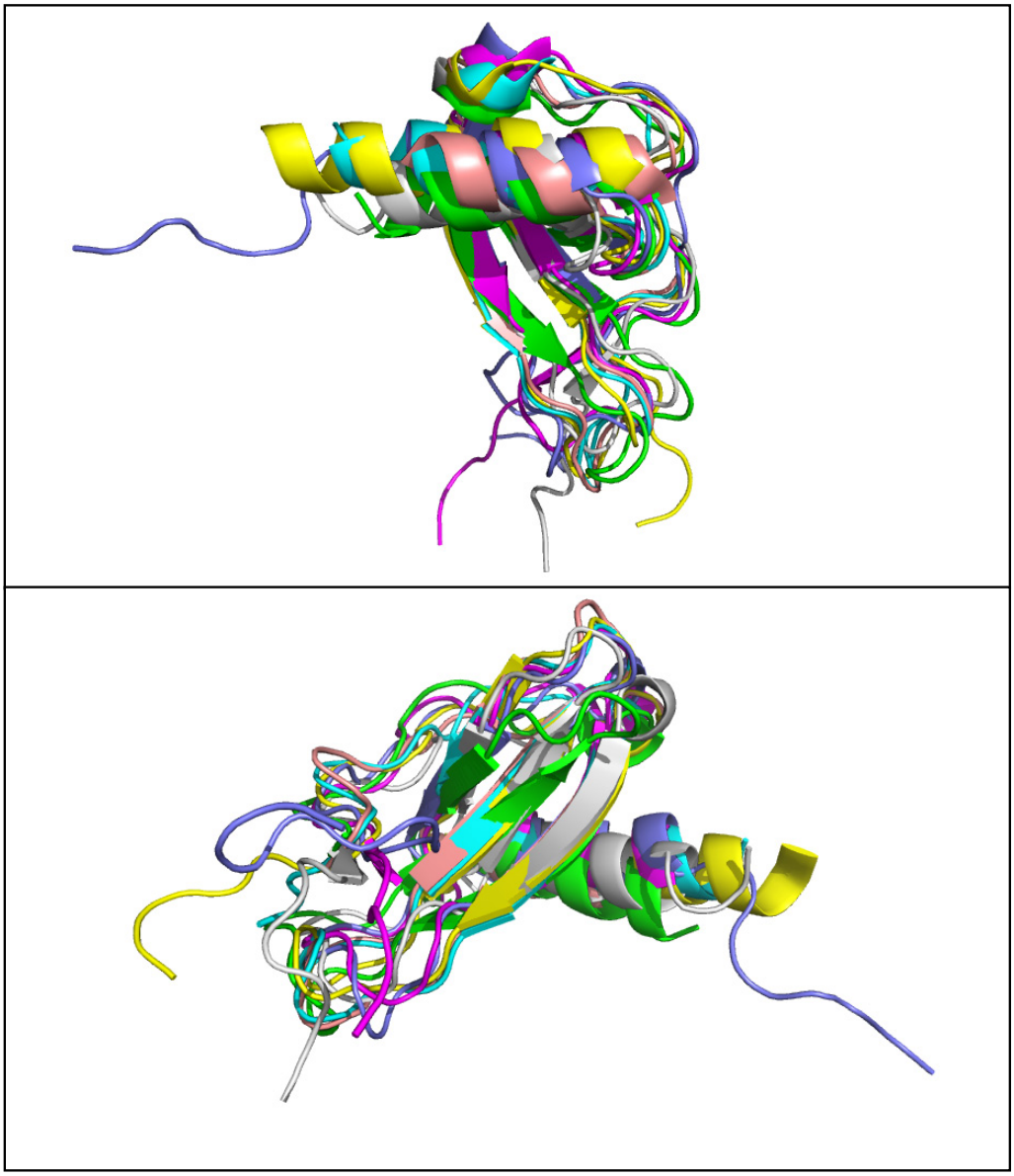

Figure 3.1: Chemokines have a similar tertiary structure. Seven chemokines were aligned using PyMOL, highlighting the similarities in the C-terminal α-helices (**top**), central β-sheet domains (**bottom**), as well as overall tertiary structure. CCL5 (RANTES, gray, PDB 1U4L); CCL13 (MCP-4, fuchsia, PDB 2RA4); CCL20 (MIP-3α, green, PDB 1M8A); CXCL4 (PF4, blue, PDB 1F9Q); CXCL7 (TC-1, purple, PDB 1BO0); CXCL8 (IL-8, yellow, PDB 1IL8); CXCL10 (IP-10, pink, PDB 1O7Z).

Figure 3.2

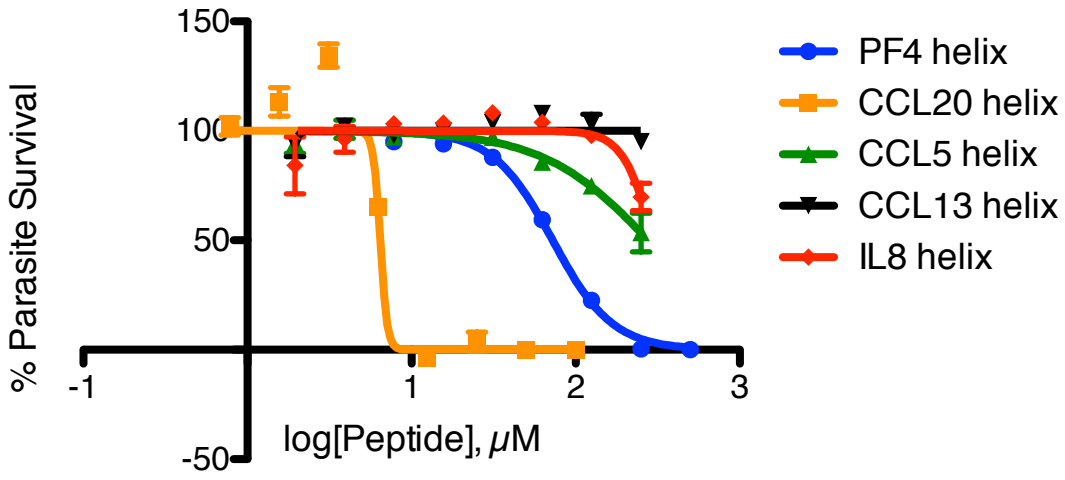

Figure 3.2: Mini-screen of chemokine helices against *P. falciparum*. Helical peptides based on the C-terminal α-helices of five chemokines, including three CC chemokines and two CXC chemokines were tested against *P. falciparum in vitro*. All have been previously shown to have AMP activity against bacteria. Shown are dose-response curves for all five peptides.

Table 3.1: Antimalarial and hemolytic activity of chemokine helices. IC50 and HC50 values are reported as means. HC50 is defined as the concentration at which there is 50% hemolysis. PF4 helix was tested with a max concentration of 500μM, n = 14; CCL20 helix was tested with a max concentration of 100μM, n = 6; all others were tested with a max concentration of 250μM n = 3. Sequences and number of amino acid residues are given for each peptide. Hemolysis was determined by measuring the absorbance at 541nm in the culture media.

Chemokine helix	Other name	IC50 (μM)	HC50 (μM)	HC50/IC50	# Residues	Sequence
CXCL4	PF4	74.9	269	3.6	12	LYKKIIKKLLES
CXCL8	IL8	>250	>250	N/A	19	KENWVQRVVEKFLKRAENS
CCL20	MIP-3α	6.8	31.3	4.6	19	KQTWVKYIVRLLSKKVKNM
CCL5	RANTES	250	>250	N/A	15	EKKWVREYINSLEMS
CCL13	MCP-4	>250	>250	N/A	13	KEKWVQNYMKHLG

CCL20 was potent against *P. falciparum* (IC50 of 6.8 μM). The hemolytic activity was also fairly potent, though the HC50/IC50 ratio was slightly improved compared to the PF4 helix (4.6 vs. 3.6, respectively).

PF4 has confirmed antimalarial activity via direct disruption of the parasite's digestive vacuole membrane [98, 101]. Because the C-terminal α-helix was necessary and sufficient to kill the parasites, and the full-length protein was also active (with ~14x increase in potency), we hypothesized that full-length CCL20 would retain antimalarial activity as well. CCL20 was slightly more potent than its helix (IC50 = 4.7 μM, Table 3.2), and surprisingly, was not hemolytic. CCL20 and its helix also killed *P. falciparum* via lysis of the DV (Figure 3.3). We next sought to explore the structure-function relationship of antimalarial activity and hemolysis in PF4 and CCL20 by testing a series of peptides based on truncations of each chemokine. We synthesized an additional 3 peptides for each PF4 and CCL20 based on portions of the various chemokine domains (Figure 3.4) via solid phase peptide synthesis (see section 3.3 Experimental Procedures). In peptides containing any unpaired cysteine residues, the cysteines were substituted to serine to prevent the formation of unwanted intra- or intermolecular disulfides that could result in polymerization.

We synthesized a peptide consisting of everything but the N-terminal chemokine receptor-activating loop, dubbed "chemokineless" peptide. We also synthesized a "long peptide," which is equivalent in length to several helical AMPs, such as melittin and magainin. The long peptide is comprised of the α-helix and a portion of the β-sheet domain to determine if even one β-strand would stabilize the helix and reduce hemolysis. Finally, we synthesized a peptide comprised of solely the central β-sheet domain. The N-terminal loop of chemokines is traditionally believed to control receptor activation, while the central β-sheet domain provides a stable scaffold, and the

Figure 3.3

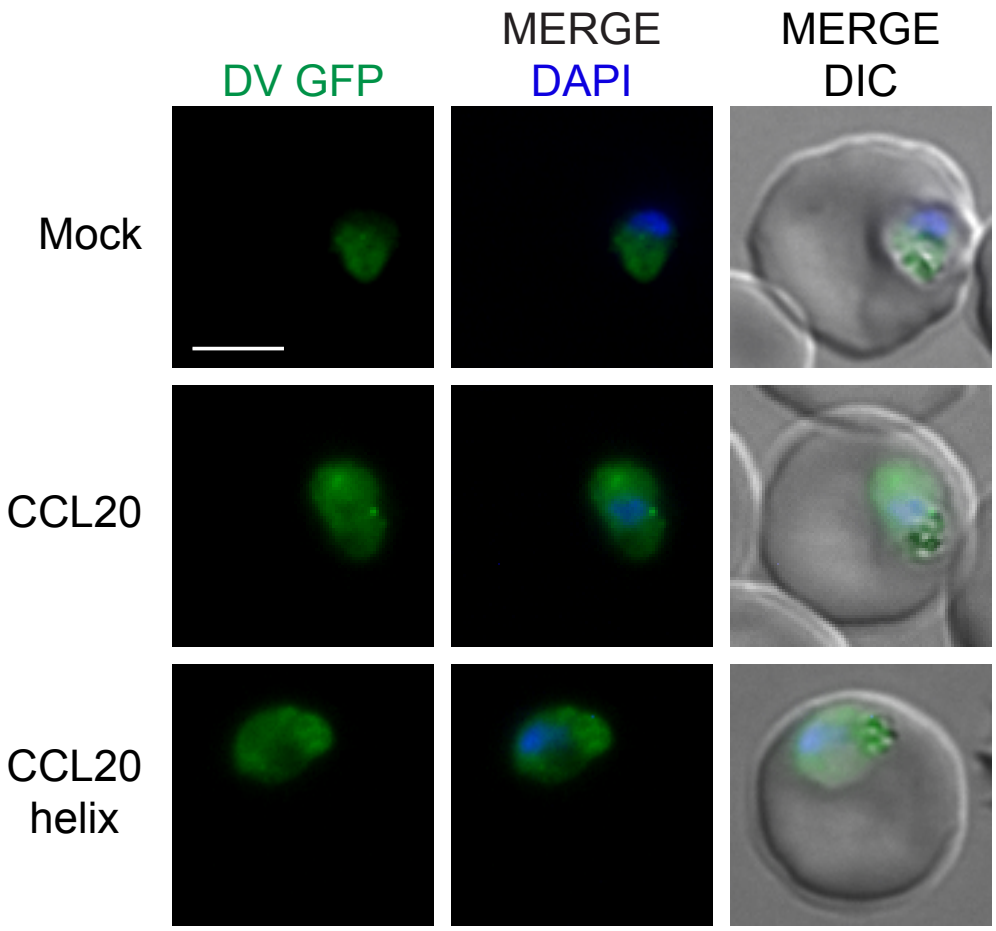

Figure 3.3: CCL20 and its helix also kill through a selective DV lysis mechanism. CCL20 (5 μM) and CCL20 helix (5 μM) treated PM-II-GFP parasites showed loss of DV integrity. Green: PM-II-GFP [DV]; blue: parasite nuclei.

Figure 3.4

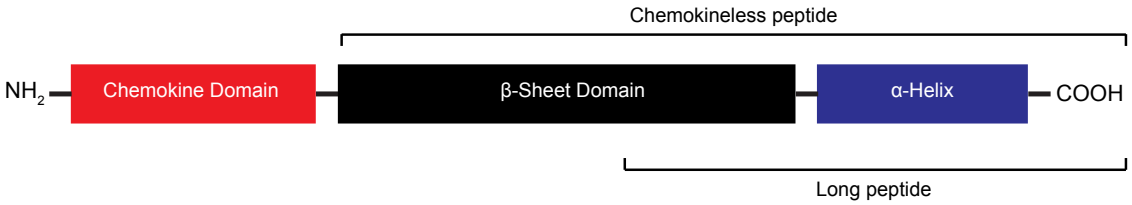

Figure 3.4: Domain analysis of PF4 and CCL20. Schematic of chemokine monomer depicting each domain and peptide truncations.

Table 3.2: IC50 and HC50 values for PF4, CCL20 and their corresponding truncated peptide series against *P. falciparum*. Values are reported as means. The α-helix is necessary and sufficient for activity against the parasites. The full protein confers protection against hemolysis.

	IC50 (μM)	HC50 (μM)	HC50/IC50
PF4	12.5	>100	N/A
Chemokineless PF4	37.5	120	3.2
PF4 β-sheet domain	>500	>500	N/A
PF4 long peptide	74.5	384	5.2
PF4 α-helix	74.9	269	3.6
CCL20	4.7	>100	N/A
Chemokineless CCL20	5.6	16.1	2.9
CCL20 β-sheet domain	>100	>100	N/A
CCL20 long peptide	6.3	27.0	4.3
CCL20 α-helix	6.8	31.3	4.6

amphipathic α-helix folds over the structure to add stability. However, we saw that any peptide lacking the N-terminal chemokine loop was less active and more hemolytic than the parent protein (Table 3.2).

To explain the differences in potency and hemolytic activity across the series of peptides, we examined the secondary structure character via circular dichroism spectroscopy (Figure 3.5, Tables 3.3,4). In the PF4 series, only the full-length protein retains any secondary structure in water (Figure 3.5A). The double minima at 208 nm and 222 nm indicate α-helical content. The secondary structure components were deconvoluted using CONTIN via DichroWeb (see 3.3 Experimental Procedures). In the CCL20 series, the full-length protein, the peptide lacking the N-terminal chemokine loop, and the β-sheet domain all displayed some α-helical character (Figure 3.5C). Upon addition of the helix-inducing trifluoroethanol (TFE, Figure 3.5B,D), all peptides showed helical character except for the PF4 β-sheet domain. Interestingly, the β-sheet domain of CCL20 was very helical with the addition of TFE (α_R = 0.25 and α_D = 0.21, Table 3.4).

Taken together with the structural data, the antimalarial activity of each series of peptides is dependent upon the presence of the C-terminal α-helix. Additionally, while it was previously believed that the α-helix folds over and provides stability to the overall structure of the chemokine, these data suggest that the N-terminal loop is also necessary to hold the structure together. Disulfide bridges are well known to confer stability in many types of proteins, including chemokines and chemokine receptors, and are often thought to be necessary for proper protein folding and function [102-104]. Therefore, without these disulfide bridges between the N-terminal loop and central β-sheet domain, the peptides are unlikely to be in their native conformations and have expected alterations in activity and hemolysis. If the peptides are unfolded or in the incorrect conformation, the α-helix may be able to blindly interact with any membrane it

Figure 3.5

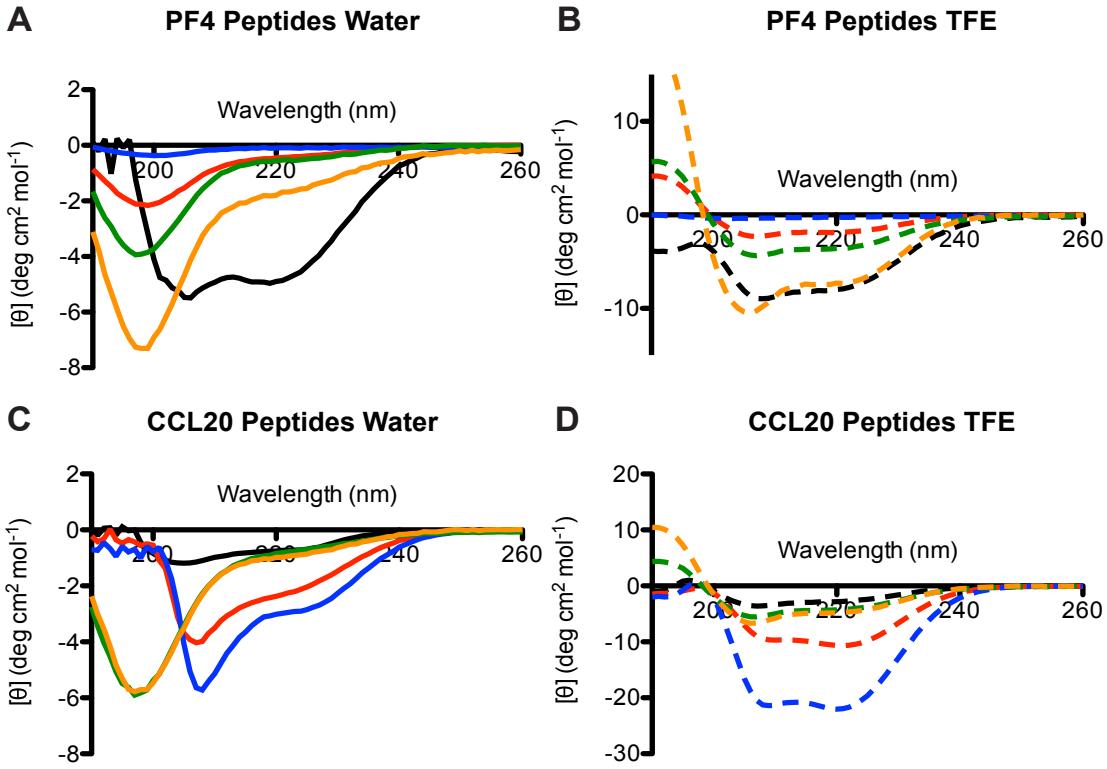

Figure 3.5: CD analysis of PF4 and CCL20 peptide series. Circular dichroism spectra of chemokines and peptides derived from domain truncations of PF4 and CCL20. Full-length protein, black; Chemokineless (CK-), red; β-sheet domain, blue; long peptide, green; α-helix, orange. The addition of TFE to induce helicity is denoted by the dotted lines in each graph. PF4 and peptides in water (**A**) and 50% TFE (**C**). CCL20 and peptides in water (**B**) and 50% TFE (**D**).

Table 3.3: Secondary structure data of PF4 and CCL20 series peptides in water. Secondary structure data were determined experimentally from independent CD spectra of each peptide as detailed in section 3.3 Experimental Procedures, and expressed as percent of structure for peptides in water. The indices R and D refer to regular and distorted structures, respectively; regular structures have a precise geometry, whereas distorted structures result from the finite size of the respective motifs.

	Helix		Strand			
Water	α_R	α_D	β_R	β_D	**Turn**	**Unordered**
PF4	0.03	0.09	0.20	0.11	0.23	0.34
CK- PF4	0.00	0.07	0.25	0.12	0.22	0.34
PF4 β-sheet	0.00	0.06	0.26	0.13	0.22	0.33
PF4 long peptide	0.00	0.07	0.25	0.12	0.22	0.35
PF4 helix	0.00	0.07	0.23	0.13	0.22	0.35
CCL20	0.00	0.06	0.25	0.13	0.22	0.33
CK- CCL20	0.04	0.09	0.22	0.12	0.22	0.32
CCL20 β-sheet	0.06	0.10	0.19	0.11	0.21	0.32
CCL20 long peptide	0.00	0.07	0.23	0.12	0.22	0.35
CCL20 helix	0.00	0.07	0.24	0.12	0.22	0.35

Table 3.4: Secondary structure data of PF4 and CCL20 series peptides in TFE. Secondary structure data were determined experimentally from independent CD spectra of each peptide as detailed in section 3.3 Experimental Procedures, and expressed as percent of structure for peptides in 50% TFE. The indices R and D refer to regular and distorted structures, respectively; regular structures have a precise geometry, whereas distorted structures result from the finite size of the respective motifs.

	Helix		Strand			
TFE	α_R	α_D	β_R	β_D	**Turn**	**Unordered**
PF4	0.09	0.11	0.18	0.09	0.20	0.34
CK- PF4	0.04	0.07	0.25	0.12	0.21	0.32
PF4 β-sheet	0.00	0.06	0.27	0.13	0.21	0.33
PF4 long peptide	0.06	0.08	0.23	0.11	0.20	0.32
PF4 helix	0.14	0.09	0.19	0.10	0.19	0.31
CCL20	0.03	0.09	0.22	0.11	0.22	0.34
CK- CCL20	0.12	0.14	0.12	0.08	0.20	0.35
CCL20 β-sheet	0.25	0.21	0.00	0.03	0.17	0.35
CCL20 long peptide	0.06	0.09	0.21	0.11	0.20	0.32
CCL20 helix	0.09	0.09	0.22	0.11	0.19	0.31

encounters, and disrupt it at high enough concentrations, relevant to the peptide's potency. We therefore conclude that the entire protein must be present, in its stabilized and folded context, to afford protection to the host cells.

Additionally, PF4 peptides show a great reduction in potency. This may be attributed to the fact that human PF4 exists naturally as a homotetramer, while human CCL20 is a monomer or a dimer at physiological conditions. These disulfide bridges between the N-terminal loop and central β-sheet domain are likely important for dimerization and tetramerization. Without the necessary quaternary structure, these peptides may not be interacting with the RBCs in the usual manner. It is believed that PF4 enters infected RBCs through interaction with the Duffy antigen [101], and in fact, conserved disulfides in the cysteine-rich *Plasmodium* Duffy Binding Like-domains (DBLs) are believed to be necessary for invasion [105]. Due to their highly conserved structural components, these antimicrobial chemokines may provide a unique and exciting scaffold from which to derive more potent antimalarial therapeutics.

3.3 Experimental Procedures

Parasite culture and IC50 determination

P. falciparum parasites were cultured in RPMI 1640 (Invitrogen) supplemented with Albumax II (Invitrogen). For synchronization, ring stage parasites were isolated by treating with 5% D-sorbitol in phosphate buffered saline at 37°C for 30 minutes [106]. For IC50 determinations, synchronized ring-stage parasites were plated at 0.5% parasitemia and 8% hematocrit in 96-well plates at a total volume of 50 µL. Serial dilutions of 2x concentration of the respective compound were added to the wells to bring the total volume up to 100 µL and 4% hematocrit. Compounds were assayed for a 72 h period, after which the cultures were fixed with a solution of 4% paraformaldehyde

and 0.08% glutaraldehyde in PBS. The cells were then permeabilized with 0.25% Triton X-100, and SYTOX Green Nucleic Acid Stain (Invitrogen) in PBS was added to a final concentration of 5 μM. DNA content, as an indicator of parasitemia, was analyzed on an Accuri C6 Flow Cytometer with C-Sampler. IC50 curves were generated using GraphPad Prism (GraphPad Software).

Assay for hemolysis

3D7 parasite-infected erythrocytes were cultured as described previously. Cultures were treated for 72 hours, and then assayed for hemolysis prior to fixing. Hemolysis was measured by removing 50 μL from each well (100 μL total in a 96-well plate) and transferring to a clear-bottom 96-well plate. Absorbance at 541 nm was measured and compared to a standard curve generated from Triton X-100-lysed erythrocytes (4% hematocrit serially diluted by 2).

Peptide synthesis

Peptides were synthesized via the solid phase method either by hand or on a CEM Liberty 1 Microwave Peptide Synthesizer at 0.092 mmol scales using Fmoc-Rink Amide resin (substitution level 0.3-0.6 meq/g; Chem-Impex International). Activation of Fmoc-amino acids (5-fold excess) was achieved with 2-(6-Chloro-1H-benzotriazole-1-yl)-1,1,3,3-tetramethylaminium hexafluorophosphate (HCTU) in the presence of 2-(N,N'-diisopropylamino) ethanol (DIPEA). The reaction solvent contains 100% *N*,*N*-Dimethylformamide (DMF, HPLC grade; Aldrich). Coupling, cleavage, and precipitation reagents were purchased from Sigma-Aldrich. Amino acids were purchased from Chem-Impex International. Side chain deprotection and simultaneous cleavage from the resin were carried out using a mixture of trifluoroacetic acid (TFA)/H_2O/Triisoproplysilane (TIPS) (46.5:2.5:1, v/v) at room temperature, for 3 hours. Crude peptide was obtained by

ether precipitation and purified by reverse-phase chromatography. The mass of all peptides was verified by ESI-MS (Agilent MSD G1956B). Analytical and preparative HPLC was performed using a C18 reverse-phase column on an Agilent 1200 series system (Agilent Technologies), with Hewlett Packard Chemstation software.

Fluorescence microscopy imaging of DV lysis

Erythrocytes infected with synchronous cultures of PMII-GFP expressing parasites were treated at 30 hours post invasion (hpi) with either 5 μM CCL20 or CCL20 helix and fixed after 5 min of treatment, stained with Hoechst and imaged by fluorescence microscopy.

Circular dichroism analysis

Peptide solutions were prepared at 50μM in water, and 25μM in 50% trifluoroethanol (TFE). Circular dichroism studies were conducted at 25˚C on an AVIV 410 spectropolarimeter equipped with a temperature control unit. Spectra were obtained from three averaged scans. Scans were conducted from 260 nm to 190 nm. Molar ellipticity was calculated via the formula $\theta = d/(l*N*c*10)$, where d = signal in degrees; l = path length (cm); N = # of amino acids; c = concentration (M). Percent α-helix, β-sheets, and turns were estimated using DichroWeb CONTIN [107].

CHAPTER 4: Conclusions and Future Directions

This work demonstrates an example of natural host defense against a pathogen that has affected humans since the dawn of man, and dissects not only how this host defense kills the parasite, but also translates this mechanism into a potential therapeutic. This natural defense is a class of proteins expressed in the bloodstream with a myriad of roles in homeostasis and inflammation, both through their abilities to affect cell trafficking and direct microbicidal activity. These proteins, called chemokines, have evolved to kill pathogens that they encounter without harming the host cells. This is likely due to their highly conserved tertiary structure, as the antimicrobial fragment alone has measurable toxicity to human red blood cells (RBCs), while the intact protein does not. These antimicrobial chemokines work through a direct membrane perturbation mechanism, which we demonstrate occurs specifically at the parasite digestive vacuole.

4.1 The identification of PF4 as an antimicrobial chemokine, and its translation to small molecule mimics of host defense peptides

Identification of PF4 as a natural antiparasitic

In this work we identified the human antimicrobial protein, PF4, as an antiparasitic molecule that kills *Plasmodium* parasites by lysing the parasite DV, a vital parasite organ responsible for digestion of host hemoglobin. Targeting the lysosome-like vesicles of protozoan parasites may be an evolutionarily selected mechanism for mammalian hosts to kill *Plasmodium* and other parasites (i.e. *T. brucei* [108]). How proteins such as PF4 enter host cells remains an open question, though uptake of human PF4 into the host erythrocyte seems to diminish following parasite DV lysis and parasite death, suggesting that perhaps an active, parasite-mediated mechanism allows entry of these HDP

molecules into the erythrocyte cytoplasm. McMorran *et al.* show evidence that this process is dependent upon PF4 interacting with the Duffy antigen on the RBC surface [101]. Since only infected cells are targeted, and parasite viability is important for uptake, this suggests that perhaps a parasite-derived or activated endocytosis-like mechanism could allow for large molecules such as PF4 to enter, while perhaps channels or pores could be responsible for small molecule uptake [109-111].

PF4 kills in an AMP-like fashion by targeting the DV membrane. AMPs are facially amphipathic, and in fact, the C-terminal peptide of PF4 requires amphipathicity for its antimalarial activity (Figure 2.12). Additionally, we have tested a natural variant of PF4, PF4var1, that has three point mutations in the C-terminus (P58→L, K66→E, L67→H) [112]. This creates a net charge of +1 on the cationic face of the PF4var1 helix vs. the +3 charge on wild-type PF4. Interestingly, we found that both parent PF4var1 and its C-terminal helical peptide were inactive against *P. falciparum in vitro* up to 10 μM and 500 μM, respectively (data not shown).

Unfortunately, controlling malaria is largely dependent upon finding low cost therapies, as the majority of the population affected is in the developing world. The high cost of production of biological therapeutics make chemokines an unlikely candidate for a malaria drug, though harnessing their mechanism of action in the small molecule mimics of host defense peptides (smHDPs) may avoid these issues while preserving the unique mechanism of action and safety. Additionally, these small molecules are more chemically tractable, and therefore may more closely fit the target product profile of malaria drugs in the pipeline. More investigation into the specificity of these molecules and proteins for the digest vacuole membrane is necessary, as well as resistance studies, development of analogues, and *in vivo* studies:

Testing PF4 and derivatives against model liposomes based on the composition of parasite digestive vacuolar membranes

To determine if PF4 selectively disrupts the DV membrane causing leakage of DV contents via direct membrane disruption, we will prepare model liposomes with similar lipid content to the parasite DV membrane and assess membrane compromise upon PF4 treatment. We will assess the composition of parasite DV membranes via the isolation of this organelle from whole parasites [113] and analysis of lipid content within these purified preparations via liquid chromatography-mass spectrometry (LC-MS) [114]. Synthetic liposomes would be prepared with the corresponding phospholipid composition of DV membranes, and then treated with PF4, its helix, or the synthetic small molecule mimics. Liposomes comprised of different phospholipids would serve as a control. Lysis of these DV-based liposomes would suggest that PF4 and its derivatives are targeting the membrane directly, and not a protein target. If there is no preference for the DV-based membranes, perhaps the specificity of lysing this particular organelle would be more dependent upon the uptake mechanism targeting these compounds to the DV than dependent upon the membranes themselves.

Investigating the selective entry of PF4 and smAMPs into infected erythrocytes

The membrane of the infected erythrocyte is vastly different than their uninfected counterparts. The maturation of the malaria parasite causes loss of the normal discoid shape, perturbations in the mechanical and adhesive properties of the cell, and alterations in the state of phosphorylation of the erythrocyte membrane skeletal proteins [115]. The increased adhesion to endothelial cells in *P. falciparum*-infected erythrocytes is affected by erythrocyte membrane protein1 (PfEMP1) binding to ICAM-1, PECAM-1, and enhanced phosphatidyl serine presentation on the red blood cell surface [116]. Our

preliminary data shows that only infected erythrocytes take up PF4 and that pretreatment with protamine sulfate blocks both entry and activity of PF4 against *P. falciparum*. We therefore hypothesize that initial interaction between PF4 and the parasitized erythrocyte is electrostatic and involves binding to negatively charged molecules on the surface. Considering that the erythrocyte surface proteins such as the glycophorins are rich with sialic acid, we can directly test whether sialic acid is involved in the initial binding events by specifically removing it using neuraminidase.

Another possible explanation for the uptake of PF4, and possibly of smAMPs, is the new permeability pathways (NPP). Erythrocytes have a myriad of membrane transport proteins including channels and porters that mediate the transfer of solutes in and out of the cell. These continue to function after infection of a malaria parasite, and undergo further changes some time after invasion to aide in the parasite's ability to gain nutrients [115], such as low molecular weight solutes including sugars, amino acids, nucleosides, vitamins, and monovalent anions and cations [117]. Certain inhibitors of the NPP have been identified, and would therefore be useful tools in determining if the NPP play a role in the uptake of PF4 and smAMPs into parasitized erythrocytes.

Generating PF4-resistant parasites

Since AMP-mediated cell death via membrane perturbation does not rely upon a specific receptor or intracellular protein target, cellular resistance to compounds that kill through membrane perturbation should be difficult to generate. In order to test this hypothesis, we will attempt to generate *P. falciparum* lines that are resistant to PF4. Chloroquine-resistant parasites (Dd2) will be serially passaged in dilutions of our experimentally determined PF4 IC50 (0.25 x IC50, 0.5 x IC50, and the full IC50 concentration) and resulting PF4 IC50 values will be determined at each passage. As a control, parallel

cultures will also be exposed to 0.5 x IC50 concentration of pyrimethamine, a well-established antiparasitic for which resistance has been reported. This will be carried out over a time period of at least 6 months. If resistant lines are successfully generated, tiling microarrays will be used to determine any genes that contribute to resistance. Resistance would indicate that PF4 might not be acting solely via membrane disruption. Conversely, if parasites fail to generate resistance to these compounds, this class of compounds may have potential as antimalarials that may elicit minimal parasite resistance.

Exploration of the in vivo role of PF4 in malaria

Due to the conflicting reports of PF4 in the pathogenesis of malaria, further investigations are necessary. We report a positive effect that PF4 reduces parasitemia in a non-lethal murine model of malaria. Srivastava *et al.* show that the presence of PF4 may negatively impact the pathogenesis and prognosis of cerebral malaria. This effect is likely through the chemokine domain [62]. As such, we hypothesize that we can harness the positive antiparasitic effects of PF4 and avoid exacerbating the cerebral symptomology by mutating the N-terminal chemokine receptor-activating loop. A similar chemokine-receptor binding and activating structure-function study has previously been explored for CCL19/MIP3-β [118], and an endogenous mutant of CCL5/RANTES has been discovered to bind to, yet not active two of its receptors, CCR1 and CCR3 [119]. Although PF4 does not have a known endogenous receptor, it does interact with the alternative splice variant CXCR3B. Cells expressing this splice variant can be used to assess whether PF4 containing a mutated N-terminus is no longer able to interact with this receptor.

After confirming *in vitro* activity of this mutated PF4 against *P. falciparum*, we would test this in both the severe anemic model of malaria using *P. yoelii* (which causes disease in the peripheral vasculature and organs) versus a model of experimental cerebral malaria caused by *P. berghei* ANKA (which causes pathology in the brain of mice). Both PF4 knockout mice [64] and wild-type littermates will be utilized to tease apart the effects of endogenous PF4 and the N-terminal chemokine mutant. Mice of each genotype will be infected with $1x10^4$ erythrocytes from mice infected with either *P. berghei* ANKA, or *P. yoelii.* If the exogenously added chemokine-mutated PF4 is able to reduce parasitemia and improve survival in the infected mice, this would highly suggest that the negative effects of PF4 are in fact mediated through its role as a chemokine. This would also support that the direct antimicrobial activity is useful as a potential therapeutic, though any potential biologic therapeutic would likely require IV infusion, and would therefore not be viable as a prophylactic and may be too expensive to be a successful antimalarial.

4.2 Exploration of the structure-function relationship of antimicrobial chemokine activity

Upon initial discovery that PF4 was active against *Plasmodium* parasites, we wondered if other similar proteins would also be antimalarial. We then hypothesized that the highly conserved tertiary structure among chemokines could lead to potential other naturally antiparasitic proteins, and first selected chemokines that had demonstrated antimicrobial activity. After screening the active portion of the proteins, the amphipathic C-terminal α-helix, we found that CCL20 was also active against *P. falciparum* in the low micromolar range. We then sought to explore which domains modulate activity against parasites, and which domains reduce toxicity against host cell. Surprisingly, we found that

hemolysis was ablated only with the intact protein, and that the N-terminal loop previously thought to only interact with chemokine receptors, likely is necessary to stabilize the whole structure. We seek to further illustrate this concept through the following studies:

Cysteine mutants of PF4 and CCL20

The key conserved features across all classes of chemokines are the cysteine residues present in the N-terminal loop. These two cysteines are either side by side (CC chemokines), or separated by any other amino acid (CXC and CX_3C chemokines), and they form two specific disulfide bonds with two other cysteines in the central β-sheet domain (Cys1-3, Cys2-4) [36, 37, 41]. While most of the literature suggests that this N-terminal loop is only necessary to recognize and activate the chemokine receptor, our data shows that this loop also likely stabilizes the overall structure. This is indicated by the antimalarial activity being preserved in any PF4 or CCL20 peptide that contains the amphipathic C-terminal α-helix, but only the parent proteins are not hemolytic at >5-fold the IC50. One way to test this hypothesis would be to remove each disulfide bond, as well as both, by replacing the cysteine residues with serine residues in both PF4 and CCL20. Another option would be to simply reduce each bond with the addition of DTT or TCEP. After destruction of the disulfide bonds, the antimalarial activity, as well as hemolytic activity, would be assessed. If our hypothesis is correct, these mutants and reduced peptides should retain most, if not all, potency against the parasite, but they may show some hemolysis compared to the wild type.

Generating antimicrobial peptide chimeras

We show evidence that the intact structure of these antimicrobial chemokines is necessary to protect against toxicity to host cells, measured via hemolysis. Therefore,

we hypothesize that potent and hemolytic helical antimicrobial peptides may be made "safe" by placing them within the chemokine scaffold. Two well characterized AMPs – melittin and magainin – will be placed within the PF4 and CCL20 scaffold to determine if the activity is retained while hemolysis is ablated. Melittin is a 26 amino acid peptide from bee venom, and is a highly lytic molecule. It is comprised of two α-helices with an overall bent configuration [120]. Magainins are a class of AMPs from the skin of *Xenopus laevis* frogs with a broad range of activity against microbes [121]. Magainin 2 is a 23 amino acid α-helical peptide [31], and surprisingly is much less hemolytic than melittin [121].

In order to show that the chemokine scaffold, stabilized by the disulfide bridges between the N-terminal loop and central β-sheet domain, is indeed protective, the "long peptide" of PF4 and CCL20 will each be replaced by the hemolytic melittin, as well as magainin 2. PF4/CCL20 and CCL20/PF4 chimeras will also be generated to show that the activity remains within these highly conserved tertiary structures. All chimeras will be expressed recombinantly in a secretable Drosophila S2 system. The expected outcomes are the PF4/CCL20 and CCL20/PF4 chimeras should retain activity, as the sequence itself does not matter, but the overall structure does. The melittin hybrids should be potent against *P. falciparum* (IC50 of melittin ~1 μM), though the hemolytic activity should be ablated or greatly decreased. The magainin 2 chimeras should also retain activity, implying that the chemokine scaffold may provide an interesting lead for non-toxic AMP therapeutics.

Development of peptidomimetics based on the α-helices of antimicrobial chemokines

In an effort to further understand the interaction of PF4 and CCL20 antimalarial activity and generate tools for use for *in vivo* mouse malaria studies, we will synthesize an array

of derivatives based on the α-helical domain of PF4 and CCL20 via standard synthetic routes. The underlying principle to the generation of these tool compounds is to increase their stability and potency *in vitro* and *in vivo* while maintaining low host toxicity. Although the full proteins have no hemolysis and IC50s in the low micromolar range, utilizing small, synthetic compounds may prove to be more viable for potential malaria therapeutics. We can optimize the antimalarial activity of this molecule using a variety of approaches, including the use of D-amino acids, replacement of neutral residues with helix promoting non-natural amino acids, stabilization of the helical confirmation to render the peptides less susceptible to proteolysis, or the synthesis of helix polymers.

BIBLIOGRAPHY

1. Organization, W.H., *World Malaria Report 2013*. 2013, World Health Organization.

2. Chima, R.I., C.A. Goodman, and A. Mills, *The economic impact of malaria in Africa: a critical review of the evidence.* Health Policy, 2003. **63**(1): p. 17-36.

3. *CDC - Malaria - About Malaria - Disease*. 2010 Feb 8, 2010 [cited 2014 Jan 9]; Available from: http://www.cdc.gov/malaria/about/disease.html.

4. Weatherall, D.J., et al., *Malaria and the red cell.* Hematology Am Soc Hematol Educ Program, 2002: p. 35-57.

5. El-Moamly, A., *Malaria elimination: needs assessment and priorities for the future.* J Infect Dev Ctries, 2013. **7**(11): p. 769-80.

6. White, N.J., *A vaccine for malaria.* N Engl J Med, 2011. **365**(20): p. 1926-7.

7. Mita, T., K. Tanabe, and K. Kita, *Spread and evolution of Plasmodium falciparum drug resistance.* Parasitol Int, 2009. **58**(3): p. 201-9.

8. Klonis, N., et al., *Artemisinin activity against Plasmodium falciparum requires hemoglobin uptake and digestion.* Proc Natl Acad Sci U S A, 2011. **108**(28): p. 11405-10.

9. Dondorp, A.M., et al., *Artemisinin resistance in Plasmodium falciparum malaria.* N Engl J Med, 2009. **361**(5): p. 455-67.

10. Burrows, J.N., et al., *Designing the next generation of medicines for malaria control and eradication.* Malar J, 2013. **12**: p. 187.

11. Wirth, D.F., *Biological revelations.* Nature, 2002. **419**(6906): p. 495-6.

12. Francis, S.E., D.J. Sullivan, Jr., and D.E. Goldberg, *Hemoglobin metabolism in the malaria parasite Plasmodium falciparum.* Annu Rev Microbiol, 1997. **51**: p. 97-123.

13. Loria, P., et al., *Inhibition of the peroxidative degradation of haem as the basis of action of chloroquine and other quinoline antimalarials.* Biochem J, 1999. **339 (Pt 2)**: p. 363-70.

14. Rosenthal, P.J. and S.R. Meshnick, *Hemoglobin catabolism and iron utilization by malaria parasites.* Mol Biochem Parasitol, 1996. **83**(2): p. 131-9.

15. Abu Bakar, N., et al., *Digestive-vacuole genesis and endocytic processes in the early intraerythrocytic stages of Plasmodium falciparum.* J Cell Sci, 2010. **123**(Pt 3): p. 441-50.

16. Hancock, R.E. and R. Lehrer, *Cationic peptides: a new source of antibiotics.* Trends Biotechnol, 1998. **16**(2): p. 82-8.

17. Finlay, B.B. and R.E. Hancock, *Can innate immunity be enhanced to treat microbial infections?* Nat Rev Microbiol, 2004. **2**(6): p. 497-504.

18. Tossi, A., L. Sandri, and A. Giangaspero, *Amphipathic, alpha-helical antimicrobial peptides.* Biopolymers, 2000. **55**(1): p. 4-30.

19. Seshadri Sundararajan, V., et al., *DAMPD: a manually curated antimicrobial peptide database.* Nucleic Acids Res, 2012. **40**(Database issue): p. D1108-12.

20. Hancock, R.E. and H.G. Sahl, *Antimicrobial and host-defense peptides as new anti-infective therapeutic strategies.* Nat Biotechnol, 2006. **24**(12): p. 1551-7.

21. Som, A., et al., *Synthetic mimics of antimicrobial peptides.* Biopolymers, 2008. **90**(2): p. 83-93.

22. Pouny, Y., et al., *Interaction of antimicrobial dermaseptin and its fluorescently labeled analogues with phospholipid membranes.* Biochemistry, 1992. **31**(49): p. 12416-23.

23. Christensen, B., et al., *Channel-forming properties of cecropins and related model compounds incorporated into planar lipid membranes.* Proc Natl Acad Sci U S A, 1988. **85**(14): p. 5072-6.

24. Ludtke, S., K. He, and H. Huang, *Membrane thinning caused by magainin 2.* Biochemistry, 1995. **34**(51): p. 16764-9.

25. Matsuzaki, K., et al., *Interactions of an antimicrobial peptide, magainin 2, with outer and inner membranes of Gram-negative bacteria.* Biochim Biophys Acta, 1997. **1327**(1): p. 119-30.

26. Matsuzaki, K., et al., *An antimicrobial peptide, magainin 2, induced rapid flip-flop of phospholipids coupled with pore formation and peptide translocation.* Biochemistry, 1996. **35**(35): p. 11361-8.

27. Scott, R.W., W.F. DeGrado, and G.N. Tew, *De novo designed synthetic mimics of antimicrobial peptides.* Curr Opin Biotechnol, 2008. **19**(6): p. 620-7.

28. Patrzykat, A., et al., *Sublethal concentrations of pleurocidin-derived antimicrobial peptides inhibit macromolecular synthesis in Escherichia coli.* Antimicrob Agents Chemother, 2002. **46**(3): p. 605-14.

29. Mosca, D.A., et al., *IB-367, a protegrin peptide with in vitro and in vivo activities against the microflora associated with oral mucositis.* Antimicrob Agents Chemother, 2000. **44**(7): p. 1803-8.

30. Ge, Y., et al., *In vitro antibacterial properties of pexiganan, an analog of magainin.* Antimicrob Agents Chemother, 1999. **43**(4): p. 782-8.

31. Tew, G.N., et al., *De novo design of biomimetic antimicrobial polymers.* Proc Natl Acad Sci U S A, 2002. **99**(8): p. 5110-4.

32. Liu, D., et al., *Nontoxic membrane-active antimicrobial arylamide oligomers.* Angew Chem Int Ed Engl, 2004. **43**(9): p. 1158-62.

33. M. Harbut, L., D., Scott, R., Greenbaum, D.C. in *ICAAC*. 2008. Washington, DC.

34. Baggiolini, M., *Chemokines and leukocyte traffic.* Nature, 1998. **392**(6676): p. 565-8.

35. Rollins, B.J., *Chemokines.* Blood, 1997. **90**(3): p. 909-28.

36. Yang, D., et al., *Many chemokines including CCL20/MIP-3alpha display antimicrobial activity.* J Leukoc Biol, 2003. **74**(3): p. 448-55.

37. Allen, S.J., S.E. Crown, and T.M. Handel, *Chemokine: receptor structure, interactions, and antagonism.* Annu Rev Immunol, 2007. **25**: p. 787-820.

38. Zimmermann, N., et al., *Chemokines in asthma: cooperative interaction between chemokines and IL-13.* J Allergy Clin Immunol, 2003. **111**(2): p. 227-42; quiz 243.

39. Esche, C., C. Stellato, and L.A. Beck, *Chemokines: key players in innate and adaptive immunity.* J Invest Dermatol, 2005. **125**(4): p. 615-28.

40. Nguyen, L.T. and H.J. Vogel, *Structural perspectives on antimicrobial chemokines.* Front Immunol, 2012. **3**: p. 384.

41. Fernandez, E.J. and E. Lolis, *Structure, function, and inhibition of chemokines.* Annu Rev Pharmacol Toxicol, 2002. **42**: p. 469-99.

42. Yeaman, M.R., *The role of platelets in antimicrobial host defense.* Clin Infect Dis, 1997. **25**(5): p. 951-68; quiz 969-70.

43. Tang, Y.Q., M.R. Yeaman, and M.E. Selsted, *Antimicrobial peptides from human platelets.* Infect Immun, 2002. **70**(12): p. 6524-33.

44. Cole, A.M., et al., *Cutting edge: IFN-inducible ELR- CXC chemokines display defensin-like antimicrobial activity.* J Immunol, 2001. **167**(2): p. 623-7.

45. Krijgsveld, J., et al., *Thrombocidins, microbicidal proteins from human blood platelets, are C-terminal deletion products of CXC chemokines.* J Biol Chem, 2000. **275**(27): p. 20374-81.

46. Yeaman, M.R., et al., *Modular determinants of antimicrobial activity in platelet factor-4 family kinocidins.* Biochim Biophys Acta, 2007. **1768**(3): p. 609-19.

47. Pain, A., et al., *Platelet-mediated clumping of Plasmodium falciparum-infected erythrocytes is a common adhesive phenotype and is associated with severe malaria.* Proc Natl Acad Sci U S A, 2001. **98**(4): p. 1805-10.

48. de Mast, Q., et al., *Thrombocytopenia and release of activated von Willebrand Factor during early Plasmodium falciparum malaria.* J Infect Dis, 2007. **196**(4): p. 622-8.

49. Mohanty, D., et al., *Fibrinolysis, inhibitors of blood coagulation, and monocyte derived coagulant activity in acute malaria.* Am J Hematol, 1997. **54**(1): p. 23-9.

50. Gimenez, F., et al., *Tumor necrosis factor alpha in the pathogenesis of cerebral malaria.* Cell Mol Life Sci, 2003. **60**(8): p. 1623-35.

51. Goodier, M.R., et al., *Cytokine profiles for human V gamma 9+ T cells stimulated by Plasmodium falciparum.* Parasite Immunol, 1995. **17**(8): p. 413-23.

52. Krupka, M., et al., *Mild Plasmodium falciparum Malaria following an Episode of Severe Malaria Is Associated with Induction of the Interferon Pathway in Malawian Children.* Infect Immun, 2012. **80**(3): p. 1150-5.

53. Rocca, B. and G.A. FitzGerald, *Simply read: erythrocytes modulate platelet function. Should we rethink the way we give aspirin?* Circulation, 1997. **95**(1): p. 11-3.

54. McMorran, B.J., et al., *Platelets kill intraerythrocytic malarial parasites and mediate survival to infection.* Science, 2009. **323**(5915): p. 797-800.

55. Moerman, F., B. Colebunders, and U. D'Alessandro, *Thrombocytopenia in African children can predict the severity of malaria caused by Plasmodium falciparum and the prognosis of the disease.* Am J Trop Med Hyg, 2003. **68**(4): p. 379; author reply 380-1.

56. Cox, D. and S. McConkey, *The role of platelets in the pathogenesis of cerebral malaria.* Cell Mol Life Sci, 2010. **67**(4): p. 557-68.

57. Wassmer, S.C., et al., *Platelet-induced clumping of Plasmodium falciparum-infected erythrocytes from Malawian patients with cerebral malaria-possible modulation in vivo by thrombocytopenia.* J Infect Dis, 2008. **197**(1): p. 72-8.

58. Brandt, E., et al., *Platelet-derived CXC chemokines: old players in new games.* Immunol Rev, 2000. **177**: p. 204-16.

59. Lasagni, L., et al., *An alternatively spliced variant of CXCR3 mediates the inhibition of endothelial cell growth induced by IP-10, Mig, and I-TAC, and acts as functional receptor for platelet factor 4.* J Exp Med, 2003. **197**(11): p. 1537-49.

60. Loscalzo, J., B. Melnick, and R.I. Handin, *The interaction of platelet factor four and glycosaminoglycans.* Arch Biochem Biophys, 1985. **240**(1): p. 446-55.

61. Lambert, M.P., B.S. Sachais, and M.A. Kowalska, *Chemokines and thrombogenicity.* Thromb Haemost, 2007. **97**(5): p. 722-9.

62. Srivastava, K., et al., *Platelet factor 4 mediates inflammation in experimental cerebral malaria.* Cell Host Microbe, 2008. **4**(2): p. 179-87.

63. Scheuerer, B., et al., *The CXC-chemokine platelet factor 4 promotes monocyte survival and induces monocyte differentiation into macrophages.* Blood, 2000. **95**(4): p. 1158-66.

64. Eslin, D.E., et al., *Transgenic mice studies demonstrate a role for platelet factor 4 in thrombosis: dissociation between anticoagulant and antithrombotic effect of heparin.* Blood, 2004. **104**(10): p. 3173-80.

65. Rauova, L., et al., *Role of platelet surface PF4 antigenic complexes in heparin-induced thrombocytopenia pathogenesis: diagnostic and therapeutic implications.* Blood, 2006. **107**(6): p. 2346-53.

66. Koenen, R.R., et al., *Disrupting functional interactions between platelet chemokines inhibits atherosclerosis in hyperlipidemic mice.* Nat Med, 2009. **15**(1): p. 97-103.

67. Lambert, M.P., et al., *Platelet factor 4 is a negative autocrine in vivo regulator of megakaryopoiesis: clinical and therapeutic implications.* Blood, 2007. **110**(4): p. 1153-60.

68. Haldar, K., et al., *Malaria: mechanisms of erythrocytic infection and pathological correlates of severe disease.* Annu Rev Pathol, 2007. **2**: p. 217-49.

69. Bruzzone, R., et al., *Infectious diseases of the nervous system and their impact in developing countries.* PLoS Pathog, 2009. **5**(2): p. e1000199.

70. White, N.J., et al., *The murine cerebral malaria phenomenon.* Trends Parasitol, 2009. **26**(1): p. 11-5.

71. Hosokawa, Y., et al., *Macrophage inflammatory protein 3alpha-CC chemokine receptor 6 interactions play an important role in CD4+ T-cell accumulation in periodontal diseased tissue.* Clin Exp Immunol, 2002. **128**(3): p. 548-54.

72. Kleeff, J., et al., *Detection and localization of Mip-3alpha/LARC/Exodus, a macrophage proinflammatory chemokine, and its CCR6 receptor in human pancreatic cancer.* Int J Cancer, 1999. **81**(4): p. 650-7.

73. Ruth, J.H., et al., *Role of macrophage inflammatory protein-3alpha and its ligand CCR6 in rheumatoid arthritis.* Lab Invest, 2003. **83**(4): p. 579-88.

74. Liao, F., et al., *STRL22 is a receptor for the CC chemokine MIP-3alpha.* Biochem Biophys Res Commun, 1997. **236**(1): p. 212-7.

75. Yang, D., et al., *Beta-defensins: linking innate and adaptive immunity through dendritic and T cell CCR6.* Science, 1999. **286**(5439): p. 525-8.

76. Hoover, D.M., et al., *The structure of human macrophage inflammatory protein-3alpha /CCL20. Linking antimicrobial and CC chemokine receptor-6-binding activities with human beta-defensins.* J Biol Chem, 2002. **277**(40): p. 37647-54.

77. Chan, D.I., et al., *Human macrophage inflammatory protein 3alpha: protein and peptide nuclear magnetic resonance solution structures, dimerization, dynamics, and anti-infective properties.* Antimicrob Agents Chemother, 2008. **52**(3): p. 883-94.

78. Gething, P.W., et al., *A new world malaria map: Plasmodium falciparum endemicity in 2010.* Malar J, 2011. **10**: p. 378.

79. Zasloff, M., *Antimicrobial peptides of multicellular organisms.* Nature, 2002. **415**(6870): p. 389-95.

80. Matsuzaki, K., et al., *Translocation of a channel-forming antimicrobial peptide, magainin 2, across lipid bilayers by forming a pore.* Biochemistry, 1995. **34**(19): p. 6521-6.

81. Kowalska, M.A., L. Rauova, and M. Poncz, *Role of the platelet chemokine platelet factor 4 (PF4) in hemostasis and thrombosis.* Thromb Res, 2010. **125**(4): p. 292-6.

82. Burkhard, B., *Rationalizing the membrane interactions of cationic amphipathic antimicrobial peptides by their molecular shape.* Current Opinion in Colloid & Interface Science, 2009. **14**(5): p. 349-355.

83. Westerhoff, H.V., et al., *Magainins and the disruption of membrane-linked free-energy transduction.* Proc Natl Acad Sci U S A, 1989. **86**(17): p. 6597-601.

84. Lehrer, R.I., et al., *Interaction of human defensins with Escherichia coli. Mechanism of bactericidal activity.* J Clin Invest, 1989. **84**(2): p. 553-61.

85. Klemba, M., et al., *Trafficking of plasmepsin II to the food vacuole of the malaria parasite Plasmodium falciparum.* J Cell Biol, 2004. **164**(1): p. 47-56.

86. Easton, D.M., et al., *Potential of immunomodulatory host defense peptides as novel anti-infectives.* Trends Biotechnol, 2009. **27**(10): p. 582-90.

87. Mensa, B., et al., *Antibacterial mechanism of action of arylamide foldamers.* Antimicrob Agents Chemother, 2011. **55**(11): p. 5043-53.

88. Knight, D.J. and W. Peters, *The antimalarial activity of N-benzyloxydihydrotriazines. I. The activity of clociguanil (BRL 50216) against rodent malaria, and studies on its mode of action.* Ann Trop Med Parasitol, 1980. **74**(4): p. 393-404.

89. Trager, W. and J.B. Jensen, *Human malaria parasites in continuous culture.* Science, 1976. **193**(4254): p. 673-5.

90. del Pilar Crespo, M., et al., *Artemisinin and a series of novel endoperoxide antimalarials exert early effects on digestive vacuole morphology.* Antimicrob Agents Chemother, 2008. **52**(1): p. 98-109.

91. Ortyn, W.E., et al., *Extended depth of field imaging for high speed cell analysis.* Cytometry A, 2007. **71**(4): p. 215-31.

92. Muskavitch, M.A., N. Barteneva, and M.J. Gubbels, *Chemogenomics and parasitology: small molecules and cell-based assays to study infectious processes.* Comb Chem High Throughput Screen, 2008. **11**(8): p. 624-46.

93. Zhang, J.H., T.D. Chung, and K.R. Oldenburg, *A Simple Statistical Parameter for Use in Evaluation and Validation of High Throughput Screening Assays.* J Biomol Screen, 1999. **4**(2): p. 67-73.

94. Chandramohanadas, R., et al., *Apicomplexan parasites co-opt host calpains to facilitate their escape from infected cells.* Science, 2009. **324**(5928): p. 794-7.

95. Fivelman, Q.L., et al., *Improved synchronous production of Plasmodium falciparum gametocytes in vitro.* Mol Biochem Parasitol, 2007. **154**(1): p. 119-23.

96. Ganz, T. and R.I. Lehrer, *Antimicrobial peptides of vertebrates.* Curr Opin Immunol, 1998. **10**(1): p. 41-4.

97. Haney, E.F., et al., *Induction of non-lamellar lipid phases by antimicrobial peptides: a potential link to mode of action.* Chem Phys Lipids, 2010. **163**(1): p. 82-93.

98. Love, M.S., et al., *Platelet factor 4 activity against P. falciparum and its translation to nonpeptidic mimics as antimalarials.* Cell Host Microbe, 2012. **12**(6): p. 815-23.

99. Bjorstad, A., et al., *Interleukin-8-derived peptide has antibacterial activity.* Antimicrob Agents Chemother, 2005. **49**(9): p. 3889-95.

100. Martinez-Becerra, F., et al., *Analysis of the antimicrobial activities of a chemokine-derived peptide (CDAP-4) on Pseudomonas aeruginosa.* Biochem Biophys Res Commun, 2007. **355**(2): p. 352-8.

101. McMorran, B.J., et al., *Platelet factor 4 and Duffy antigen required for platelet killing of Plasmodium falciparum.* Science, 2012. **338**(6112): p. 1348-51.

102. Sevier, C.S. and C.A. Kaiser, *Formation and transfer of disulphide bonds in living cells.* Nat Rev Mol Cell Biol, 2002. **3**(11): p. 836-47.

103. Legendre, B., et al., *The disulfide bond between cysteine 10 and cysteine 34 is required for CCL18 activity.* Cytokine, 2013. **64**(1): p. 463-70.

104. Feng, Z., et al., *Human beta-defensin-3 structure motifs that are important in CXCR4 antagonism.* FEBS J, 2013. **280**(14): p. 3365-75.

105. Singh, S.K., et al., *Structural basis for Duffy recognition by the malaria parasite Duffy-binding-like domain.* Nature, 2006. **439**(7077): p. 741-4.

106. Lambros, C. and J.P. Vanderberg, *Synchronization of Plasmodium falciparum erythrocytic stages in culture.* J Parasitol, 1979. **65**(3): p. 418-20.

107. Whitmore, L. and B.A. Wallace, *Protein secondary structure analyses from circular dichroism spectroscopy: methods and reference databases.* Biopolymers, 2008. **89**(5): p. 392-400.

108. Ortiz-Ordonez, J.C., J.B. Sechelski, and J.R. Seed, *Mechanism of lysis of Trypanosoma brucei gambiense by human serum.* J Parasitol, 1994. **80**(6): p. 924-30.

109. Baumeister, S., et al., *Evidence for the involvement of Plasmodium falciparum proteins in the formation of new permeability pathways in the erythrocyte membrane.* Mol Microbiol, 2006. **60**(2): p. 493-504.

110. Kirk, K. and H.A. Horner, *In search of a selective inhibitor of the induced transport of small solutes in Plasmodium falciparum-infected erythrocytes: effects of arylaminobenzoates.* Biochem J, 1995. **311 (Pt 3)**: p. 761-8.

111. Elford, B.C., et al., *Heterogeneous and substrate-specific membrane transport pathways induced in malaria-infected erythrocytes.* Blood Cells, 1990. **16**(2-3): p. 433-6.

112. Green, C.J., et al., *Identification and characterization of PF4varl, a human gene variant of platelet factor 4.* Mol Cell Biol, 1989. **9**(4): p. 1445-51.

113. Goldberg, D.E., et al., *Hemoglobin degradation in the malaria parasite Plasmodium falciparum: an ordered process in a unique organelle.* Proc Natl Acad Sci U S A, 1990. **87**(8): p. 2931-5.

114. Ham, B.M., et al., *Identification, quantification and comparison of major non-polar lipids in normal and dry eye tear lipidomes by electrospray tandem mass spectrometry.* J Mass Spectrom, 2004. **39**(11): p. 1321-36.

115. Cooke, B.M., N. Mohandas, and R.L. Coppel, *Malaria and the red blood cell membrane.* Semin Hematol, 2004. **41**(2): p. 173-88.

116. Wautier, J.L. and M.P. Wautier, *Molecular basis of erythrocyte adhesion to endothelial cells in diseases.* Clin Hemorheol Microcirc, 2013. **53**(1-2): p. 11-21.

117. Kirk, K. and K.J. Saliba, *Targeting nutrient uptake mechanisms in Plasmodium.* Curr Drug Targets, 2007. **8**(1): p. 75-88.

118. Ott, T.R., et al., *Determinants of high-affinity binding and receptor activation in the N-terminus of CCL-19 (MIP-3 beta).* Biochemistry, 2004. **43**(12): p. 3670-8.

119. Capoulade-Metay, C., et al., *A natural CCL5/RANTES variant antagonist for CCR1 and CCR3.* Immunogenetics, 2006. **58**(7): p. 533-41.

120. Terwilliger, T.C. and D. Eisenberg, *The structure of melittin. II. Interpretation of the structure.* J Biol Chem, 1982. **257**(11): p. 6016-22.

121. Zasloff, M., *Magainins, a class of antimicrobial peptides from Xenopus skin: isolation, characterization of two active forms, and partial cDNA sequence of a precursor.* Proc Natl Acad Sci U S A, 1987. **84**(15): p. 5449-53.